

BLL ID NO D 18530/77

LOUGHBOROUGH  
UNIVERSITY OF TECHNOLOGY  
LIBRARY

AUTHOR/FILING TITLE

SELBY, K

ACCESSION/COPY NO.

023911/02

VOL. NO.

CLASS MARK

<del>13 JUN 1977</del>	<del>LOAN COPY</del>	
<del>29 SEP 1977</del>	<del>2 JUL 1980</del>	
<del>DATE</del>	<del>1 JUL 1981</del>	<del>6 JUN 1995</del>
<del>2.8.77</del>	<del>-2 JUL 1982</del>	<del>30 1995</del>
<del>12 JUN 1979</del>	<del>-1 JUL 1983</del>	<del>6 OCT 1995</del>
<del>4.1979</del>	<del>-2 JUL 1983</del>	
<del>-2 JUL 1980</del>		
	0 MAY 1995	

002 3911 02





A STUDY OF THE FRACTURE, MECHANICAL  
BEHAVIOUR AND MORPHOLOGY OF AN EPOXY RESIN SYSTEM

by  
Kevin Selby B.Sc.

A DOCTORAL THESIS SUBMITTED IN PARTIAL FULFILMENT  
OF THE REQUIREMENTS FOR THE AWARD OF DOCTOR OF  
PHILOSOPHY OF THE LOUGHBOROUGH UNIVERSITY OF  
TECHNOLOGY

SEPTEMBER 1976

Supervisors: L. E. Miller Ph.D.\*  
M. O. W. Richardson Ph.D.  
Department of Materials Technology  
\*Formerly Department of Materials Technology  
© by Kevin Selby, 1976.

Loughborough University of Technology Library	
Date	Dec. 76
Class	
Acc. No.	023911/02

## SYNOPSIS

### A STUDY OF THE FRACTURE, MECHANICAL BEHAVIOUR AND MORPHOLOGY OF AN EPOXY RESIN SYSTEM

by

K. Selby

The fracture and mechanical properties of an epoxy resin system have been investigated as a function of changes in stoichiometry and heat treatment. Relationships between the various macroscopically measured properties and the microscopic characteristics of the cured resin are described. The investigation shows that the concept of fracture surface work,  $\gamma$ , measured by a cleavage technique, is a sensitive parameter for monitoring changes in the resin's fracture properties and that the Irwin-Kies and Berry analyses can provide a more sensitive monitor of  $\gamma$  than the Gurney method, in some circumstances. The investigation also demonstrates how the elastic and visco-elastic properties of the resin can effect plasticisation at the tip of a crack, with consequent improvement in fracture toughness. To aid the interpretation of the mechanical data, a morphological characterisation of the cured resin will be described in which quantitative infrared spectroscopy, thermo-mechanical analysis, solvent uptake resistance, chemical and ion-beam etching methods have been used.

# C O N T E N T S

## SYNOPSIS

### PART 1 - Morphology of Epoxy Resins and the Relation between Morphology of Materials and Mechanical Behaviour.

#### Chapter 1 Introduction Page

1.1. Epoxy Resins 5

1.2. Properties and Morphology of Materials 6

#### Chapter 2 Morphology of Epoxy Resins Page

2.1. Chemical Morphology 7

2.2. Physical Morphology 8

#### Chapter 3 Fracture Parameters and the Cleavage Technique Page

3.1. Fracture Parameters 10

3.2. The Influence of Plastic Deformation 12

3.3. The Cleavage Technique 12

#### Chapter 4 Fracture Parameters Applied to the Study of Polymer Morphology Page

4.1. General Comments 14

4.2. Effect of Structure Modification by Cross-linking 14

#### Chapter 5 Aims and Justification of Present Work Page

5.1 17

### PART 2 - Experimental Detail

#### Chapter 6 Production of Cured Epoxy Resin and Initial Testing Page

6.1. Raw Materials 18

6.2. Preparation of Cured Slabs and Specimens 18

6.3. Initial Tests 19

#### Chapter 7 Mechanical and Fracture Test Methods Page

7.1. General Comments 21

7.2. Measurement of Fracture Surface Work and Plane Strain Fracture Toughness 22

7.3. Tensile Fracture and Tensile Modulus Tests 26

7.4.Compression Testing	26
7.5.Crack Tip and Fracture Surface Observations	27
Chapter 8 Characterisation of Cured Resin	Page
8.1.General Comments	28
8.2.Infra-red Spectroscopy	28
8.3.Thermo-mechanical Analysis	29
8.4.Solvent Uptake	29
8.5.Density	30
8.6.Etching Methods	30
PART 3 - Results and Discussion	33
Chapter 9 Mechanical and Fracture Properties of Epikote 828/Epikure DDM	Page
9.1.General Comments	34
9.2.Effect of Resin/DDM Ratio	34
9.3.Effect of Variations in Cure Cycle	40
9.4.Effect of Varying Testing Speed	41
9.5.Comments on Mechanical Behaviour	42
Chapter 10 Morphological Characterisation	Page
10.1.General Comments	43
10.2.Thermo-mechanical Analysis	43
10.3.Solvent Uptake and Density	43
10.4.Infra-red Spectroscopy	44
10.5.Chemical and Ion-beam Etching	45
Chapter 11 Crack Tip and Fracture Surface Characteristics	Page
11.1.In-situ Cleavage Tests on the Projection Microscope	51
11.2.Optical and Electron Fractography	52

Chapter 12	Discussion	Page
12.1.	General Comments	55
12.2.	Comparison of Fracture Surface Work Values Obtained by Irwin-Kies', Berry's and Gurney's Analyses	55
12.3.	The Variation of Properties as a Function of DDM content	58
12.4.	Physical Morphology of 828/DDM and its Contribution to Mechanical Behaviour	67
12.5.	Variation of Properties as a Function of Cure Cycle	70
12.6.	Effect of Testing Speed on Mechanical and Fracture Properties	71
12.7.	Comments on Fracture Surface Features and Their Relation to Crack-tip Processes	72
PART 4	- Conclusions and Suggestions for Future Work	Page
Chapter 13	Conclusions	74
Chapter 14	Suggestions for Future Work	Page
14.1.	General Comments	76
14.2.	Specific Studies of Epikote 828/DDM	76
14.3.	Use of Fracture Parameters and Etching Techniques as Characterisation Methods	76
14.4.	Matrices for Composites	77
14.5.	Author's Concluding Remarks	77
	REFERENCES	79
	ACKNOWLEDGEMENTS	86
	APPENDICES	Page
1.	Concepts of Fracture Mechanics	96
2.	Machining of Test Specimens	105
3.	Statistical Analysis of Fracture Data	106
4.	Calculation of Young's Moduli	112
5.	Tabulated Data for Cross-Reference with Graphical Figures	115



ABBREVIATIONS AND SYMBOLS USED

- $\gamma$  - Fracture Surface Work
- $K_{IC}$  - Plane Strain Fracture Toughness
- $G_C$  - Critical Strain Energy Release Rate
- $E_C$  - Compressive Young's Modulus
- $E_T$  - Tensile Young's Modulus
- U.T.S. - Ultimate Tensile Strength
- D.C.B. - Double-Cantilever-Beam
- T.D.C.B. - Tapered Double-Cantilever-Beam
- A - Absorption or Absorbance Ratio (in Infra-red Analysis)

PART 1 - Morphology of Epoxy Resins and the Relation between  
Morphology of Materials and Mechanical Behaviour

CHAPTER 1 Introduction

1.1. Epoxy Resins

The epoxy resin family of materials is very widely used in the industrial world. Typical applications are for castings (rods, spheres, gears, bushes etc.), potting of electrical components, encapsulating, sealing, laminating and as matrices in modern composites. There are many epoxy adhesives and they also enjoy considerable use in civil engineering applications for flooring, road and bridge coating, repair and soil consolidation.

Epoxy resins require chemical 'cross-linking' or curing, a process which may be achieved by adding a curing agent. Discussion of the various cure reactions is included later. Suffice it to mention that there are a great number of resin/curing agent/additive systems in existence, the exact formulation used being dependent on the ultimate application of the polymer. (1-4)

Although epoxy resins have been used for many years on their own and, more recently, as constituents in engineering composites, little work on the inter-relationship of physical morphology and physical and mechanical properties has been done on the resins per se. A considerable body of literature is available on the chemistry of epoxy resins (see reference 1 for example) and their curing agents. Studies have included kinetics of cross-linking and the characterisation of the cured product by means of standardised mechanical, electrical and chemical tests. What is missing, however, is a description of the physical morphology of a typical resin system and of the behaviour of the structural features comprising the resin when subjected to stress. The work described in this thesis was carried out with the intention of providing such a description of morphology and behaviour, and to relate existing characterisation techniques to any new

morphological description of a resin.

## 1.2. Properties and Morphology

The natural connection between morphology and properties which exists in all materials prompts the question:-

'which property is most likely to respond to a change in morphology'?

Since morphology can be defined at levels ranging from the atomic to the supramolecular, the property variations that may be induced by changes in morphology may require investigation at several levels of observation. Of primary interest to many engineers and materials scientists are the bulk mechanical and fracture properties. Since these properties are representative of the material in bulk and are of direct practical use, it was decided to monitor changes in mechanical and fracture behaviour as functions of stoichiometric variation in formulation and heat treatment. In parallel with this, a morphological investigation by conventional chemical and physico-chemical methods was carried out. Furthermore, a study of the resin by chemical and ion-beam etching was undertaken, together with fractographic and crack-tip observations.

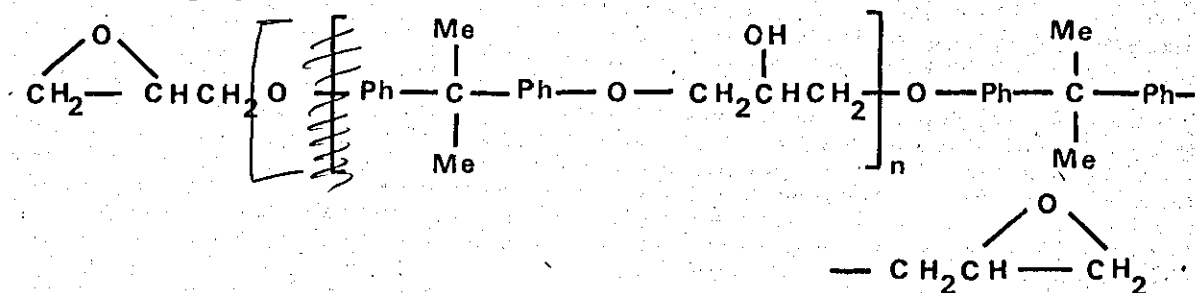
In the following pages, a resumé of existing knowledge of the morphology of epoxy resins is given. This is followed by a brief summary of the fracture mechanics concepts employed in this study and their application to polymeric materials. This will provide a foundation upon which the major mechanical and fracture properties of the resin system Epikote 828\*/Epikure DDM\* can be presented and discussed in morphological terms. A more detailed discussion of fracture mechanics concepts is given in Appendix 1.

\* Trade names of Shell Chemical Co. See Section 2.1. and 6.1. for chemical description.

CHAPTER 2 Morphology of Epoxy Resins

2.1. Chemical Morphology

Epoxy resins are frequently based upon the di-glycidyl ether of bisphenol A (DGEBA). Many variations on this basic theme exist, but conventional descriptions of the generalised DGEBA epoxy molecule employ the following chemical formula:



Among the methods of characterisation which have been used on uncured epoxies are fractional precipitation,<sup>(2)</sup> thin layer chromatography,<sup>(5,6)</sup> gel permeation chromatography,<sup>(7)</sup> and infra-red spectroscopy.<sup>(8-15)</sup> Infra-red spectroscopy has also been used for studying cured resins.<sup>(8)</sup>

At this stage it would be informative to consider some aspects of the chemistry of cross-linking reactions in epoxy resins, in order to provide a basis for later discussion. Generally, the curing agents used for these materials are of two types - catalytic or polyfunctional - and curing may be effected through the hydroxyl or the epoxy groups on the resin molecule. Homopolymerisation of the resin results from the use of a catalytic initiator. In the case of polyfunctional agents, near stoichiometric quantities of curing agent are generally used, the product being a three dimensional network of resin cross-linked by curing agent. The curing agent thus acts as a co-monomer. The reactions are usually free from by-products and usually exothermic. Substances containing active hydrogen atoms e.g. phenols, thiols, alcohols, primary and secondary amines and carboxylic acids will act as polyfunctional curing agents.

Tertiary amines, Lewis bases and many acids are catalysts for resin cure. (1-3)

Although the reaction schemes suggested as explanations of resin cure are fairly simple in nature,<sup>(1)</sup> there is tremendous variety in terms of the formulation of a resin system. Simultaneous reactions, suppression or promotion of a reaction may occur.

Additives such as mono-functional flexibilisers, plasticisers and viscosity control agents can influence the product. An extensive coverage of these aspects of resin cure would serve no useful purpose here. Detailed discussion of the chemistry of Epikote 828/Epikure DDM is left until later (Section 12.3.).

## 2.2. Physical Morphology

Very little work has been done on the elucidation of physical morphology in epoxy resins. For many years the assumption that a cross-linked resin is one giant molecule, possibly sponge-like in character, has been implicit in the references to mechanical behaviour and its dependence on, for example, resin chemical structure. However, a growing body of evidence suggests that a sub-unit of structure may be instrumental in making up the large mass of material produced by cross-linking.<sup>(16-20)</sup> In particular, the work by Cuthrell<sup>(18-20)</sup> suggests that the curing epoxy has a colloidal nature, and that the resulting cross-linked mass retains some of the essential features of a two-phase structure, i.e. a dense floccular phase tens of  $\mu$  (microns) in diameter, dispersed in a matrix of less dense material which resembles the uncured resin. Cuthrell also implied that a regular arrangement of floccules may be obtained. If this is so, it is reasonable to suppose that such a two-phase structure would influence mechanical and fracture properties.

Floccular or globular morphologies have been the subject of some research fairly recently.<sup>(20a)</sup> For example, amorphous polycarbonate,<sup>(21,22)</sup> phenolic resins and DAP (di-allyl phthalate),<sup>(16,17)</sup> have all been studied and were found to exhibit nodular structures. The role that nodular structures play in determining the bulk properties of both thermo-plastics and thermo-setting resins is by no means clear. Much of the research carried out to determine the physical morphology of glassy polymers has involved thermoplastics some of which are crystallisable. (See, for example, the review by Geil<sup>(22a)</sup>). However, the existence of nodular fibrillar textures in sheared regions and crazed regions of glassy polymers,<sup>(23)</sup> the suggestion of ordering phenomena in epoxies, both in the bulk,<sup>(20)</sup> and in interfacial regions in composites<sup>(24)</sup> adds weight to the view that the interaction between such structural entities is of major importance. Questions left unanswered in some of the work already cited are associated with the intra-nodular structures and their relation to cure and processing conditions and the response that nodular agglomerates exhibit when subject to mechanical deformation. It will be seen that the behaviour of material adjacent to a crack tip provides an insight into the morphology of the material.

The following chapter describes the basic parameters of fracture mechanics and outlines a suitable method of measuring these parameters.

CHAPTER 3 Fracture Parameters, and the Cleavage Technique

3.1. Fracture Parameters

It is now necessary to consider the meaning of two terms frequently encountered in fracture studies:

- (a) Fracture surface work, (F.S.W.,  $\gamma$ ).
- (b) Fracture toughness,  $K_C$  (Critical stress intensity factor).

The original concept of fracture surface energy is due to Griffith.<sup>(25)</sup> He considered the energy changes that occur when a cracked body undergoes fracture and defined  $\gamma$  as the work required to produce unit area of fracture surface. His treatment of the process depends ultimately on elementary linear elastic stress analysis for the description of the state of stress around a crack tip.<sup>(26)</sup> This is a situation which is not entirely satisfactory (see Appendix 1). However, the thermodynamic approach to the problem employed by Griffith is still regarded as valid by many workers and the FSW concept, when properly defined, has found considerable use as a fracture parameter and as a material 'constant'.

$\gamma$  can be evaluated in a number of different ways<sup>(27-29)</sup> but the feature common to all methods is the energy balance invoked to estimate the work done in propagating a crack.

The fracture toughness term arises as a natural consequence of an analysis of crack tip stresses performed by Irwin.<sup>(30)</sup> The essential difference between Griffith's and Irwin's analyses is that Griffith considered the energetics of the whole system and equated the loss of free energy on crack propagation to the work of fracture, whereas Irwin analysed near-tip regions only, to develop his argument. (A lucid account of the two approaches is provided by Berry in (31)). The fracture toughness parameter is found to be dependent on the geometry of the system and the mode of failure of the specimen (see Appendix 1 and Fig. 1). However,  $K_C$

can be related mathematically to  $\gamma^{(32)}$ , provided the equivalence of the testing conditions is established. Various methods are available<sup>(33)</sup> for evaluating  $K_C$ , the details of which do not concern us here. It is found that a relationship between  $K_C$ , modulus of elasticity  $E$ ,  $\gamma$ , and another parameter arising from Irwin's analysis,  $G_C$ , exists such that

$$K_C^2 = 2 E \gamma = E G_C \text{ for plane stress.}$$

or 
$$K_{IC}^2 = \frac{E G_{IC2}}{1 - \nu} \text{ for plane strain (see below)}$$

where  $\nu$  is Poisson's ratio.

$G_C$  is called the critical strain energy release rate. (Both  $G_C$  and  $K_C$  are often referred to as the 'fracture toughness' of a particular material. ' $\gamma$ -fracture-toughness' is another term which has been used. Unfortunately, it is possible to be misled by the improper or inappropriate use of these terms. From the author's viewpoint, the use of the symbol  $\gamma$  is preferred, representing fracture surface work for macroscopically plane strain fracture. (The reason for this will become clear in section 3.2.)). It should be noted that  $K_C$  is material and geometry dependent but  $K_{IC}$ , the lower limiting value of  $K_C$  as specimen thickness increases, is regarded as a material constant. (See Appendix 1).

The fundamental criterion in Irwin's analysis is that  $K_C$  is constant at fracture. It is the correct evaluation of  $K_C$  which has been the object of fracture mechanics for many years. The development of new criteria for fracture and relationships between  $K_C$  and these new concepts has now become of paramount importance, particularly in dealing with polymeric materials and other materials which undergo considerable plastic deformation at the tip of a crack.



### 3.2. The Influence of Plastic Deformation

The original analyses of Griffith and Irwin took no account of plastic deformation near the tip of a crack and relied on assumptions of perfect elasticity up to the point of fracture. However, Orowan et al<sup>(34-36)</sup> and Irwin<sup>(30)</sup> recognised the role that plastic deformation must play in crack development and produced modifications to the earlier treatment (see Appendix 1). The details of these treatments are omitted here but it is necessary to say that all real, experimental values of  $\gamma$ ,  $G_C$ ,  $K_C$  or  $K_{IC}$  obtained from cracked specimen tests necessarily include the effects of crack tip micro-plasticity. They therefore represent the total work done during crack growth.

The main contribution that plastic deformation makes to the behaviour of the tip of a crack is effectively to make it less sharp and to relieve stresses in the vicinity of the tip.<sup>(32)</sup> The nett effect is to toughen the material. In the case of rate sensitive materials, it is evident that visco-elastic processes may markedly affect the toughness of the material.

### 3.3. The Cleavage Technique

A useful method of evaluating  $\gamma$  or  $K_C$  or  $G_C$  employs an experimental system which fractures a pre-cracked specimen in the opening mode of crack advancement (Fig. 1.). While pure cleavage on a microscopic scale is rarely, if ever achieved,<sup>(32,37)</sup> the term cleavage is used in a generic sense to describe this mode of failure. The geometry of the test piece determines the exact form of mathematical treatment of the results. A general energy balance analysis by Irwin and Kies,<sup>(28)</sup> a treatment by Berry,<sup>(27)</sup> and a method presented by Gurney<sup>(29)</sup> have all been used in cleavage tests to evaluate fracture parameters.<sup>(38-44)</sup>

In the author's work, all three analyses have been used<sup>(44)</sup> to establish which is the most appropriate for monitoring morphological changes in epoxy resins. The analyses are described in Chapter 7.

In essence, the cleavage test consists in propagating a crack through a material in such a way that its direction of motion is controlled. The parameters load, crack length, specimen end deflection and (in recent years) near-tip crack opening displacement (C.O.D.) are measured during the test. Control of the crack direction is usually achieved by machining grooves along the sides of the specimen (Fig. 2.).

Before considering the cleavage technique in detail, some fracture studies on polymers will be briefly mentioned.

## CHAPTER 4 Fracture Parameters Applied to the Study of Polymer Morphology

### 4.1. General Comments

Berry<sup>(45)</sup> has provided an excellent review of the general problem of fracture in polymeric glasses. In particular, he discusses the application of the Griffith theory, the inherent flaw concept, the influence of experimental conditions on fracture properties, the significance of fracture parameters, crazing, characteristics of fracture surfaces and mechanisms of fracture as well as time dependent fracture. Many different polymers have been investigated using classical fracture mechanics techniques and the more modern plastic zone analyses (see Appendix 1). Polystyrene, polycarbonate and poly (vinyl chloride)<sup>(46)</sup> have all been investigated using the Dugdale plastic zone analysis,<sup>(47)</sup> as have poly (methyl methacrylate) and poly (ethylene terephthalate)<sup>(48)</sup>. However, the section of literature most relevant to the present investigation of epoxy resins deals with structural modification by cross-linking.

### 4.2. Effect of Structure Modification by Cross-linking

This aspect has some considerable potential as a research tool on account of the control that can be exercised over the extent of cross-linking. It is surprising that so little work has been published on the topic.

The objective has been to systematically vary the 'structural unit' by copolymerisation and/or cross-linking and to correlate these variations with changes in fracture properties. Work has been done on co-polymers of methyl methacrylate (MMA) and ethylene glycol dimethacrylate (EGDMA), some commercial methyl methacrylate co-polymers<sup>(50)</sup> and on polyester and epoxy resins.<sup>(50,51)</sup> The two latter systems probably provide greater scope for variation in terms of resin/cross-linking agent proportions because they

will tolerate quite substantial changes in formulation before becoming difficult to cast or machine and are less susceptible to shrinkage stresses than the more linear co-polymers. (In the case of MMA/EGDMA co-polymers, Berry<sup>(49)</sup> was unable to produce a material with >10% dimethacrylate because of shrinkage cracking).

Fracture surface work,  $\gamma$ , can be decreased in MMA/EGDMA relative to the linear PMMA<sup>(49)</sup> and can be made to decrease with increased cross-linking. Polyester/styrene cross-linked systems<sup>(50)</sup> again show an overall reduction in  $\gamma$  compared to the linear polyester, but a slight increase in  $\gamma$  on increasing styrene content up to about 50% by weight is observed.

Although a great deal of work has been carried out on the mechanical behaviour of epoxy resins and composites, little has been reported concerning variations of fracture properties in unfilled resins. In particular, the use of stoichiometry as a variable in fracture investigations has only been covered very briefly,<sup>(51)</sup> without reference to the morphological reasons for changes in values of  $\gamma$ . Fracture surface work and fracture toughness values are available for stoichiometric unfilled resin, however.<sup>(50-55)</sup> In general, the unfilled resins have not been regarded as tough materials, suitable for use on their own in structural members. Typical values of fracture surface work for unfilled epoxies are 25-200 Jm<sup>-2</sup>.

The reason for using cross-linking to study fracture behaviour is based on the evidence (see (45)) that the major contribution to measured  $\gamma$  values is the energy expended during deformation of material adjacent to the crack tip. It is logical to expect a systematic variation in fracture properties if the

deformation process can be modified in a controlled manner. In view of the ease with which the crosslink-agent, its proportion of the total, and the cure schedule can be varied in epoxy resins without presenting insurmountable practical difficulties it is expected that epoxy systems can provide controlled structures for fracture mechanics and fracture mechanism investigations. Also, the work described above has established that fracture and mechanical parameters can be used to monitor morphological changes in polymers. (Including changes induced by processing<sup>(45)</sup>). With these points in mind, the use of fracture parameters as engineering and characterisation aids is a logical course of action.

CHAPTER 5 Aims and Justification of Present Work

5.1.

From what has been written in Chapters 1-4, it is evident that there is a need not only to relate traditional chemical characteristics of epoxy resins to their mechanical behaviour, but also to establish new relationships between the chemical and physical descriptions of the resins. The mechanical behaviour of any material is fundamentally determined by its chemical identity. However, it is well known that processing conditions are a major factor in determining the final properties and performance in practice. If a morphological entity exists in epoxy resins which can respond to mechanical forces, it would be a major step forward if this entity could be identified and monitored in some way and used for the effective rationalisation of property variations. Apart from aiding the description of mechanical behaviour of the resin alone, such information may prove to be valuable in the composites field, where matrix/second phase interaction plays such an important role.

Part 2 of this thesis outlines the experimental work carried out and lays the foundation for presenting results.

PART 2 - Experimental Detail

CHAPTER 6 Production of Cured Epoxy Resin and Initial Testing

6.1. Raw Materials

The resin used for this particular investigation was Epikote 828, a commercial di-glycidyl ether of bisphenol A (DGEBA, see section 2.1.). The resin has a molecular weight (quoted by manufacturer) of approximately 370. This value of MW means that n in the generalised epoxy molecule has a value between 1 and 3. The crosslinking agent was 4-4'-diamino-diphenyl-methane (DDM), which has the formula.



DDM is also known as 4,4'-methylene dianiline (MDA). The nominal stoichiometric proportions for this system are 27 parts DDM per 100 of resin (by weight). The term 'parts DDM' is used throughout this text and indicates the weight of DDM used, per 100 weight units of resin, for the mixing of the original casting compounds.

6.2. Preparation of Cured Slabs and Specimens

Various ratios of resin and DDM were mixed and cured as indicated in Table I. Resin at 353°K (80°C) and DDM at 383°K (110°C) were mixed and de-gassed prior to casting into steel moulds. The moulds had been pre-heated to 373°K (100°C) after the application of a silicone release agent. After casting, the moulds were replaced in the curing oven. The temperature of the curing mixture was monitored by a thermocouple inserted through the top of the mould and dipping just under the upper surface of the liquid resin. (Consequently, a small length of thermocouple was sacrificed for each cast). On completion of the appropriate cure cycle, the mould

was allowed to cool, in still air, to room temperature before removal of the sheet of cured resin. The point of casting was usually reached within 960 seconds (16 minutes) of the start of mixing.

Tapered double-cantilever-beam cleavage test pieces were machined from the .006m thick sheets of resin, the geometry of the test piece being defined in Fig. 2. (For convenience, these specimens are referred as TDCB specimens).

Tension and compression test pieces were also machined from the cured resin. Their geometries are defined in Fig. 3. Excess material was utilised in characterisation studies described in Chapter 8.

Further details concerning the machining operations are given in Appendix 2.

### 6.3. Initial Tests

In order to establish that material produced by the above method was of adequate quality and homogeneity, a series of tests was done which involved simple procedures and which could be relied upon to prove the suitability of the material and the method of production. For this purpose, tensile Young's modulus was chosen as a suitable parameter. Also, some fracture tests were carried out in order to show that the fracture surface work parameter was capable of differentiating between resin formulations of various DDM content. Details of the testing and calculation procedures are given in Chapter 7, and Appendix 4.

The results of these early tests are included in the more extensive resumé of results, in particular in Figs. 9 and 11. It is sufficient to note here that both the tensile Young's modulus and fracture surface work (measured by Irwin-Kies or Berry's method) variation within a given formulation was quite small. In the worst cases ~8% variation for modulus measured at  $.017\text{mms}^{-1}$  ( $0.1\text{mm. min}^{-1}$ )



crosshead speed and  $\sim 9\%$  variation for  $\gamma$  were recorded. Both parameters were also capable of differentiating between formulations containing different amounts of DDM. It was concluded that batch reproducibility was adequate and that mechanical test parameters, which could monitor variations, were available.

Having established that the material could be produced consistently and monitored adequately, a more exhaustive investigation of mechanical properties and morphological characterisation was started. The testing methods employed are described in the following two chapters.

## CHAPTER 7 - Mechanical and Fracture Test Methods

### 7.1. General Comments

For the reader's convenience, the mechanical parameters measured during this work are listed below and test methods are given later in the Chapter.

- (a) Fracture surface work,  $\gamma$ , and plane strain fracture toughness  $K_{IC}$ .
- (b) Tensile Young's modulus,  $E_T$ .
- (c) Compressive Young's modulus,  $E_C$ .
- (d) Compressive proof stress (1%).
- (e) Tensile strength (U.T.S. or fracture stress).
- (f) Deformation characteristics, particularly in compression. Details of these particular parameters are given in the relevant sections on results and discussion.
- (g) Crack tip observations and fracture surface examination.

The majority of the above parameters were investigated as functions of:

- (i) Stoichiometric ratio i.e. 828/DDM ratio,
- (ii) Cure conditions. (Temperature and time),
- (iii) Testing rate,

in order to assess the response of the morphology of the resin to processing variables and mechanical service conditions.

The logic behind choosing DDM content as a major variable has already been outlined in Chapter 4. The reasons for monitoring changes in cure cycle are straight forward. If the curing resin is subjected to variations in thermal treatment it is possible that different extents of reaction will prevail. This in turn might affect mechanical properties. Copious information on the effect of cure

cycle for a variety of resin systems is available.<sup>(1)</sup> However, it was considered necessary to establish the extent to which variation can be induced in 828/DDM for confidence in interpreting other data collected during this study. The influence of testing speed on the measured properties of visco-elastic materials is an important point to consider in the assessment of a material's performance. It was therefore considered advisable to acquire some information on the rate sensitivity of at least two parameters i.e.  $\gamma$  and  $E_T$ .

All mechanical testing was carried out on an Instron TTM (floor model) machine. All tests were conducted at room temperature. Further details are given in the following sections.

## 7.2. Measurement of Fracture Surface Work and Plane Strain Fracture Toughness

### 7.2.1. Test Piece Description

Two forms of the double cantilever beam (DCB) cleavage test piece are illustrated in Fig. 2.

- (a) the parallel test piece
- (b) the tapered test piece (TDCB).

The essential difference between the two geometries is that their compliance ( $\frac{1}{\text{load/unit deflection}}$ ) v. crack length characteristics are different. The parallel DCB specimen has a non-linear compliance v. crack length relationship whereas the TDCB geometry provides a linear plot. It is this plot which is of paramount importance to the calculation of  $\gamma$ ,  $G_C$  or  $K_C$  by Irwin-Kies equation. An advantage of both the DCB and TDCB specimens over many other fracture toughness test configurations is that they will allow several datum points per specimen to be easily obtained. Hence there are statistical advantages in using DCB or TDCB specimens.

### 7.2.2. Berry's Analysis of DCB Systems

By invoking beam theory and postulating that the deflection behaviour of a DCB test piece conforms to an equation of the form

$$f = (ac^{-n}) \delta$$

where  $f$  = load applied to free ends of cantilever beams

$a$  = constant

$n$  = constant

$c$  = crack length

$\delta/2$  = end deflection of one half of the DCB specimen,

Berry<sup>(27)</sup> has established that plots of  $\log f/\delta$  v.  $\log c$  and of  $f\delta/w$  v.  $c$  ( $w$  being the width of the crack plane) should be linear. From the slopes of the two graphs, a value for  $\gamma$  can be obtained.

$$\gamma = \frac{\text{slope 1} \times \text{slope 2}}{4}$$

### 7.2.3. The Irwin-Kies Equation

One form of the equation developed by Irwin and Kies<sup>(28)</sup> is:

$$2\gamma = G_C = \frac{f^2}{2w} \cdot \frac{dR}{dc}$$

where  $R$  is the compliance of the specimen. Thus, if a plot of  $R$  v.  $c$  is drawn for any specimen geometry, its slope at a particular value of  $f$  and  $c$ , (and hence a particular value of  $R$  and  $c$ ) can be measured and  $\gamma$  can be evaluated. It is to be noted that a linear plot of  $R$  v.  $c$  would be advantageous. To a first approximation, the equation<sup>(56)</sup>

$$\frac{dR}{dc} = \left( \frac{3c^2}{h^3} + \frac{1}{h} \right) \frac{8}{EB}$$

where  $h$  = half height of the complete DCB specimen

$B$  = gross thickness of the specimen

defines such a situation. Thus, if the bracketted term remains constant,

so does  $dR/dc$ . This last equation, deduced from simple beam theory, defines a cubic profile, but in practice it is found that a straight-edged, tapered test piece will produce an approximately linear  $R$  v.  $c$  plot. It is the approximate profile which was employed during this study. It should also be noted that for constant  $G_c$ , failure at constant load would be expected for TDCB specimens, (Fig. 4).

#### 7.2.4. Gurney's Analysis

The area under a load-extension curve obtained from a DCB fracture test represents the amount of elastic and plastic work done during the loading and rupture of the specimen to a crack length  $c$ . Gurney<sup>(29)</sup> has pointed out that if the component of area corresponding to crack propagation is measured and converted accordingly to an energy value, then a figure for  $\gamma$  can be obtained by dividing this energy value by the fracture surface area. The simplicity of the method makes it very attractive for fracture studies. However, there are situations when the method can give rise to misleading results.<sup>(44)</sup> This point is considered in more detail in Chapters 9 and 12.

#### 7.2.5. Fracture Tests - Procedure

For fracture toughness or  $\gamma$  calculations, the following parameters were measured.

- |  |       |
|--|-------|
| (a) Force,                             | N     |
| (b) Crosshead movement,                | m     |
| (c) Crack length,                      | m     |
| (d) Crack surface width,               | m     |
| (e) Area under force-deflection graph, | $m^2$ |

All fracture toughness tests were done on the Instron machine using a CTM load cell of 0-4905N capacity. The high sensitivity range for load measurements was used in some tests (when failure loads were less than  $\sim 50N$ ). Crosshead speed was varied according to the particular investigation, but most work was done at  $.017mm\ s^{-1}$

( $0.1\text{mm}\cdot\text{min}^{-1}$ ). Crosshead movement was measured from the chart record (Y axis as mounted in the machine), by applying the appropriate factor to allow for the chart/crosshead speed ratio. Crack length was measured either:

- (a) during the test, when a continuous tearing mode of propagation was prevalent, by observing the movement of the crack tip between graduations on the specimen and using a chart event-marker to indicate the appropriate force-deflection-crack length datum point.
- or (b) after the test, when 'crack jumping' phenomena allowed the position of the crack, at various stages of the test, to be located by arrest marks on the fracture surface. A wooden rule was found to be adequate for crack length measurement in these circumstances. (See section 11.2.).

Fracture surface width was measured, using a micrometer

- (a) in several places on specimens which failed in a stable manner (continuous tearing)
- (b) at arrest points, and at least one intermediate point per crack-jump, for specimens which failed in an unstable manner.

Areas under force-deflection graphs, for Gurney's analysis, were calculated from the general relation,

$$\text{Area of triangle ABC} = \frac{1}{2} ab \sin C$$

where the capital and sub-case letters have the usual mathematical significance. (The linearity of the load-extension curves generated during fracture tests which allowed the use of the above formula for area, is discussed in section 9.2.1.).

Pre-cracking of specimens prior to testing was achieved by clamping the specimen in a vice so that approximately .050 m (measured from the loading end) projected. A single-edged razor blade was then tapped into the end of the specimen until a sharp

natural crack, .02-.05m long, formed. All tests were conducted at room temperature.

### 7.3. Tensile Fracture and Tensile Modulus Tests

Tensile testing was carried out using ASTM D638-71a as a guide. Actual specimen dimensions differed from those in D638 but the essential features of the test piece shown in Fig. 3 are similar to the type 2 specimen described by ASTM. For modulus measurements, an Instron G11-57-M-A (0-10%) strain gauge extensometer was used, over a load range of 0-2000N and at crosshead speeds of .017-.17mm s<sup>-1</sup> (0.1-10.0 mm.min<sup>-1</sup>), according to the investigation. Modulus testing was done in two ways (a) by a single application of the load and (b) by repeated applications separated by 60s periods of relaxation and recovery (see section 9.2.2. and Appendix 4). All tests were done at room temperature and the FRM load cell was used.

### 7.4. Compression Testing

ASTM D695-69 was used as a basis for the compression testing. However, the slenderness ratio of the specimens was approximately one half of that recommended in the ASTM standard (Fig. 3). This enabled a greater number of specimens to be obtained from each slab of resin.

Compressive moduli and 1% proof stresses were calculated after correcting for machine deflection at the test loads. (See also Appendix 4). This correction was obtained simply by performing a compression 'test' without a specimen. The resulting deformation (equivalent chart length) at the required load was subtracted from the indicated deformation for the real test. Corrections were applied to both the normal and the relaxation/recovery techniques (see section 9.2.2.) for measuring compressive modulus. A GRM load cell

was used over the range 0-20000N for tests to ultimate failure. For measuring modulus by the relaxation/recovery method, the 0-2000 N range was used.

## 7.5. Crack Tip and Fracture Surface Observations

### 7.5.1. In-situ Cleavage Tests on a Projection Microscope

In order to study crack tip processes in detail, a small cleavage apparatus (Fig. 5) was designed which enabled miniature DCB specimens to be fractured while being viewed on a Reichert projection microscope. The small specimens were hand-made with the aid of a junior hacksaw and a groove was cut in one face only, allowing the opposite face to be viewed through the microscope. Some specimens were polished or polished and etched prior to testing. A wedge load was applied to the pre-cracked end of the specimen and photographs of the crack tip were taken at various strains. Results of these experiments are included in Chapter 11.

### 7.5.2. Fractography

Optical, scanning-electron and transmission-electron microscopy were all employed at some stage in order to examine fracture surfaces. A Reichert projection microscope was used for optical methods and the Cambridge Instruments Stereoscan and the E.M.6 machines were used for scanning and transmission electron methods respectively.



## CHAPTER 8 - Characterisation of Cured Resin

### 8.1. General Comments

An outline of the methods of characterisation employed is given in this Chapter. Infra red spectroscopy, thermo-mechanical analysis, solvent uptake, density, chemical and ion-beam etching have been used to obtain a broad view of the characterisation problem.

### 8.2. Infra red Spectroscopy

#### 8.2.1. Production of Specimens

Standard potassium bromide discs<sup>(57)</sup> containing particulate epoxy samples were produced in the following manner. The sample was filed off a portion of the bulk material (using a clean needle file) into an agate mortar. Approximately 3mg. of material was required for dispersion in spectroscopic grade KBr. The pre-dried KBr and sample were mixed (without milling) and pressed into thin discs in a conventional die-set. The discs were subsequently stored in a dessicator. It was discovered during the early trials that a satisfactory disc could be made without milling the sample. In fact, it was sometimes observed that a more cloudy disc was produced when the constituents had been subject to comminution by ball milling. The diversity of mechanical properties exhibited by the resin formulations was seen to affect the degree of comminution of the as-filed resin. For this reason, adequate dispersion within the disc was more easily achieved in the more brittle resins.

#### 8.2.2. Spectroscopic Analysis

Two infra-red (I-R) spectrophotometers have been used for this study. Initially, samples were analysed in a Pye-Unicam SP200G (by courtesy of the Institute of Polymer Technology at Loughborough).

The need for quantitative data across the whole range of I-R wavelengths was the deciding factor in favour of an SP200 model (by courtesy of Chemistry Department at Loughborough). The SP200 enabled a single trace to be obtained without interrupting the scan at any stage and it was considered advisable to maintain the analysis conditions as unperturbed as possible. All the I-R data quoted in this thesis was obtained from traces made on the SP200 model. Nominally identical treatment of material during sampling, disc making and storage was ensured.

Quantitative data was obtained by the baseline density method<sup>(58,59)</sup>. A typical I-R trace and the principle of the measurement are shown in Fig. 6.

### 8.3. Thermo-mechanical Analysis

A DuPont 941 thermo-mechanical analyser (TMA), linked to a model 900 thermal analyser, was used in the penetrometer mode. Full slab thickness (.006m) was a convenient sample height and specimens were cut from the cured slabs so that the face which made contact with the penetrometer probe was a cast surface. Heating rate was maintained at  $.33^{\circ}\text{K s}^{-1}$  ( $20^{\circ}\text{C min}^{-1}$ ) (nominal) and a penetrometer load of .010 kg was used in each case. At the transition temperature of the material under test, an inflexion or a sharp change in slope of the penetrometer displacement v. temperature curve is obtained. An example of a penetrometer curve is shown in Fig. 7. It should be pointed out that the transitions referred to are not necessarily glass-transitions.

### 8.4. Solvent Uptake

The solvent uptake or solvent sorption behaviour of the various resin/DDM formulations was investigated by immersion of a small specimen cut from the bulk material, in the appropriate solvent. At selected

times after immersion, the samples were removed from the solvent, dried on tissue and weighed immediately. All solvent uptake tests were performed at room temperature in screw-capped sample bottles, one specimen per bottle. The specimens were usually rectangular in section, having two as-cast faces and weighing approximately .0002 kg before immersion. Several organic solvents were used, including methylene chloride, acetone and tetrahydrofuran.

### 8.5. Density

A limited number of density measurements were made by the Archimedes (immersion in water) method.

### 8.6. Etching Methods

#### 8.6.1. Philosophy of Etching

In view of the paucity of information with regard to etching of polymers for characterisation purposes it is worthwhile considering the philosophy behind the adoption of etching as a characterisation method.

Etching of polymers has not received very much attention from the point of view of characterisation. Methods which have been used include solvent etching,<sup>(60-62)</sup> acid etching,<sup>(63,64)</sup> alkaline hydrolysis<sup>(65)</sup> and gas discharge etching<sup>(66-72)</sup>. It had been considered by the author that a complete picture of mechanical behaviour in relation to morphology could not be obtained without some effort being applied to the determination of physical morphology. The application of etching in metallurgical research is widely known and its value as a characterisation tool cannot be over-emphasised. Polymers, however, provide a particularly daunting prospect. Not least of the problems in epoxy resins is their extremely good chemical resistance. Again, the lack of knowledge of physical morphological characteristics in these materials meant that the investigation had to be quite wide in scope, in order to separate artifacts from reliable, real information.

### 8.6.2. Etching Methods

Two methods of developing an etched surface were used,

- (a) chemical etching in chromic and mixtures of chromic, phosphoric and sulphuric acids.
- (b) ion-beam etching.

The ion-beam method was specially developed for this work and employed apparatus designed and built originally within the Department of Materials Technology by Mr. D. W. Tomkins<sup>(73)</sup> and modified by the author and Tomkins.

Both methods of etching have proved to be of considerable value in the investigation of physical morphology of epoxy resins.

#### 8.6.2.1. Chemical Etching

Chemical etching of epoxy resins has been carried out previously by Cuthrell<sup>(18-20)</sup>. His conclusions were outlined in Chapter 2. The method used in the present study was that of immersing the samples in the etching fluid under a reflux condenser. A variety of mixtures of chromic, phosphoric and sulphuric acids were used, at a number of temperatures between 343 and 373°K. Time of immersion was varied between .120 and 28.8 ks and several different surface pre-treatments were considered.

#### 8.6.2.2. Ion-beam Etching

Ion beam techniques for etching materials have been in use for some considerable time<sup>(74-78)</sup>. However, very little work has been published on the effect of ion bombardment of polymeric solids<sup>(66-72)</sup>.

The apparatus used consisted essentially of a hollow anode glow discharge ion gun from which a beam of ionised gas molecules could be extracted. A canal aperture cathode was used to direct a collimated beam towards the target mount. The material to be bombarded was located on the mount. The conditions of bombardment could be altered by means of the following variables.

- (a) gun potential (0-10kv),
- (b) identity of bombarding ion,
- (c) beam current,
- (d) specimen temperature.

(d) was incorporated as a direct result of the work carried out on the epoxy resin system. Its importance is clarified in Chapter 10.

Fig. 50 shows the general arrangement of the specimen mount in its final form. (See also section 10.5.2.).

PART 3 - Results and Discussion

In the interest of clarity of presentation, the author has tried to establish trends and report observations as briefly and succinctly as possible and to reserve critical analyses until a general discussion in Chapter 12. However, it has been necessary, in some areas, to make critical comments or outline a modification to a test procedure in order to maintain continuity.

CHAPTER 9 - Mechanical and Fracture Properties of Epikote  
828/Epikure DDM

9.1. General Comments

For convenience, the properties considered in this Chapter are dealt with in three sections. The first looks at the effect of resin/crosslink agent ratio on the mechanical and fracture properties, the second examines the effects of changes in cure cycle and the third reports on the testing - rate sensitivity of the system. Examples of the methods of evaluating fracture surface work,  $\gamma$ , and Young's moduli are given in Appendices 3 and 4. At the end of the Chapter some comments, on the results reported in the preceding sections, are made.

9.2. Effect of Resin/DDM Ratio on Fracture and Mechanical Properties

All samples considered in this section were cured for 3.6ks at 373°K and 7.2ks at 373 448°K (see table 1).

9.2.1. Variation of Fracture Surface Work,  $\gamma$ , with DDM Content

The data obtained from TDCB tests is typified by that in tables 2 to 5 and Figs. 8 to 14. It can be seen from the data that the expected behaviour of the TDCB fracture toughness specimen i.e. failure at constant load over a considerable range of crack lengths, is observed and that a linear relationship exists between compliance,  $R$ , and crack length,  $c$ , within the range of interest. (See also Appendix 3). Values of  $\gamma$  were determined using the equations given in section 7.2, by substitution of the appropriate values of load ( $f$ ),  $\frac{dR}{dc}$ , and crack plane width, ( $w$ ) in Irwin-Kies' equation (section 7.2.3.) or by substitution of  $\frac{d(\log f/\delta)}{d(\log c)}$  (= slope 1 in section 7.2.2.) and  $\frac{d(f\delta/w)}{dc}$  (= slope 2 in section 7.2.2.) in Berry's equation. The relevant energy term for Gurney's analysis, as mentioned in section 7.2.4, was obtained by measuring the area under the load-extension graph and using a multiplying factor appropriate to the crosshead displacement

rate, the chart speed used on the Instron testing machine and the full scale load calibration for the test. Worked examples for all three methods are given in Appendix 3.

The load-extension graphs for the specimens considered in tables 2 to 5 are shown in Fig. 8. Comparing these graphs with the idealised forms in Fig. 4 it is evident that the specimens behaved in a linear elastic manner. The use of a trigonometric formula for measuring area under load-extension curves is therefore justified. It was noted that the load-extension graphs for all resin/DDM ratios were linear up to the critical load at each crack jump. In a very small number of cases there was a 'levelling' of the load prior to rapid propagation (see Fig. 8a for an example of this behaviour), but this was most likely associated with slow crack advance rather than a gross yielding or creep phenomenon. This is illustrated by the observation that the extrapolated load-displacement graphs did not show a positive displacement at zero load. Any creep in the specimen arms or near loading points would be expected to give rise to a positive shift (along the displacement axis) of the load-displacement graph. Also, the specimens which did show a levelling-off of load were always those containing 20 parts DDM. They tended to fail by very small unstable increments in crack length or by stable "tearing" or by a combination of both. This tendency to stable crack growth would give rise to a flattening of the load-extension graph near the "average" propagation load.

Tabulation of all the intermediate data derived from primary data generated during fracture testing would require far more space than could be sensibly allocated in this thesis. The examples chosen typify the behaviour of the system, however, and it is hoped that the reader finds them adequate from the illustrative viewpoint.



Appendix 5 includes all primary fracture test data.

A peak in the  $\gamma$  v. DDM curve was evident, the maximum value occurring at about 35 parts DDM (fig. 15). All resins containing greater than 20 parts DDM exhibited unstable crack propagation during testing i.e. the crack increased in length by sudden jumping and subsequent arrest at a new position along the crack line. As mentioned above, material containing 20 parts DDM failed primarily in a stable manner, for crack lengths between approximately .03m and .08m. There was a marked increase in the length of a given crack-jump as  $\gamma$  increased. This led to fewer crack-jumping events per specimen as the toughness increased. The statistical effect of this behaviour is considered in Appendix 3.

The differences in propagation behaviour were seen to markedly affect the variation in  $\gamma$  as a function of DDM content, according to the method of evaluating  $\gamma$ . This is clearly shown in Fig. 15. It is worth noting the similarity between the trends in  $\gamma$  values obtained from the Berry and Irwin-Kies analyses. This should be compared with the relative insensitivity of the Gurney analysis as a function of DDM content. Appendix 3 contains further information concerning the three methods of evaluating  $\gamma$ .

Summarising the fracture tests showed that the resins containing different proportions of DDM were significantly different in fracture surface work terms. It was therefore possible that some morphological change was occurring as DDM content was varied. The efforts to define the nature of such changes are described in Chapter 10.

NOTE: Because the Irwin-Kies analysis involves only one graph and is able to distinguish between resins on a fracture surface work basis, subsequently quoted values of  $\gamma$  should be recognised as values obtained from Irwin-Kies' equation).

9.2.2. Tensile and Compressive Young's Moduli,  $E_T$  and  $E_C$  and General Tensile Behaviour

$E_T$  and  $E_C$  were measured in two ways:

- (a) by uninterrupted, constant crosshead speed testing.
- (b) by employing a cyclic, stress relaxation/recovery technique where the crosshead is stopped (see points  $R_1$  and  $R_2$  in Figs. 16 and 17) at the maximum and minimum loads in a series of crosshead displacements. The two extremes of load are made to approach each other until the relaxation (from the maxima) and the recovery (from the minima) balance each other. The modulus test proper then proceeds as normal, within the limited load range dictated by the final cycle. This method, it is claimed,<sup>(79)</sup> gives results which are more representative of the elastic component of behaviour in visco-elastic materials.

Typical, worked examples of evaluating the moduli are given in Appendix 4. The appropriate load extension curves relating to these particular specimens are shown in Figs. 16 and 17. These curves also exemplify the behaviour of the different resin formulations as described in section 9.2.5. and later in this section.

Whichever test method was used, the general trend in moduli was the same. Low DDM content material (20 parts DDM) always had a higher value of  $E$  than all other formulations and the general form of the  $E$  v. DDM curve indicated that material of near-stoichiometric (i.e. intermediate) composition possessed the lowest modulus. Intermediate compositions were also the most visco-elastic in nature. This is most clearly evident, for the tensile mode, if the load-extension curves shown in Fig. 16 are compared. Relaxation at points  $R_1$  is greatest for 27 parts DDM. If the compressive tests are compared, again for low and intermediate resin compositions (fig. 17), a similar conclusion is reached. There is also a notable difference in yield behaviour, which is more fully considered in sections 9.2.4. and 9.2.5. A shallow increase in  $E$  was noted for

resins in the range 27-40 parts DDM. These modulus variations are shown in Figs. 18 and 19.

The occurrence of the highest modulus at 20 parts DDM was not expected since it had been assumed that increased DDM content was synonymous with increased cross-link density and hence, increased resistance to elastic deformation. It is worth noting that E values from relaxation/recovery tests exceeded those obtained from uninterrupted tests. It should be borne in mind, however, that different load ranges (in the case of  $E_C$ ) were used for the two methods.

Table 6 summarises the tensile and some compressive characteristics as a function of DDM content. Note that two of the 20 parts DDM specimens fractured prior to any load-drop or deviation from linearity, whereas all other tensile specimens exhibited deviation from linearity. Also, a maximum load followed by a load-drop, was evident only at 20, 35 and 40 parts DDM. Typical tensile load extension curves are shown in Fig. 20. (Since no extensometer was used for these tensile tests no scale has been included in Fig. 20. The curves are, however useful for comparison).

### 9.2.3. Plane Strain Fracture Toughness, $K_{IC}$

Values of  $K_{IC}$ , computed from the data on  $\gamma$  (Irwin-Kies) and  $E_T$  are plotted v. DDM content in Fig. 21. (The factor  $1-\nu^2$ ) in the equation relating K, E and G has been ignored for the purposes of the calculation (see section 3.1.) because little error is introduced, assuming  $\nu = .3$  for thermosets). The peak in  $\gamma$  at approximately 35 parts DDM is retained in the  $K_{IC}$  v. DDM trend, even though  $E_T$  is less for resins containing  $>20$  parts DDM.

#### 9.2.4. Yield Stress and 1% Proof Stress (Compressive)

Values of yield stress and 1% proof stress (see Appendices 4 and 5) are shown in Fig. 22. Not all of the resins displayed a characteristic yield point in compression which was associated with a drop in load. The nominal stoichiometric composition (27 parts DDM) did not show any yield drop in compression. It was found that 1% proof stress was a more sensitive function of stoichiometry than yield stress was.

#### 9.2.5. Other Deformation Characteristics

In order to complete the picture of compressive deformation v. DDM content some 'unconventional' parameters were evaluated. These are indicated in Fig. 17 (points R1) and Fig. 23. Firstly, the 'compressibility' (Fig. 23) of the standard .006 x .006 x .012m sample after the yield region (or point of inflexion on the load-extension curve) was measured. This parameter is effectively the post-yield compressive strain that can be tolerated by the sample prior to ultimate failure. It is expressed, in Fig. 24, as mm of recorder chart. The results indicated a minimum value of post-yield compressibility at stoichiometric composition. Secondly, the actual value of the drop in load at yield was measured. The difference between the 20 parts DDM material and the rest was quite remarkable. (See also section 9.2.4.). The yield characteristic of the low DDM samples was quite marked (Fig. 23). The resins containing 27-40 parts DDM, while they showed a greater propensity to yield sharply at higher DDM contents, did not exhibit a sudden onset of gross plastic deformation (Fig. 25).

Thirdly, during the relaxation/recovery method of measuring compressive modulus, it was noted that the near stoichiometric resins behaved in a more visco-elastic manner than those at the two extremes of DDM content. This behaviour is illustrated in Fig. 24

as the relaxation (in Newtons), from an initial compressive load of 1800N, which occurred in  $\sim 12$ s. (This period of time was chosen for convenience during the modulus test, rather than for specific stress relaxation studies). Load extension curves for the resins of extreme DDM contents were more linear than those of intermediate composition also.

Finally, the occurrence of shear bands at approximately  $45^\circ$  to the compression axis was observed in some specimens. The bands were usually associated with stress raisers such as discontinuities along a vertical edge of the sample. It was possible to generate quite sharply defined bands by compressing a specimen with a hole drilled through it. All compositions of resin behaved in this way, although there was a tendency for intermediate compositions to acquire less well defined shear boundaries. The 'barrelling' tendency, which is a common feature in compression testing, was also less evident for intermediate compositions.

### 9.3. Effect of Variations in Cure Cycle

#### 9.3.1. Extended Cure Time at $448^\circ\text{K}$

Material for this investigation was of stoichiometric composition, cured 3.6ks at  $373^\circ\text{K}$  then 7.2ks  $373\text{--}448^\circ\text{K}$  followed by a maximum of 5.76ks extra cure at  $448^\circ\text{K}$ . The reason for carrying out extended cure at  $448^\circ\text{K}$  was the uncertainty (at the time) of the extent of reaction in stoichiometric material cured for the nominal 3.6ks at  $373^\circ\text{K}$  plus 7.2ks at  $373\text{--}448^\circ\text{K}$ .

Tensile modulus,  $K_{IC}$ , and transition temperatures (by TMA - see Chapter 10) showed no significant variation with extended cure time at  $448^\circ\text{K}$  within the range 0-5.76ks (Table 7). Based on the statistical evidence in Appendix 3, there was a slight upward trend in  $\gamma$ . However, this trend was not well established in comparison with the changes induced by DDM content variation. The  $\gamma$  values have been included in Fig. 26.

### 9.3.2. Effect of Varying Gel Temperature

For this series of casts, the pre-heat temperature of the steel mould was held at 323, 333 or 348°K prior to casting. Three compositions were investigated: 20, 27 and 40 parts DDM. After 3.6ks at 323, 333 or 348°K, the customary 7.2ks, heating within the appropriate temperature range to a maximum of 448°K was carried out. The term 'gel temperature' therefore refers to the initial stage of the cure cycle.

The variation in  $\gamma$  with gel temperature was rather larger than the variation with extended cure time at 448°K, but the variations taken as a whole were not very great (Fig. 26). Again, based on the evidence presented in Appendix 3, the variation of  $\gamma$  with gel temperature was significant. Other mechanical properties investigated did not correlate with changes in  $\gamma$ . Compressibility, relaxation characteristics, compressive and tensile moduli were unable to differentiate between resins gelled at the four temperatures in a manner which was consistent with variations in fracture surface work, (Figs. 27 and 28). Yield drop in compression (Fig. 27b) was the only parameter which showed some correlation with  $\gamma$  and this was only observed at 20 parts DDM.

### 9.4. Effect of Varying Testing Speed

Both  $\gamma$  and  $K_{IC}$  were reduced in value by testing at faster crosshead rates, despite an increase in  $E_T$  (Figs. 29 and 30). Fig. 31 indicates that this is true of all compositions between 20 and 40 parts DDM although there is no clear connection between the % change in  $\gamma$  with crosshead speed and other mechanical characteristics.

The discrepancy between values of  $\gamma$  obtained by Gurney's method and those obtained by Irwin-Kies analysis was smaller at higher crosshead speeds, (Fig. 29). Also, the crack jumps occurring

at higher testing rates were smaller than at low rates.

The tensile strength of the stoichiometric resin tended to increase at higher testing rates, (Fig. 32). There was an accompanying tendency for the scatter in tensile strength values to diminish at higher rates, although this was not the case for  $\gamma$  or  $E_T$ .

#### 9.5. Comments on Mechanical Behaviour

It is evident from the results presented in this Chapter that changes in resin stoichiometry have a marked effect on the mechanical and fracture behaviour of Epikote 828/Epikure DDM. Changes in initial cure temperature and post cure time at 448°K (175°C) do not appear to drastically affect mechanical and fracture properties.

As one might expect for a visco-elastic material, the rate of testing does affect the value of a particular property. The most interesting result, however, is the observation that resin containing less than the nominal stoichiometric amount of DDM behaves in a less visco-elastic manner than other resin compositions. The low DDM material also has a higher Young's modulus in tension and compression. On the basis of an assumption that an increase in DDM content results in a more highly cross-linked material, this behaviour is difficult to understand.

The following Chapter describes experiments designed to determine the reasons for this apparently anomalous behaviour, as part of the general investigation of epoxy resin morphology.

## CHAPTER 10 - Morphological Characterisation

### 10.1. General Comments

In this Chapter the results of some conventional characterisation studies will be described, along with the results of etching investigations. The effects of DDM content and changes in cure cycle are not covered separately because this would not enhance the presentation of the results. Unless otherwise stated, resins were cured 3.6ks at 373°K plus 7.2ks at 373-448°K.

### 10.2. Thermo-mechanical Analysis

The range of transition temperatures determined as a function of DDM content is shown in Fig. 33. The presence of at least two distinct transitions in the 353°K-443°K (80-170°C) range at low and high DDM contents but only one at intermediate composition, is one point to be noted. The other observation is that the stoichiometric resin exhibited a transition at higher temperatures than the rest of the formulations.

The effect of cure cycle on thermo-mechanical behaviour has not been reliably established because of difficulties with the apparatus at the time of testing (and of writing). However, the TMA evidence available suggests that low and high DDM content materials are more significantly affected by changes in gel temperature than stoichiometric resins are, (Fig. 34). It must be emphasised that at the time of writing the reliability of this set of results is not established. Consequently, they play no part in later discussion and, if substantiated, are not likely to alter any major conclusions drawn.

### 10.3. Solvent Uptake and Density

Fig. 35 summarises the general behaviour of three of the resin formulations when immersed in three different organic solvents. It can be seen that the stoichiometric composition is least affected by solvents, an indication that the material is



chemically most fully cured at that composition. It is worth mentioning that for some applications a material with high solvent resistance is desirable. However, that material does not necessarily possess optimum overall properties.

The behaviour of the low DDM content material, compared to the others, is illustrated in Fig. 36. The rate of uptake is considerably higher in the low DDM content resin.

The effect of varying gel temperature on solvent uptake characteristics of two resins (20 and 40 parts DDM) is shown in Fig. 37. There is no apparent correlation between rate of uptake and gel temperature.

Density variation as a function of DDM content is shown in Fig. 38. The scatter is very large, but there is a tendency for intermediate compositions to be less dense than the others.

#### 10.4. Infra-red Spectroscopy

The absorption bands of interest (1,2) in this system are at:

- (a)  $918\text{cm}^{-1}$ , attributed to the epoxy ring,
- (b)  $1110\text{cm}^{-1}$ , ether linkages formed during cure,
- (c)  $810\text{cm}^{-1}$ , associated with para-substituted- $\text{CH}_2$  on the Epikote 282 benzene ring,
- (d)  $830\text{cm}^{-1}$ , associated with the  $\text{-NH}_2$  group in DDM,
- (e)  $1040\text{cm}^{-1}$ , alkyl-aryl ether linkages present in cured Epikote 828.
- (f)  $3300\text{-}3600\text{cm}^{-1}$ , associated with  $\text{-OH}$  groups.

The band at  $1040\text{cm}^{-1}$  was used as an internal reference so that the various absorption levels in different specimens could be directly compared. (The alkyl-aryl ether does not become involved in the cross-linking reactions and can therefore act as a baseline or comparator for absorption at other frequencies).

Figs. 39-41 summarise the I-R data for material cured 3.6ks at  $373^\circ\text{K}$  and 7.2ks at  $448^\circ\text{K}$ . The data in Fig. 39 provides

an estimate of the likely error in the method. The points plotted on the A830/A810 (absorption ratio) scale represent relative amounts of resin and DDM, as measured from I-R traces, at known ratios of resin/DDM. The second graph in Fig. 38 represents the residual epoxy content of the cured material. A steady increase in conversion of epoxy to other species, with increasing DDM content, is indicated.

Fig. 40 shows the variation in the number of ether linkages formed on curing, relative to the number of alkyl-aryl ether bridges present in the sample. An increase in ether links is observed, which starts to tail-off at about 35 parts DDM.

Finally, Fig. 41 shows how the relative absorbances at  $3530\text{cm}^{-1}$  and  $1110\text{cm}^{-1}$  varied as a function of stoichiometry. The whole range of values has been shown in Fig. 41 to illustrate the relatively high scatter in the results. There is, however, a recognisable trend in that the resins containing 30-35 parts DDM have a greater-OH/ether ratio than the other compositions. There also appears to be a sharp change in this ratio near the stoichiometric composition.

The infra red method was unable to differentiate between resins which had received different heat treatments by way of varying gel temperature.

#### 10.5. Chemical and Ion-beam Etching

##### 10.5.1. Chemical Etching

Essentially two kinds of result were obtained by chemical etching of all compositions. These are shown in Figs. 42 and 43. It was found to be experimentally difficult to obtain an evenly attacked surface which revealed features like those in Fig. 43. In some cases a film of material obscured the feature and in others, colours provided enhancement of contrast. Attempts to show that the features in Fig. 43 might be due to the contraction

of a swollen surface layer proved to be inconclusive. Slow cooling, water quenching and liquid nitrogen quenching of the etched article immediately after removal from the etching fluid did not produce consistent variation in the size of the feature. Stereoscan observation of the etched surfaces (e.g. Fig. 44) revealed the presence of craters and hillocks but did not serve (on its own) to prove the validity of the structures. A further investigation was required before the validity of the result shown in Fig. 42 could be established.

This comprised of etching some of the material that had been used for mechanical (compression) testing. It was reasonable to argue that a structural entity would respond to gross mechanical deformation. Therefore, material which had been compressed beyond the yield point was etched in chromic acid. The result is shown in Fig. 45. It is obvious from Fig. 45 that there is a feature which responds to mechanical deformation. The distortion was not evident in specimens strained to below the yield point or in regions remote from the strain bands in permanently deformed specimens. (Shear band contour is responsible for the focusing problem in Fig. 45).

Similar evidence of deformation is illustrated in Fig. 46, which is an etched region of rapid crack propagation on a TDCB fracture surface. The influence of the groove-cutting wheel can be seen from the degree of distortion of features near the edge of the specimen. Proof that the distortion was not produced during the fast-fracture process is provided by the following observation. The orientation of the distorted features correlated with the direction of rotation of the cutter. The method of slot cutting would result in oriented features on both sides of the fracture surface, in

opposing senses. This was seen to be the case. Thus, the orientation was not created by a fast-fracture event.

Further evidence for the existence of structural features in the resins is given in section 10.5.2.

The effect of surface pre-treatment on the characteristics of chemically etched surfaces was investigated by etching as cast material, samples polished to different surface finishes and fracture surfaces. The general appearance of the etched surface did not change, regardless of the preparation technique. There was, however, additional evidence on the material's response to mechanical treatment in that scratch marks on polished surfaces were associated with deformed etch-features. Fig. 47 shows an example of this. As-cast surfaces were less amenable to etching, possibly because of contamination by release agent, although there is no evidence of such contamination from other results.

With regard to the variation of etching characteristics as a function of DDM content, the general behaviour was such that material with high or low DDM contents etched faster than intermediate formulations. This is in accordance with the chemical behaviour of the system in terms of solvent uptake and TMA results. Any dimensional variations in etched features as a function of DDM content was not evident. (Feature dimensions were  $\sim 5-15 \mu\text{m}$ ). A simple line-intercept count using photomicrographs was unable to distinguish between the resins, although there was a slight variation with surface preparation technique and etching conditions. The statistical significance of these counts has not been assessed, but there is a case for further investigation of etch feature sizes. A major problem is likely to be the discrimination between adjacent features. As Fig. 47 indicates, the degree of overlap or inter-dependence of features could be troublesome (indeed it was so!) in

any quantitative assessment. However, some help may be forthcoming if the ion-beam technique described in the following section is utilised in parallel with chemical methods.

#### 10.5.2. Ion Beam Etching

In the initial experiments, the operating conditions for argon ions were maintained at 7kv gun potential, 3mA gun current,  $4 \times 10^{-5} \text{ mA m}^{-2}$  beam current, 300s bombardment time and  $1.06 \text{ Nm}^{-2}$  chamber pressure.

Bombardment of a bulk sample of 27 parts DDM polished to a  $1 \mu\text{m}$  diamond finish, revealed a severely wrinkled surface together with evidence of residual polishing damage even at the bottom of the eroded zone. The experiment was repeated using fracture surfaces of bulk material as the target. Surface wrinkling of the kind shown in Fig. 48, and some evidence of charring were produced, to varying degrees, at all crosslink-agent concentrations. Repeating the bombardment experiments at lower gun potential and for shorter times (4.5kv and .30s) produced ion cleaning of the surface without the development of surface features. The use of helium instead of argon produced essentially similar results, except that the degree of surface erosion was lower in the helium bombarded specimens.

The evidence of charring and wrinkling indicated that high specimen surface temperatures (possibly  $600^{\circ}\text{K}$  or above) were being achieved. A separate experiment was conducted in which a bulk specimen was wound with nichrome wire and the wire flash-heated, to red-heat, in vacuo. The result was a surface wrinkling effect (Fig. 49) very similar, though of different dimension, to the features seen in Fig. 48.

The specimen mount was modified to allow cooling with liquid nitrogen. Bombardment was then carried out on an epoxy resin cast directly onto the cold finger. The resultant surface,

although free from wrinkles and charring, was unsuitable for examination due to the presence of a network of small cracks. Cracks were produced in all epoxy casts (at all DDM contents) upon introduction of liquid nitrogen to the cold finger. In some cases, the resin was seen to peel off the mount.

To combat this problem, a mixture of carbon tetrachloride, chloroform and solid  $\text{CO}_2$  was substituted for liquid nitrogen and the specimens were cast onto small aluminium discs which could be held against the cold finger by means of a screw cap (Fig. 50). Using this arrangement, reproducible results were obtained, by careful attention to cooling and bombardment times, with samples having resin/DDM ratios between 100/20 and 100/40.

The results of these experiments are typified by Figs. 51 and 52. They represent areas immediately adjacent to the central eroded zone. It appears from these micrographs that either a surface layer is present or that excessive bombardment has occurred in some areas. However, the most interesting result is that bombardment has produced regularly structured erosion zones (see Fig. 52). The terrace-like features in Fig. 52 were not observed in the four samples of resin containing only 20 parts DDM, except in one area, where the contour of the specimen surface would have presented a shallow angle of incidence to the beam. Ten samples containing 27 parts DDM or more, showed evidence of terracing after cryogenic bombardment.

Material from the same castings as the mechanical test specimens was also bombarded using the cold finger arrangement. For example, Fig. 53 shows the effect of bombarding a thin polished section ( $\sim 1$  mm thick) of 27 parts DDM material. There is a similarity between the features of Figs. 52 and 53. Again, an as cast

surface (Fig. 54) which was taken from the meniscus at the top of a slab shows discreet areas of attack after ion bombardment.

The influence of mechanical deformation during surface preparation was also seen in some ion-bombarded specimens. Some areas of Fig. 53 indicate linear arrays similar to those seen on scratched, chemically etched material.

The consistency of the ion etching process for revealing features in the thin sections from bulk material was not as good as one might desire. Sometimes, quite heavy erosion was achieved with short bombardment times and occasionally a wrinkled product was obtained. In the latter cases it was possible to attribute the wrinkles to poor thermal contact with the cold finger. The peripheral clamping effect may have created an arched specimen, thus reducing the effective cooling contact area.

However, the balance of available evidence is in support of the situation described above and illustrated in Figs. 51 and 52.

A most striking observation from this work is the similarity between the chemically-etched material depicted in Fig. 47 and that shown in Fig. 51.

The  $\text{CrO}_3/\text{H}_2\text{O}$  etch produces features (at all resin compositions) which are very like those produced by a 'light' ion etch. The terracing and sub-structural features obtained by ion bombardment have not yet been fully investigated. The author feels that it is in this area that more meaningful information concerning the morphological characteristics of the resins may be forthcoming.

Having established, by two independent paths, that there is a morphological entity of interest, it was necessary to consider how this entity related to the fracture process. The following Chapter provides some evidence of a link between the deformation of the features described above and crack tip processes.

CHAPTER 11 - Crack Tip and Fracture Surface Characteristics

11.1 In-situ Cleavage Tests on the Projection Microscope  
(See also section 7.5.1.)

The main observation from this work was that considerable blunting occurred at the crack tip in resins of 27 to 40 parts DDM. The 20 parts DDM material would not accommodate significant strain at the crack tip prior to sudden propagation. (The discontinuous manner in which the crack propagated in 20 parts DDM resin is a direct result of changes in strain rate and specimen geometry, compared with macroscopic (20 parts DDM) TDCB specimens).

The difference between the resins was also manifested in the shape of the zone of deformation near the crack tip. The tougher resins exhibited surface zones of deformation which were quite extensive in the direction perpendicular to the plane of the crack (Fig. 55). The appearance of a 'tough-tip' was that of an extensively dimpled surface, combined with a blunt tip. The 20 parts DDM resin, however, was less extensively deformed close to the tip, although a region of deformation, extending some distance towards the open end of the crack, could be seen near the arrest locations (Fig. 56). This region was confined to a narrow width in the direction perpendicular to the plane of the crack, and has some interesting features associated with it which are described in section 11.2. A narrow fish-tail geometry was seen ahead of the arrest point in 20 parts DDM material and no crack blunting was observed prior to rapid propagation.

Etched specimens provided some interesting observations of the movement of material around the crack tip prior to sudden propagation. Fig. 57 indicates how the crack can progress during slow growth in a tough resin. This particular specimen's surface



had not responded well to the chromic acid etch. (It was an as-cast surface, see section 10.5.1.). However, deformation bands, in the vicinity of the crack tip were observed. It is worth noting that the material bridging the two crack faces in Fig. 56 was quite visco-elastic. It was possible to see the slow movement of the flap of material just after its detachment from one of the crack faces. A similar effect was noted when the experiment was done on an etched 20 parts DDM specimen. Fig. 58 indicates multiple 'bridging' in the region of an arrest location in this material. In this case, the partially detached flaps were formed on deceleration of the crack.

The effect which etching may have had on the response of the surface regions is difficult to estimate. However, the behaviour of the etched material near crack tips is reminiscent of craze phenomena in thermoplastics. It may be that the hostile environment to which these specimens were subjected degrades the crosslinked resin to the point where it behaves more like a thermoplastic, when stressed after etching.

The response of a polished and pre-cracked cleavage specimen to etching in chromic acid is shown in Fig. 59. In this instance, the material has etched successfully and has provided evidence of the distortion of structure around the crack tip in the same manner as the material in compression tests has.

## 11.2. Optical and Electron Fractography

Examination of both large and small cleavage test pieces on the projection microscope and in the S.E.M. provided information on the behaviour of the crack front. The essential characteristics of all fracture surfaces studied are shown in Figs. 60-62. In Fig. 60 it is seen that the region which is crescent-shaped has a considerably rougher surface than the majority of the fracture surface.

The 20 parts DDM specimens did not have these very rough zones. Arrest locations were, however, visible in some specimens of low DDM content (Fig. 62), particularly the small DCB samples, where unstable propagation was more frequent.

The size of the rough zones in the TDCB specimens was found to be a function of DDM content and in fact correlated very well with  $\gamma$  and  $K_{IC}$  values (Figs. 63 and 67). The rough zone size (and its variability) also decreased as testing speed increased, as the data in Fig. 63 shows. The existence of the crescent-shaped rough zone leads to some ambiguity about the value of crack length that should be adopted in calculating fracture parameters. However, the size of the zone relative to the required accuracy of crack-length measurement meant that any ambiguity in crack-length determination was masked by the influence of DDM content or testing rate. This point is further considered in Chapter 12, in relation to the measurement of fracture toughness by compliance methods (see section 12.2.).

Other points of interest on the fracture surfaces were:

- (a) the multiplicity of fracture planes within the rough zone.
- (b) the existence of curved features, usually emanating from the rough zone (layer lines) and linear features which occurred at random locations within the smooth area of propagation. These were sometimes associated with air bubbles or inclusions.
- (c) the sharp angular displacement between rough and smooth regions on the advancing side of the rough zone.
- (d) the 'brushmarks'<sup>(80)</sup> which were present throughout the fracture surfaces at all DDM contents. (See Fig. 64 background markings).

One particularly interesting observation in 20 parts DDM material was the triangular feature illustrated in Fig. 62. These were rarely seen outside the region near the arrest location. In fact, the zone of deformation shown in Fig. 56 corresponded to the area containing the triangular features. Stereoscan observation (Fig. 64) of these features showed that they represented

a minor bifurcation of the crack plane. Occasionally, a pore or inclusion site was associated with them, as seen in Fig. 65.

Transmission electron micrographs taken of single stage (carbon) and two-stage (acetate-carbon) replicas of fracture surfaces were certainly no more informative than stereoscan observations. In fact the production of a replica from the smoother areas was a difficult process and it was considered an uneconomic exercise in terms of return for effort and time. It was therefore decided not to proceed with an extensive study using transmission techniques. Fig. 66 shows the transmission electron micrograph equivalent of Fig. 64.

## CHAPTER 12 - Discussion

### 12.1.. General Comments

The main aim of this Chapter is to demonstrate relationships between the mechanical and fracture data already presented, crack tip behaviour and the morphological characterisation of the resin. However, it is necessary to comment in some detail on the results of the fracture tests before any correlations are established between properties and morphology. It is essential to clarify the meaning of the fracture parameter measured in order to understand its relationship to the other parts of his work.

### 12.2. Comparison of Fracture Surface Work, $\gamma$ , Values obtained by Irwin-Kies', Berry's and Gurney's Analyses

In principle, the three analyses should give the same result, provided that the crack propagates at constant speed.  $\gamma$  in this context is therefore a propagation value. It is well established<sup>(81-83)</sup> that  $\gamma$  can vary with crack speed. For materials which fail in a stable manner during a TDCB test, it is to be expected that all three analyses would yield the same value of  $\gamma$  because crack speed does not vary in such circumstances. This was confirmed for 20 parts DDM, where propagation was primarily continuous. (Unstable behaviour was seen at very short crack lengths. The stability of the system at very short crack lengths is likely to be different from that at intermediate crack lengths since the geometry of the specimen deviates from the ideal. The effective loading rate will then be significantly different).

If the stability conditions for the TDCB test are not satisfied by the material at a given rate,<sup>(81)</sup> unstable cracking will occur. Therefore, the material will have been subject to varying crack speeds during a crack jump. The area-under-curve

method of Gurney will then provide an undefined mean value of  $\gamma$ . The range of crack speeds during unstable propagation will influence the weighting of this mean value. The methods employing crack initiation loads, however, would be expected to agree under crack jumping situations. Crack jumping has been observed previously during DCB tests on epoxy resins<sup>(53,54,84)</sup>, polyurethanes<sup>(85)</sup> and poly(vinylchloride)<sup>(43)</sup> and, as mentioned previously, is related to the specimen geometry, the type of testing machine employed, the testing speed, and the identity of the material. The possibility that crack tunnelling (the crack leading in the centre of the crack plane, see section 11.2.) results in higher  $\gamma$  values by compliance methods is not considered important for TDCB specimens. This is because of the linear relationship between compliance and crack-length. It is not possible to over-estimate  $dR/dC$  for TDCB specimens merely by under-estimating crack length. It is possible to do so when using parallel DCB specimens. The reason is that the parallel specimen exhibits a non-linear compliance v. crack length relationship and a value of  $dR/dC$  must be determined at a particular crack length and load for evaluating  $\gamma$  by Irwin-Kies' equation. If crack lengths are measured during a stable test, variations in tunnelling behaviour may give rise to under-estimates of crack length. Gurney's method, however, uses differences in crack length for area measurement when calculating  $\gamma$ . Therefore, provided a near equilibrium tunnelling situation has developed in stable cracking, a more realistic value of  $\gamma$  may be obtained if Gurney's method is employed.

The fracture data for Epikote 828/Epikure DDM systems are in accordance with expectations as far as the methods of evaluation of  $\gamma$  is concerned. It is reasonable that the two analytical methods (Berry's and Irwin-Kies') should agree more closely because they

employ data from equivalent situations. The averaging caused by application of Gurney's method, and the fact that the 'area' figure is below the 'initiation' figures at all compositions means that care must be taken when interpreting area-under-curve results or when comparing them with  $\gamma$  values for other materials whose rate sensitivity of  $\gamma$  may be grossly different. Mai and Atkins have recently pointed out<sup>(81)</sup> that it is possible to stabilise a test situation with the aid of external stabilisers such as adhesive tape or the use of composite test pieces. It is therefore possible to employ Gurney's method for materials which normally fail in an unstable manner in TDCB tests, provided the specimen is modified to induce stability. With regard to the work reported here, the unmodified TDCB specimen has proved to be quite satisfactory. In fact, its very susceptibility to unstable cracking was instrumental in suggesting some of the studies of mechanical behaviour reported in earlier Chapters. Knowing that  $\gamma$  can vary with crack speed (an immediate implication from unstable cracking in TDCB tests) and knowing also that the resin's visco-elastic characteristics can be altered, the interpretation of fracture toughness variations is facilitated if one has knowledge of these visco-elastic characteristics and how they relate to crack tip behaviour.

From the point of view of the usefulness of the fracture surface work parameter, it is true that in an engineering sense there is still much debate about how  $\gamma$  or  $K_{IC}$  should be evaluated or applied, especially for very tough materials where attainment of plane strain conditions demands very thick specimens. It is evident from this work, however, that  $\gamma$  for Epikote 828/DDM epoxies is a sensitive parameter, especially with regard to stoichiometric variations. It is to this aspect that our attention is now turned.

### 12.3. The Variation of Properties as a Function of DDM Content

#### 12.3.1.

A striking feature is the variation in  $\gamma$  and  $K_{IC}$  with DDM content. An approximate five-fold increase in  $\gamma$  (at  $.017\text{mms}^{-1}$  testing speed) is obtained by changing DDM content from 20 to 35 parts. At this testing speed, the  $\gamma$  v. DDM curve possesses a pronounced peak, but there is no discontinuity. Thus, it is tempting to suggest that an increase in DDM content up to stoichiometric amount (fully cured) would increase the cross-link density and toughen the resin. An excess of DDM might result in crack tip plasticisation so that the material could become even tougher. A gross excess of DDM might induce such plasticisation that the material would become less fracture-tough again. Hence, a peak in toughness would be expected. The crack tip plasticisation effect has been illustrated in Figs. 55 and 59. But what mechanism can be invoked for the accommodation of DDM in such excess quantities? How does general mechanical behaviour fit the simple view of toughening outlined above?

Unfortunately, the evidence from mechanical tests other than fracture toughness tests does not support such a simple view of what is undoubtedly a microscopically complex process. For example, the variations of Young's moduli  $E_C$  and  $E_T$ , are in direct conflict with what one would expect by assuming that increasing DDM content results in an increased crosslink density. The visco-elastic behaviour of the resins, exemplified by stress-relaxation and non-linearity (Fig. 24 and Table 6), also conflicts with this simple assumption. On the other hand, by consideration of the variation of thermo-mechanical transitions and solvent uptake with

DDM content, it is possible to conclude that the stoichiometric resin is the most highly cross-linked. The existence of at least two thermo-mechanical transitions for compositions on either side of stoichiometric could be attributed to

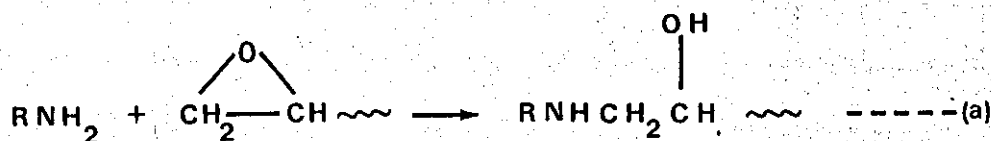
- (a) uncured resin and cured resin in low DDM material,
- (b) unreacted DDM and cured resin in high DDM material.

This is likely to be a grossly over-simplified explanation. However, it is the fact that the transitions are highest for intermediate compositions which implies a high degree of cross-linking at these DDM contents. The lowest rate of solvent uptake at stoichiometric composition (regardless of solvent identity) also implies that it is a highly cross-linked material or at least highly "converted" chemically.

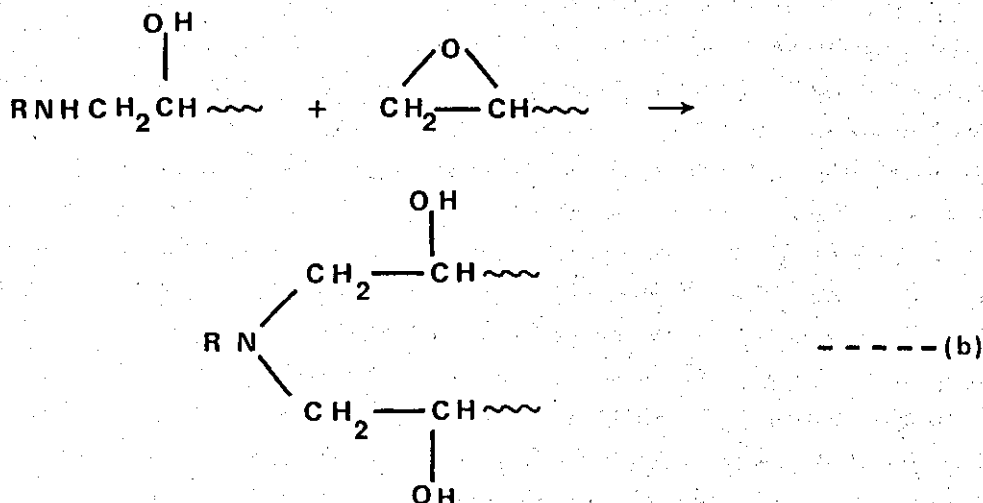
In view of these apparent discrepancies between mechanical properties and conventional characterisation parameters, it is fruitful to consider the chemical aspects of curing and to try to establish the meaning of the term 'cross-link'.

### 12.3.2. The Mechanism of Epoxy - Amine Reactions

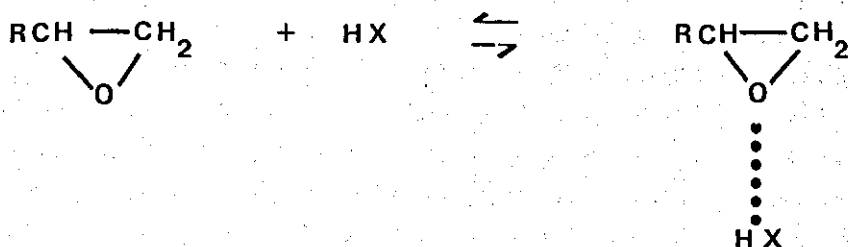
This topic has been investigated by a number of workers<sup>(86-92)</sup>. The following reaction sequences are usually suggested<sup>(1,2)</sup> when an epoxy resin is cured with a primary amine

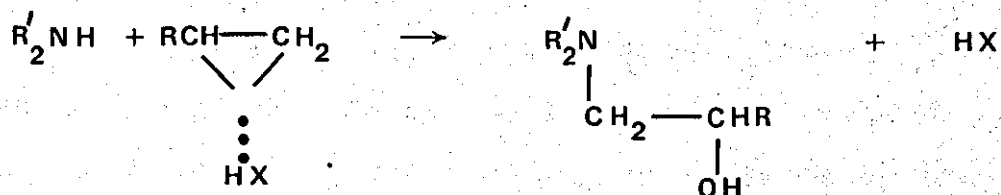






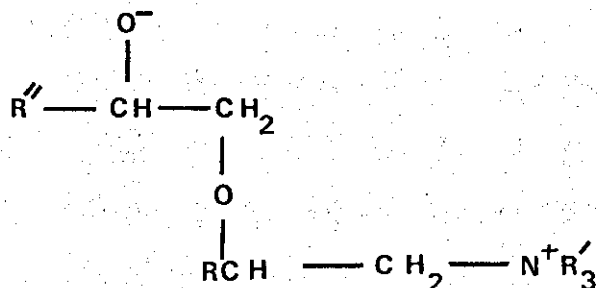
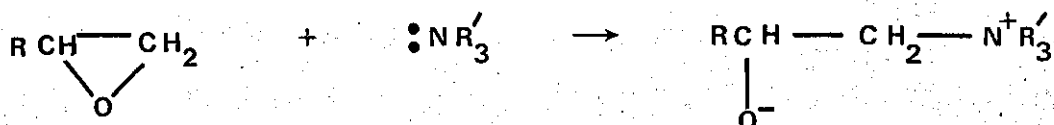
The tertiary amine so produced may be capable of catalytic homopolymerisation of the epoxy groups. However, its effectiveness is dependent upon steric factors and environmental conditions<sup>(91)</sup>. In fact the reaction between epoxide groups, catalysed by tertiary amine is also dependent upon the - OH concentration<sup>(91)</sup>. The influence of hydroxyl groups (present as constituents of curing agents, modifiers or the basic epoxy molecule as well as those formed during cure) is considered to be very important<sup>(1,2,92)</sup>. Kinetic studies by Smith<sup>(87)</sup> and calorimetric investigations by Horie et al<sup>(88)</sup> support the idea that a termolecular mechanism can explain the reaction kinetics. The reaction scheme proposed by Smith is





where HX is a hydrogen bond donor. Thus, the presence of -OH groups in the reaction system could have a profound effect on reaction kinetics. In fact, hydroxyl groups present on the epoxy molecule have been cited as catalytic agents by Whiting and Cline<sup>(93)</sup>.

The latter workers have also pointed out the difference between Smith's reaction scheme and that proposed earlier by Narracott<sup>(86)</sup> and Newey<sup>(92)</sup>, in terms of the linearity of the product. The Narracott scheme, which applied to tertiary amine cure is:



It should be noted that the product contains the C-O-C ether linkage whereas the product of the Smith scheme contains the -OH group.

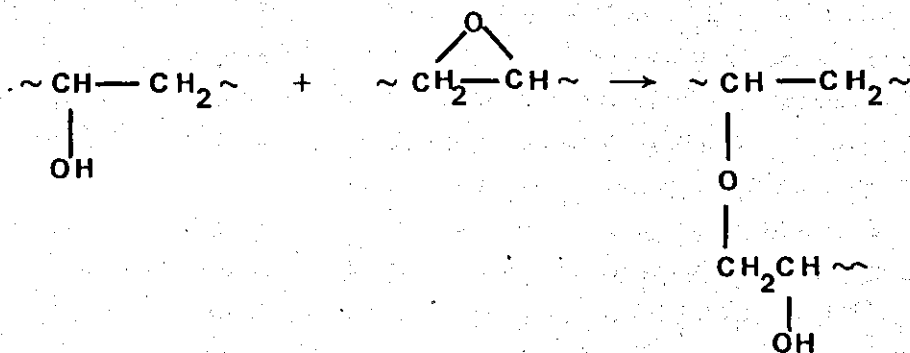
Summarising, the suggestion made by Whiting and Cline is that two competing reaction schemes will influence the linearity of the molecular species formed during cure. This, in turn, should affect the mechanical properties of the product. The fact that

tertiary amine and - OH groups are formed during cure may also affect the result.

Whiting and Cline's investigation of Epon 828 cured with N, N'-diethyl-1,3-propanediamine (DEAPA) showed that the relative amounts of - OH and C-O-C groups in the product varied with DEAPA content. The variation was such that the - OH/C-O-C ratio (measured by infra-red spectroscopy) was an almost linearly increasing function of DEAPA content over the range 10-50% of stoichiometric amount of DEAPA. It was suggested that since Epon 828 and DEAPA are bifunctional with respect to Smith's reaction scheme, linear molecules will be formed. Hence at higher DEAPA contents, the product is linear in nature. Conversely, lowering the DEAPA content reduces the number of active hydrogens able to react according to Smith's scheme, which means that a reaction of the kind outlined by Narracott is favoured. The functionality of an Epon 828 molecule in such circumstances is increased to four. Therefore, a branched system, containing a high percentage of C-O-C linkages could be obtained.

It is obvious that Epikote 828/DDM is not subject to quite the same analysis in terms of functionality, since DDM is tetrafunctional anyway and Epikote 828 is at least bifunctional. However, the availability of active hydrogen in the form of DDM can be regarded as a significant variable. Following Whiting and Cline's reasoning, low DDM contents could give rise to a predominance of the Narracott scheme, and the formation of more ether linkages relative to hydroxyl groups. Some support for this idea is found in the infra-red data of Fig. 41. It is seen that 20 and 27 parts DDM resins have a lower - OH/C-O-C ratio than the toughest resins. The findings of Shechter et al.<sup>(89)</sup> also show that the presence of primary and secondary amine excludes the - OH/epoxy reaction (see below) which is a logical step following the formation

of - OH.



Effectively, ether linkages are not expected to predominate in formulations containing a high proportion of primary and secondary amine. The predominance of a particular species is therefore dependent upon the identity and proportions of resin and cure agent and on the cure schedule, if steric hindrance plays a major role in the reaction.

The above analysis poses two further problems. One of these is concerned with the fact that the stoichiometric resin has an - OH/C-O-C ratio closer to that of the 20 parts DDM formulation than to the others'. But its general mechanical behaviour is more like that of resins containing 30-40 parts DDM. In particular, its Young's moduli are very similar to the latter resins' moduli and it behaves in a more visco-elastic manner than the 20 parts resin. This point is considered more fully in section 12.4.

Considering the infra red data on consumption of epoxy, ether linkage concentration and hydroxyl/ether ratio in relation to general mechanical behaviour it appears that a reduced conversion of epoxy in low DDM resin is compensated for in the stiffness of the appropriate bond. A more linearly elastic, rigid material might be produced, which is unable to accommodate high stress levels after yielding. Intermediate DDM contents, despite having higher actual ether levels could be more linear or have different molecular weight distribution (if such a term can be applied to cross-linked networks) or different spatial and geometric characteristics.

Therefore, they may have lower elastic moduli, higher crack tip plasticity and behave in a more visco-elastic manner.

The other problem arising from Whiting and Cline's type of analysis is that according to Fig. 41, a decrease in hydroxyl  
ether ratio occurs between 30 and 40 parts DDM. It may be that as DDM content increases beyond 27 parts the exotherm generated during the initial stages of the reaction is sufficient to mobilise the tertiary amines formed during cure. It is worth noting here that tertiary amines have been detected at a very early stage of reaction during cure with primary amines<sup>(8)</sup>. In such circumstances, a tertiary amine catalysed reaction of the Narracott type might occur. This would lower the hydroxyl/ether ratio. Temperature/time records of castings during gelling indicated a higher peak temperature for the 40 parts DDM material than for 27 or 20 parts DDM. It was also seen that the higher DDM content produced a peak temperature earlier in the cure cycle. The temperatures of the various resins at the point of casting also showed systematic variation, the higher DDM contents giving rise to higher pouring temperatures. (All casts were made from charge weights of the same order of magnitude and all batches received nominally identical treatment prior to casting). Lee and Neville<sup>(1,8)</sup> point out, however, that tertiary amines generated during cure by primary and secondary amines are sterically hindered or immobile. Therefore, they do not easily catalyse polymerisation through hydroxyl groups.

There have to be reservations about the applicability of these ideas if the infra red and other chemical analyses are considered to be the only parameters of significance. The near equality of the -OH/C-O-C ratios for resins of high and low DDM content is not matched by a near equality of modulus values for example. Nevertheless, characterisation studies should involve more than chemical morphology and it is with this in mind that

comments are made about physical morphology later in this discussion.

### 12.3.3. General Comments on Fracture Toughness and Mechanical Behaviour

From the point of view of crack tip plasticity, the variations in fracture toughness, visco-plastic yielding and tensile Young's moduli are quite consistent. The inability of low DDM material to sustain large crack opening displacements prior to propagation is consistent with its low fracture toughness. Only a small amount of energy is dissipated because the material at the crack tip is less amenable than high DDM material to visco-plastic deformation at the testing speeds employed. The crack tip remains relatively sharp and therefore the stress concentration effect is high. When the material yields, it does so rapidly and this event is closely followed by bond rupture. The low crack opening displacement is also in keeping with its observed higher modulus, since the tensile (brittle) fracture stresses for all the resins are similar. A lower strain at failure might therefore be expected for the material with the higher modulus. Dibenedetto and Wambach<sup>(94)</sup> have also found that Epon 828, cured with a eutectic mixture of aromatic amines (probably DDM and metaphenylenediamine), when subjected to stoichiometric variation, has a modulus trend similar to that reported here. A corresponding increase in  $\gamma$  was recorded as their cure agent concentration was increased. No peak in  $\gamma$  was reported, but they did not extend the variation in composition very far beyond the stoichiometric point. Griffiths and Holloway<sup>(51)</sup> have reported an increase in  $\gamma$ , for an epoxy cured with phthalic anhydride (Araldite CT200/HT901), on increasing the amount of crosslink agent, but there was no peak in the curve. They did not give the value of the stoichiometric

composition but from the information on epoxide equivalent it is estimated that 30 parts of phthalic anhydride would be required for full cure. Their investigation did not cover anhydride contents in excess of 30 parts, so that the presence of a peak in  $\gamma$  cannot be ruled out. Modulus values quoted by Griffiths and Holloway do not wholly support the present results on 828/DDM but there are complications due to the fact that their system used an anhydride rather than an amine curing agent.

It might be argued that the 20 parts DDM resin's greater post-yield compressibility should allow considerable crack blunting to occur. It should be borne in mind, however, that the more visco-elastic resins begin to 'yield' at lower stress levels. This allows the crack tip more scope for accommodating increases in load. There is also the question of yield kinetics and subsequent stability of the testing system to consider, apart from the wider problem of applying compressive data to plane strain tensile opening mode situations. It is perfectly valid to assess a material's behavioural character by compression testing but the precise matching of trends is not a likely occurrence in a study of this nature.

Behaviour in compression does indicate that low DDM material yields in the classical manner i.e. a sudden yield associated with a drop in load. This sudden onset of permanent (at room temperature) deformation also implies that the rupture of primary chemical bonds is involved or that the agency providing resistance to plastic deformation is less extensive than in resins containing intermediate levels of DDM. The work of Ishai<sup>(95,96)</sup> and of Steg and Ishai<sup>(97)</sup> has shown that 'delayed' yielding in a flexibilised epoxy-Versamid\* system is attributable to the disruption of what they call 'physical' rather than chemical bonds. The physical bond they allude to is, in their opinion, a hydrogen bond. This is in keeping with the results obtained for the Epikote 828/DDM system at intermediate compositions.

\* Trade name for General Mills, Inc. polyamide flexibilisers.

Whichever of the parameters plotted in Figs. 22 and 24 is chosen to describe the mechanical behaviour of the resin, the trend is one which does not endorse the simple idea that increased DDM content automatically increases crosslink density (even if the limited range 20-27 parts is considered). Other physical characteristics of the morphology must be investigated. The majority of the mechanical property trends indicate that the 20 parts DDM resin is significantly different from the others. In particular, the yield point characteristics considered above are quite noticeable. The relationship between yield behaviour and fracture surface work is not likely to be a simple one. The tendency for the tougher resins to exhibit less well defined yielding in compression, though well established by the results in general, cannot provide an exact correlation between  $\gamma$  and, for example, yield drop in compression. However, the existence of a sharp yield either in tension or compression does give some indication of the relative toughnesses of the resins. (See Fig. 24 and Table 6).

Having considered the variation of properties as a function of the chemistry of the system, it is necessary to examine the role of physical morphology, in order to rationalise some of the results.

#### 12.4 Physical Morphology of 828/DDM and its Contribution to Mechanical Behaviour

It should be made clear at this point that no quantitative data is available for the correlation of mechanical property trends in terms of physical morphological parameters. The subject is in its infancy. However, what is known is that a feature is observed which responds to mechanical forces.

It cannot be disputed that the effect of mechanical deformation beyond the yield point results in permanent distortion of this feature. The sequence of events employed for revealing this effect,



i.e. deform-chemically etch-examine, does not allow the feature to be regarded merely as an artifact. The fact that distortion is observed in areas which have not been subjected to direct abrasive action rules out the possibility that the act of polishing a specimen gives rise to these particular etch features. A particular surface contour which is amenable to non-uniform chemical attack may be envisaged - with the result that an artifact is generated - but in this case the feature is too far removed from the surface to have been generated in such a way (Fig. 46).

Again, the development of identical features (Figs. 47 and 51) by two completely different routes supports the validity of the result. A question of fundamental importance with regard to the etched feature is: 'What is there within the entity which can influence mechanical properties'? Parameters which become worthy of investigation are:

- (a) size and size distribution of features,
- (b) identity and distribution of chemical bonds within a feature,
- (c) shape factor.

The effects of heat treatment, stoichiometry, mould wall preparation and mechanical deformation during cure on such parameters are as yet unknown. A preliminary investigation of size v. DDM content, surface preparation and chemical etching conditions (see section 10.5.1.) failed to isolate any significant trend. Unfortunately, due to time limitations, an extension of these investigations has not been possible.

One possible trend has emerged, however, as illustrated by a comparison of Figs. 51 and 52. The existence of terraced structures within the erosion zones of some ion-bombarded specimens may be significant. Of equal significance would be the absence of terracing in resins containing 20 parts DDM. The reasons for these differences are not fully understood. However, the possibility of a structural difference, resulting in a change of intermolecular bonding or packing arrangement,

is one way of interpreting the evidence. With this in mind, the variations in mechanical behaviour may be rationalised:

low DDM material, having low ether-link content and low conversion of epoxy, may still be rigid in a modulus test because the predominant factor is the primary bond. Low conversion of epoxy means low hydroxyl (from epoxide ring opening) concentration. Therefore, the only bonds contributing significantly to a modulus value are strong primary bonds.

A stoichiometric resin may possess a higher ether-link content (primary bonds), but the material may suffer a change in molecular conformation because of this. The relatively constant hydroxyl/ether ratio in the range 20-27 parts DDM may not be the over-riding factor in determining mechanical properties. However, at higher DDM contents, the influence of this ratio on mechanical properties may become greater because there is relatively little change in physical morphology in the range 27-40 parts DDM. The shallow increase in modulus in the range 27-40 parts DDM may reflect the variation in hydroxyl/ether ratio rather than a significant variation in basic physical morphology.

The mechanical properties must be a function of both chemical identity and physical disposition of the microscopic repeating units. The variation in properties with DDM content may be compatible with the infra-red analysis, if due allowance is made for physical morphological changes.

In the absence of information concerning the kinetics of these 828/DDM reactions it is not possible to establish which reaction schemes are predominating at particular times during cure and therefore one can only speculate on the origin of the morphology. Such information could prove very useful in clarifying the relationship between chemical and mechanical behaviour.

Evidence for the existence of a structural entity in resinous substances has been obtained by other workers. Apart from the work of Cuthrell<sup>(18-20)</sup>, which is considered later, there have been significant contributions by Erath and Spurr<sup>(16)</sup>, Erath and Robinson<sup>(17)</sup>, Frank et al<sup>(22)</sup> and by Lin and Kramer<sup>(21)</sup>. The evidence provided in references 16, 17 and 22 consists largely of electron micrographs of shadowed replicas produced from the surfaces of several thermosetting resins. The micrographs provide evidence of the existence of globular formations which have an apparent diameter of approximately 0.01-0.09  $\mu\text{m}$  (100-900  $\text{\AA}$ ). There is also evidence<sup>(16)</sup> which suggests that the globules (or nodules or miscelles) can be arranged in a filamentary manner, the filament presumably having arisen in the earlier stages of polymerisation.

Some thin section electron microscopy has also been done, using a phenolic resin<sup>(16)</sup>, which again indicated the existence of a nodular structure. Electron micrographs of replicated epoxy showed that nodularity was enhanced after leaching with acetone<sup>(16)</sup>. This, it has been suggested, is further support for the concept of dense nodules embedded in a less dense matrix, the latter being rather more easily attacked by solvents and etchants. (See also section 2.2. and below).

When comparing the dimensions of the nodules reported in references 16 and 17 with those of the features revealed by chromic acid etching of Epikote 828/DDM one finds an immediate discrepancy. The electron microscopic observations give rise to nodule diameters of the order of 0.1  $\mu\text{m}$  (1000  $\text{\AA}$ ) whereas the etched features in 828/DDM are of the order of 10  $\mu\text{m}$  (100,000  $\text{\AA}$ ). However, closer examination of fig.43 for example, indicates a fine structure which may be composed of nodules of the order of 1.0  $\mu\text{m}$  in dimension. It appears that chromic acid etching may not reveal the smallest sub-unit of structure

whereas other methods of examination may do so. It is conceivable that different etchants will reveal features of a different dimension. In fact, the suggestion has been made<sup>(17)</sup> that a variety of organic etchants, with polarities compatible with the materials to be removed, might provide better evidence of the chemical identity of inter-nodular species. The work reported in this thesis has also suggested that the identity of the etchant has some influence on the result (compare the effects of etching Epikote 828/DDM with mixed acids and with chromic acid alone) although the consistency achieved by etching 828/DDM with chromic acid, together with the concurring evidence from ion-beam etching experiments indicates that the structural feature of interest is quite large.

The difficulty in defining the dimensions of a structural entity in resins has been encountered previously. Frank et al<sup>(22)</sup> examined ion-bombarded surfaces of "amorphous" polycarbonate and showed that a feature similar to those of fig. 43 and those in references 16 and 17 could be revealed. The dimensions of an apparent network of "grains" were seen to vary with heat treatment. These changes were not discernable in unetched samples. They also reported dynamic mechanical measurements in support of the apparent structural changes induced by various heat treatments. Their investigation, which involved platinum-shadowed carbon replicas, indicated "grain" dimensions of  $0.01 \mu\text{m}$  ( $100 \text{ \AA}$ ).

In all the above cases, it has been reported that the globular morphologies of resinous materials have characteristic dimensions much less than  $1 \mu\text{m}$ . However, the work reported in this thesis suggests that there is a response not only to etching but also to mechanical deformation, which extends for distances of the order of several  $\mu\text{m}$ . The concept of a "supermodule"\* has, in fact, been proposed by Klement and Geil<sup>(97a)</sup> in the case of polyethylene terephthalate.

\* Equivalent to Geil's term used to describe an area of agglomerated nodules.

Although the dimensions of these proposed supernodules in PET were still much less than  $1\ \mu\text{m}$ , the idea may be worth investigating in the case of epoxy resins.

The only published results which lend quantitative support to the author's findings are those obtained by Cuthrell<sup>(18-20)</sup>. Using a number of techniques, including multiple micro-hardness measurements, micropenetrometer traces and sessile drop contact angle measurements he was able to conclude that some cured epoxies consisted of "floccular" aggregates approximately  $20-90\ \mu\text{m}$  in diameter. He concluded also that floccule dimensions were determined primarily by the thermal conditions during the early stages of cure, higher initial heat transfer rates to the samples giving rise to smaller floccules. Correlations between floccule size, physical, chemical and electrical properties were suggested by Cuthrell. The underlying theme of his discussion was based upon the periodicity of the measurements he undertook and it was evident that he did not rule out the existence of partially ordered structures. Unfortunately, very little pictorial evidence of the existence of floccular aggregates was provided in references 18-20. Therefore, a comparison with the work reported here is not possible. However, the fact that a periodicity with a half cycle dimension of  $20-90\ \mu\text{m}$  was detected supports the author's view that there could be a large structural entity in Epikote 828/DDM which is capable of responding to mechanical deformation. The distortion revealed by etching (e.g. fig. 45) must be attributed to some microstructural element even though it is difficult to see an immediate link between that element and, for example, the features on a fracture surface. (Some comfort is drawn from the observation that fracture topography is not easily correlated with the known morphological characteristics of metallic materials). In the absence of any evidence of floccular morphology in undeformed epoxy, it might be argued that the deformed, etched features are a manifestation of micro-shear bands. They may represent the result of micro shear

processes but the fact remains that they bear a remarkable physical resemblance to the undeformed etched features typified by those in fig. 42.

Accepting, for the purposes of discussion, the reality of such a structural unit one may consider the permanent distortion of the resin to represent a form of ordering. Ordering might be achieved during cure by residual shrinkage stresses. This mechanism has been proposed by Manson and Chiu<sup>(24)</sup> in order to explain anomalous water permeability characteristics in a glass-filled epoxy (Epon 828 cured with a polyamide). Although they suggested that the residual stress was the result of a mismatch between coefficients of expansion of the resin and filler, the agency creating the order would still be a mechanical force. Cuthrell<sup>(18)</sup>, in his work on epoxies, indicated that residual strain bands were prevalent in samples cured at lower temperatures i.e. in resins characterised by larger floccules, higher glass transition temperatures and greater resistance to solvent etching. The larger interfloccular spaces, it was implied, allowed diffusion controlled curing processes to continue after gelation.

In the light of the above discussion, of Cuthrell's work in particular, it may seem strange that differences in etched feature dimensions were not readily apparent in Epikote 828/DDM. However, it should be noted that fairly severe cure schedules were employed for the majority of the work reported here, implying that any internodular post-gelation reactions were fully encouraged in all formulations. The most striking differences in mechanical behaviour and the only apparent significant physical morphological change occurred somewhere in the region 20-27 parts DDM. The less striking differences, in Young's moduli for example, occurred between 27 and 40 parts DDM between which limits there was no visual evidence of a significant

physical morphology change. If it is accepted, in the absence of evidence to the contrary, that floccule diameters and floccule shape factors in 828/DDM have not changed as a function of stoichiometry, one must conclude that a combination of stoichiometric control of intra-nodular morphology and 'remanent' stoichiometric control of inter-nodular chemical reactivity are the influential parameters in determining the properties of Epikote 828/Epikure DDM. The development of a quantitative stereological method of characterising the etched features in this resin would certainly be a very useful tool for clarifying the situation. Quantitative stereology, combined with more than one etching technique, may help in deciding whether the floccular features observed after chromic acid etching are "supernodules" and whether they influence the properties of the resin.

## 12.5. Variation of Properties as a Function of Cure Cycle

Consideration of the results presented in section 9.3. leads to the conclusion that initial gel temperature is not a variable which greatly influences mechanical properties in 828/DDM, when a two-stage cure schedule is employed. The only correlation between fracture and mechanical behaviour occurred in the low DDM resin. In this case, yield drop in compression showed a similar trend to fracture surface work. (A similar correlation was noted in section 12.3.3.).

The two other resin compositions were largely unaffected by changes in gel temperature, except for  $\gamma$  values. The variation in  $\gamma$  was very much less than that obtained as a function of DDM content. Analyses of infra-red absorption at  $3530\text{cm}^{-1}$  and  $1110\text{cm}^{-1}$  (-OH and C-O-C groups) were unable to distinguish between resins of the same initial composition which had been subject to different gel temperatures. Thermo-mechanical transitions appeared to be sensitive to gel temperature (Fig. 34) but the reliability of this result has already been questioned in Chapter 10. Of the mechanical parameters measured,  $\gamma$  was the most sensitive to changes in cure cycle. Young's modulus was particularly insensitive to variation in gel temperature. Identical remarks can be made with regard to extending the cure time of 27 parts DDM resin at  $448^{\circ}\text{K}$ . The apparent insensitivity of the system to changes in gel temperature might be explained by regarding the final stage of cure at elevated temperature to be the controlling factor for a given composition. This contrasts with evidence in the literature<sup>(98)</sup>, that the rheological behaviour during cure of epoxy/anhydride systems is dependent upon the cure temperature relative to the maximum glass transition temperature of the system and relative to the glass transition temperature at



the gel point. If the reaction sequence in 828/DDM is more sensitive to temperature variations early in the gellation process (possibly even during mixing) then it is conceivable that little change in properties will be induced by varying initial gel temperature 960s (16 mins.) after the reaction has been started. Even so, fracture surface work,  $\gamma$ , appears to be a sensitive parameter for monitoring these small changes.

#### 12.6. Effect of Testing Speed on Mechanical and Fracture Properties

Some variation in mechanical and fracture properties with testing speed would be expected for visco-elastic materials. The response of the material at the tip of a crack will influence the amount of deformation and slow crack growth that occurs prior to sudden propagation. This point is well illustrated by the decrease in rough zone size which accompanies an increase in testing speed, (Fig. 63). The strong correlation between  $\gamma$  and rough zone size observed for variations in stoichiometry also applied for testing speed variation, (Fig. 56).

The closer agreement between  $\gamma$  values obtained by Gurney's and Irwin-Kies' analyses at high testing speed is logical if one considers the likely velocity profile during crack movement. The major part of the propagation length is covered at high speed (crack movements of 50-100mm took much less than 1s). However, the agency responsible for the storage of large amounts of elastic energy prior to rapid crack propagation in a low speed test is probably associated with the slow growth (i.e. blunting) of the crack. At low testing rates, the visco-elastic and visco-plastic processes which are now known to occur in this resin system (section 12.3.3.) are given time to operate. The greater the stored energy, the longer the propagation length after instability is reached. This accounts for the shorter crack jumps at lower fracture toughnesses and higher testing rates. At high testing rates, the visco-elastic processes

are likely to be subdued and the high speed propagation step becomes more significant as a contribution to the total energy consumed.

It has already been mentioned that  $\gamma$  in epoxy resins varies with crack speed in stabilised testing systems<sup>(81)</sup>. The trend is that  $\gamma$ , at low rates, is very much higher than at high testing rates and the curve is asymptotic i.e. there is a strong negative  $\gamma$  v. crack speed characteristic at low speeds and relatively little change in  $\gamma$  at extremes of crack speed. Therefore it is easy to visualise a crack jumping situation at a relatively high testing rate where the rapid propagation step contributes significantly to the value of  $\gamma$  and has a relatively constant value. The Gurney analysis would then be more appropriate than at low testing speeds.

#### 12.7. Comments on Fracture Surface Features and their Relation to Crack-tip Processes

It has already been noted in Chapter 11 that there was no fundamental difference between the fracture surfaces of the various resins except for the predominance of the triangular areas in Fig. 62 (in 20 parts DDM) and the size of the rough zone. The existence of such features (Fig. 62) in this system supports the earlier observations of Lilley and Holloway<sup>(99)</sup>. They observed an identical effect near crack arrest locations and attributed it to crazing in their Araldite CT200/HT901 epoxy. They also reported that crazes grew in a direction perpendicular to the local principal stress and that the craze density around crack tips loaded at room temperature for approximately 360ks (100 hours) was small in comparison with that obtained at elevated temperatures. In contrast to Lilley and Holloway's findings, the narrowly confined zone in which these features occur in Epikote 828/Epikure DDM was only observed at low DDM contents. There may, however, be a rate or temperature dependence characteristic which excludes the formation of such 'crazes' in

fully\* cured 828/DDM at the testing speeds employed. Long term static loading may prove necessary for their formation at room temperature in the fully\* cured material. It is also of interest that Lilley and Holloway observed larger crazes in CT200/HT901 formulations of below stoichiometric amount of HT901.

The only other major feature of interest on fracture surfaces was the rough zone, near the initiation area of propagation. The extent of the rough zone, as seen in Figs. 63 and 67 correlates well with fracture parameters measured from initiation data. Prior to sudden propagation, an amount of slow growth occurs during the application of load. The extent of this growth is determined by the natural visco-elastic response of the material and the effective loading rate at the crack tip. Given time to respond, the material near the tip will relax the local stresses and extend the area of deformation either in the form of crazed regions (typified by thermoplastics) or by multiple crack plane formation and associated macroscopic crack blunting (the latter particularly in areas of plane stress). An assessment of the relative contributions of these mechanisms is difficult to make. However, if the fractographic evidence and crack tip morphology are considered, the initiation  $\gamma$  or  $K_{IC}$  values in Epikote 828/DDM at normal testing rates do not appear to rely on crazing as a major contribution. Within certain crack speed ranges, though, the behaviour of an under-cured (low DDM) resin does seem to be related to a craze-like phenomenon.

\* This term is used in its conventional sense in this section, to describe a stoichiometric resin which has received extensive cure treatment.

PART 4 - Conclusions and Suggestions for Future Work

CHAPTER 13 - Conclusions

13.1.

The mechanical and fracture properties of Epikote 828/Epikure DDM systems are highly dependent on the relative amounts of resin and cross-linking agent, particularly at low testing rates. The crack tip phenomena which are observed during fracture tests can be related to the fracture properties and to the general mechanical behaviour of the material.

13.2.

The variation in fracture and mechanical properties of Epikote 828/Epikure DDM systems cannot be explained in terms of the simple concept of cross-link density. Chemical and physical characterisation techniques have been used to establish that two competing reaction schemes may be responsible for the observed variations in properties.

The relationship between chemical and physical morphology is not clear. However, chemical and ion-beam etching methods have been developed and have been used to establish the existence of a morphological entity which responds to mechanical forces. Moreover, ion-beam methods have been able to identify some potentially significant structural trends in this system which may clarify the relationship between chemical and physical characteristics.

13.3.

The mechanical and fracture properties of Epikote 828/Epikure DDM systems are only slightly affected by changes in initial gel temperature and by moderate increase in post-cure time at 448<sup>o</sup>K.

It is not known whether this is because the reaction sequence may be determined at a very early stage of cure (by stoichiometric and thermal influences) or because the post-cure at 448°K may be sufficient to compensate for minor differences during gellation.

13.4.

The mechanical and fracture properties of Epikote 828/Epikure DDM systems are rate sensitive. In particular, higher testing rates result in lower fracture toughnesses. The rate sensitivity is not unique to any one composition of resin. Rate-sensitive crack tip processes are believed to be responsible for changes in macroscopic parameters.

13.5.

Comparison of fracture surface work values for material/specimen/testing machine combinations which behave in an unstable manner should only be carried out using initiation data, if maximum sensitivity of the fracture parameter is to be ensured.

13.6.

The failure mechanism in Epikote 828/Epikure DDM systems tested at normal rates does not appear to be closely related to crazing phenomena, except for resins containing considerably less than stoichiometric quantity of DDM.

13.7.

The fracture surface work parameter, measured with the aid of the TDCB fracture test piece, is a very useful and sensitive measure of changes in the resin system. It is a statistically reliable parameter when measured thus and can be evaluated without sophisticated instrumentation.

## CHAPTER 14 - Suggestions for Future Work

### 14.1. General Comments

Broadly, the lines of approach recommended for future work can be categorised as:

- (a) specific studies of Epikote 828/DDM, particularly with regard to chemical and physical morphologies.
- (b) extension of the techniques described and developed during the course of this work to other materials, including composite systems.

### 14.2. Specific Studies of Epikote 828/DDM

This material is an important example which typifies many of the industrially used resins. Therefore, detailed knowledge of its behaviour is useful. With regard to the relationship between morphology and mechanical behaviour it would be worthwhile investigating the kinetics of the crosslinking reactions. Such a study might clarify the ideas about the competitive reactions producing ether and hydroxyl groups. A more detailed analysis of the system by chemical and ion-beam etching would also be useful. In particular, quantitative stereological analysis of etched surfaces could be carried out with the aid of image analysing systems. Armed with this knowledge, a quantitative correlation between physical, chemical and mechanical characteristics could be attempted.

### 14.3. Use of Fracture Parameters and Etching Techniques as Characterisation Methods

The fracture surface work parameter has been shown, in this study, to be a sensitive one. Its practical application as a method of generating engineering data could be supplemented by its use as a 'characterisation' device. Materials other than epoxy resins are candidates for study.

The etching methods described in this thesis are as yet non-quantitative. The suggestion of stereological analysis has already been made. Another possible fruitful investigation would be concerned with ion beam etching of composites. Interface regions are extremely important in composite systems and their characterisation would prove to be a valuable contribution to the understanding of the mechanics and chemistry of composites. Chemical etching of polymer composites (e.g. deformed epoxy/fibre composites) may indicate how well theoretical treatments of the mechanics of deformation match the real situation. It is now known that in epoxy resins, a feature which responds to deformation can be revealed by chemical etching. If sampling problems can be overcome, better analysis of deformations in composites may be possible.

#### 14.4. Matrices for Composites

One point which emerges from the investigation of mechanical behaviour in Epikote 828/DDM is that a wide variety of behaviour can be achieved. It is possible that not enough attention has been given in the past to the modification of matrix properties in existing epoxy composites. In this context, therefore, interface and matrix characterisation offers considerable scope for experimental study.

#### 14.5. Author's Concluding Remarks

Throughout the three year span of this work, the author has become progressively more aware of the complexities of even a 'simple' system such as Epikote 828/DDM. It is tempting to suggest that many of the questions raised by this work are unanswerable. However, it has also become more obvious that the solution of these problems can only be effected by way of carefully planned experiment,

not necessarily with the aid of sophisticated equipment. There is no substitute for logic. It is hoped that the reader will find this thesis of some use, if only in the application of his own logic to the numerical data, where the author's has failed.



REFERENCES

1. H. Lee and K. Neville  
Epoxy Resins - Their Applications and Technology,  
McGraw-Hill Book Co. Inc., New York. (1957).
2. W. G. Potter  
Epoxy Resins, Plastic Institute,  
Publ. by Iliffe Books, London. (1970).
3. Epoxy Resin Technology  
Ed. P. F. Bruins,  
Interscience Publishers, John Wiley & Sons Inc., New York. (1968).
4. I. Skeist and G. R. Somerville  
Epoxy Resins  
Reinhold, New York. (1958).
5. H. L. Spell and R. D. Eddy  
American Chem. Soc. Symp.  
148th Meeting. (1964).
6. R. G. Weatherhead  
Analyst, London, 91, (1966), 445.
7. B. H. Miles  
American Chem. Soc. Symp.  
148th Meeting. (1964).
8. H. Lee and K. Neville  
Handbook of Epoxy Resins  
McGraw-Hill, New York. (1967).
9. W. A. Patterson  
Analyt. Chem. 26, (1954), 823.
10. J. Bomstein  
Analyt. Chem. 30, (1958), 544.
11. O. D. Shreve, M. R. Heether, H. B. Knight and D. Swern  
Analyt. Chem. 23, (1951), 277.
12. H. Lee and L. Vincent  
Adhesives Age, 4, 9, (1961), 22.
13. R. E. Kagarise and L. A. Weinberger  
U.S. Govt. Report PB 111438 (1954).
14. H. Dannenberg and W. R. Harp  
Analyt. Chem. 28, (1956), 86.
15. H. Dannenberg  
S.P.E. Trans., 3, (1963), 78.
16. E. H. Erath and R. A. Spur  
J. Poly. Sci, 35, (1959), 391.
17. E. H. Erath and M. Robinson  
J. Poly. Sci. c, Polymer Symposium No. 3. (1963).

18. R. E. Cuthrell  
J. Appl. Poly. Sci, 11, (1967), 949.
19. R. E. Cuthrell  
J. Appl. Poly. Sci, 11, (1967), 1495.
20. R. E. Cuthrell  
J. Appl. Poly. Sci, 12, (1968), 1263.
- 20a. G. S. Y. Yeh  
Crit. Reviews. Macromol. Sci, 1, (1972), 173.
21. W. Lin and E. J. Kramer  
J. Appl. Phys. 44, 10, (1973), 4288.
22. W. Frank, H. Goddar and H. A. Stuart  
Polymer Letters 5, (1967), 711.
- 22a. P. M. Geil  
Polymeric Materials - Relationships between Structure and  
Mechanical Behaviour  
ASM Seminar (Sept. 1973) Chap. 3. (Published by ASM 1975).
23. G. S. Y. Yeh  
J. Macromol. Sci.-Phys. B 7, 4, (1973), 728.
24. J. A. Manson and E. H. Chiu  
Polymer Reprints 14, 1, (1973), 469.
25. A. A. Griffith  
Trans. Phil. Soc. A221, (1920), 163.
26. C. Inglis  
Trans. Inst. Naval Archit. London 55, (1913), 219.
27. J. P. Berry  
J. Appl. Phys, 34, (1963), 62.
28. G. R. Irwin and J. A. Kies  
Welding J. Res. Suppl. 33, (1954), 193s.
29. C. Gurney  
Physical Basis of Yield and Fracture,  
Oxford Conference, England. (1966).
30. G. R. Irwin  
Encyclopaedia of Physics. 6, Springer, Heidelberg. (1958).
31. J. P. Berry  
Fracture Processes in Polymeric Solids  
Ed. Rosen, Interscience (1964), 157.
32. A. S. Tetelman and A. J. McEvily  
Fracture of Structural Materials,  
Wiley, New York. (1967). Ch. 2.
33. Experimental Techniques in Fracture Mechanics  
Ed. A. S. Kobayashi  
S.E.S.A. Monograph No. 1 (1973). Publ. Iowa State Univ. Press.  
and S.E.S.A. Conn. U.S.A.
- ✓ 34. E. Cowan  
Reports on Progress in Physics. 12, (1948), 185.

- ✓35. E. Orowan and D. K. Felbeck  
Welding Journal Res. Suppl. (1955), 570.
36. E. Orowan  
Trans. Inst. Eng. Shipbuild. Scotland, 89, (1945), 165.
37. K. R. Linger and D. G. Holloway  
Phil. Mag. 18, 156, (1968), 1269.
38. P. P. Gillis and J. J. Gilman  
J. Appl. Phys., 35, (1964), 647.
39. P. P. Gillis  
J. Appl. Phys., 36, (1965), 1374.
40. J. W. Obreimov  
Proc. Roy. Soc. A.127, (1930), 290.
41. J. J. Benbow and F. C. Roesler  
Proc. Phys. Soc. B70, (1957), 201.
42. R. G. Hoagland  
J. Basic Eng. (Sept. 1967), 525.
43. L. E. Miller, K. E. Puttick and J. G. Rider  
J. Poly. Sci, 33c (1971), 13.
44. K. Selby and L. E. Miller  
J. Material Sci. 10, (1975), 12.
45. J. P. Berry  
Fracture Ed. Liebowitz, 7, Academic Press. New York. (1972).
46. R. J. Ferguson, G. P. Marshal and J. G. Williams  
Polymer 14, (1973), 451.
47. D. S. Dugdale  
J. Mech. Phys. Solids, 8, (1960), 100.
48. R. J. Ferguson and J. G. Williams  
Polymer 14, (1973), 103.
49. J. P. Berry  
J. Poly. Sci., A1, 993.
50. L. J. Broutman and F. J. McGarry  
J. Appl. Poly Sci, 9, (1965), 609.
51. R. Griffiths and D. G. Holloway  
J. Material Sci, 5, (1970), 302.
52. J. O. Outwater and D. J. Gerry  
Modern Plastics, (Oct. 1967), 156.

53. A. D. S. Digwaa  
Polymer 15, (1974), 101.
54. W. T. Evans and B. I. G. Barr  
J. Strain Anal., 9, 3, (1974), 166.
55. A. C. Meeks  
Brit. Poly. J. 7, (1957), 1.
56. S. Mostovoy, B. P. Crossley and E. J. Ripling  
J. Materials JMLSA, 2, 3, (1967), 661.
57. Laboratory methods in Infra-red Spectroscopy,  
Eds. Miller and Stace, 2nd Edition, Heyden and Son, (1972), 119.
58. H. A. Willis and R. G. Miller  
Molecular Spectroscopy, Heywood, London, (1961), 279.
59. V. J. I. Zichy  
Laboratory Methods in Infra-Red Spectroscopy  
Eds. Miller and Stace 2nd Edition, Heyden and Son, (1972), 48.
60. H. Keskkula and P. A. Traylor  
J. Appl. Ply Sci, 11, (1967), 2361.
61. L. Bartosiewicz and Z. Mencik  
J. Poly. Sci. 12, (1974), 1163.
62. D. A. Blackadder and P. I. Vincent  
Polymer, 15, (1974), 2.
63. C. B. Bucknall, I. C. Drinkwater and W. E. Keast  
Polymer, 13, (1972), 115.
64. C. B. Bucknall and I. C. Drinkwater  
Polymer 15, (1974), 254.
65. G. C. Eastmond and E. G. Smith  
Polymer 14, (1973), 509.
66. B. J. Spitt  
Polymer, 4, (1963), 109.
67. F. R. Anderson and V. F. Holland  
J. Appl. Phys., 31, (1960), 1516.
68. S. L. Strong  
J. Material Sci., 2, (1974), 993.
69. S. B. Warner, D. R. Uhlmann and L. H. Peebles  
J. Material Sci., 10, (1975), 758.
70. Commonwealth Scientific Corp. Bulletin 45-71.
71. J. Lilley  
Ph.D Thesis, University of Keele, England. (1973).

72. A. Kolbeck  
Ph.D Thesis, Mass. Inst. of Tech. U.S.A. (1975).
73. D. W. Tomkins  
Private Communication.
74. D. J. Barber  
J. Material Sci., 2, (1970), 1.
75. R. L. Cunningham  
J. Appl. Phys., 31, (1960), 839.
76. R. A. Dugdale and S. D. Ford  
Trans. Brit. Ceram. Soc., 65, (1966), 165.
77. A. H. Heuer  
Rev. Sci. Instr. 42, (1971), 1177.
78. J. W. Ward  
Microstructures, 2, (1971), 11.
79. Instron Ltd.  
Technical Literature.
80. M. J. Doyle, E. Maranci and S. Stork  
Proc. Roy. Soc., A329, (1972), 137.
81. Y. W. Mai and A. G. Atkins  
J. Material Sci., 10, (1975), p. 2000.
82. T. Kobayashi  
Ph.D Thesis, Illinois Inst. of Tech. (1972).
83. J. G. Williams  
Inst. J. Fract. Mech. 8, (1972), 393.
84. R. Griffiths  
M.Sc. Thesis, University of Keele, England, (1968).
85. H. Arican  
Private Communication.
86. E. S. Narracott  
British Plastics, (April 1953), 120.
87. I. T. Smith  
Polymer, 2, (1961), 95.
88. S. Horie, H. Huiira, M. Sawada, I. Mita and H. Kambe  
J. Poly. Sci., A1, 8, (1970), 1357.
89. L. Shechter, J. Wynstra and R. Kurkijy  
Ind. Eng. Chem., 48, (1956), 94.

90. M. Acitelli, R. Prime and E. Sacher  
Polymer, 12, (1971), 335.
91. L. Shechter, J. Wynstra  
Ind. Eng. Chem., 48, (1956), 86.
92. H. A. Newey  
Gordon Research Conf. on Polymers, New London, U.S.A. (1955).
93. D. A. Whiting and D. E. Kline  
J. Appl. Poly. Sci., 18, (1974), 1043.
94. A. T. Dibenedetto and A. D. Wambach  
Int. J. Polymeric Materials, 1, (1972), 159.
95. O. Ishai  
J. Appl. Poly. Sci., 11, (1967), 963.
96. O. Ishai  
J. Appl. Poly. Sci., 11, (1967), 1863.
97. J. Steg and O. Ishai  
J. Appl. Poly. Sci., 11, (1967) 2303.
- 97a. J. J. Klemm and P. H. Geil  
J. Macromol. Sci. (Phys) B5, 2, (1971), 535.
98. J. K. Gillham, J. A. Benci and A. Noshay  
J. Poly. Sci., Symp. 46, (1974), 279.
99. J. Lilley and D. G. Holloway  
Phil. Mag. 28, 1, (1973), 215.
- ✓ 100. I. N. Sneddon  
Proc. Roy. Soc., A187, (1946), 229.
- ✓ 101. P. C. Paris and G. C. Sih  
ASTM STP No. 381, (1965), 30.
102. A. H. Cottrell  
Mechanical Properties of Matter, Wiley, New York, (1964), p. 345.
103. J. Friedel  
Fracture, Ed. Averbach et al., M.I.T., Wiley, New York, (1959), 498.
104. G. R. Irwin  
Metals Engineering Quarterly, (1963), 324.
105. G. R. Irwin  
Proc. of 1960 Sagamore Research Conf. on Ordnance Materials.
- ✓ 106. B. A. Bilby, A. H. Cottrell and K. H. Swinden  
Proc. Roy. Soc., A272, (1963), 304.
107. P. T. Heald, G. M. Spink and P. J. Worthington  
Material Sci. and Engineering, 10, (1972), 129.
108. G. C. Sih, Eng. Fract. Mech., 5, (1973), 365.

109. J. F. Knott  
Fundamentals of Fracture Mechanics, Butterworth (1973), 154.
110. J. R. Rice  
J. Appl. Mech., 35, (1968), 379.
111. J. F. Knott  
As. 109, Page 174.
112. Methods of Analysis and Solutions to Crack Problems  
Edited by G. C. Sih, Wolters-Noordhoff, (1972).
113. R. R. Barr, D. Elliott, P. Terry and E. F. Walker  
Metal Construction, 7, 12, (Dec. 1975), 604-610.

ACKNOWLEDGEMENTS

The Author wishes to thank the following for their assistance during the past three years.

The Science Research Council for providing funds.

The Department of Materials Technology, Loughborough University of Technology, for provision of research facilities.

The Departments of Chemistry, Polymer Technology and the Centre for Industrial Studies (all at Loughborough) for the loan of equipment.

Dr. L. E. Miller\* and Dr. M. O. W. Richardson (Lecturer, Department of Materials Technology) for their help and encouragement during the course of this work, and for many helpful discussions.

Mr. D. W. Tomkins for his assistance with the ion-beam etching problem. Also Dr. D. S. Coleman for permission to use the apparatus.

Dr. A. C. Meeks (Shell Chemical Co. Ltd.,) for advice on the casting, curing and characterisation of epoxy resins.

The technical staff of the Department of Materials Technology.

The Shell Chemical Co. Ltd., for providing raw material.

Miss A. Rook for typing this thesis despite my handwriting.

- - - - -

I, Kevin Selby, accept responsibility for the work submitted in this thesis and I declare that, except for the acknowledged assistance of the above, the work reported was conducted by myself and no other persons.

\* Formerly Lecturer in the Department of Materials Technology.



TABLE 1

CAST NO.	DDM CONTENT (PARTS PER 100 OF RESIN) BY WEIGHT	CURE CYCLE
12-14	27	3.6ks at 373°K + 7.2ks 373 / 448°K
15	20	3.6ks at 373°K + 7.2ks 373 / 448°K
16	30	3.6ks at 373°K + 7.2ks 373 / 448°K
17	20	3.6ks at 373°K + 7.2ks 373 / 448°K
18	30	3.6ks at 373°K + 7.2ks 373 / 448°K
19	35	3.6ks at 373°K + 7.2ks 373 / 448°K
20	40	3.6ks at 373°K + 7.2ks 373 / 448°K
21	20	3.6ks at 373°K + 7.2ks 373 / 448°K
22	27	3.6ks at 373°K + 7.2ks 373 / 448°K + 1.8ks at 448°K
23	27	3.6ks at 373°K + 7.2ks 373 / 448°K + 3.6ks at 448°K
24-27	27	3.6ks at 373°K + 7.2ks 373 / 448°K
28	27	3.6ks at 373°K + 7.2ks 373 / 448°K + 5.76ks at 448°K
29	35	3.6ks at 373°K + 7.2ks 373 / 448°K
30	32	3.6ks at 373°K + 7.2ks 373 / 448°K
31	33	3.6ks at 373°K + 7.2ks 373 / 448°K
32	40	3.6ks at 373°K + 7.2ks 373 / 448°K
33	10	3.6ks at 373°K + 7.2ks 373 / 448°K
34-40	20-40	3.6ks at 373°K + 7.2ks 373 / 448°K small samples for ion beam etching. Two steel moulds in oven to act as thermal load.
41	20	3.6ks at 323°K + 7.2ks 323 / 448°K
42	20	3.6ks at 333°K + 7.2ks 333 / 448°K
43	20	3.6ks at 348°K + 7.2ks 348 / 448°K
44	27	As cast 41
45	27	As cast 42
46	27	As cast 43
47	40	As cast 42
48	40	As cast 41
49	40	As cast 43

Casts 12-21 and 29-32 were used to investigate the effect of DDM content on properties.

Casts 22, 23 and 28 were used to investigate the effect of post-cure time at 448°K.

Casts 24-27 were used to investigate the effect of testing speed.

Casts 41-49 were used to investigate the effect of initial gel temperature.

TABLE 2

## Typical Primary Data from TDCB Tests

SPECIMEN NUMBER	LOAD f (N)	DEFLECTION (m) $\times 10^4$	CRACK LENGTH C (m) $\times 10^2$	CRACK PLANE WIDTH W (m) $\times 10^3$
17B	39.5	9.0	8.4	2.1
	42.0	10.4	9.0	
	40.0	11.6	10.2	
	40.0	12.4	10.7	
	40.5	13.2	11.3	
	40.0	14.0	12.0	
	40.0	14.6	12.5	
	42.5	16.4	13.0	
20A	66.5	3.0	2.1	2.0
	68.5	3.6	2.4	
	65.0	4.5	3.0	
	63.0	5.7	3.7	
	55.0	6.6	4.5	
	62.0	8.6	5.0	
	60.5	12.0	6.5	
	62.0	17.7	8.45	
	65.0	27.6	11.6	
20B	70.0	4.1	2.7	2.04
	60.0	4.8	3.5	
	63.5	6.1	3.8	
	63.0	8.0	4.8	
	63.0	11.4	6.1	
	63.5	16.8	8.1	
	67.5	26.3	11.1	

TABLE 3 Typical Data for Evaluating  $\gamma$  by Berry's Method  
 (See section 7.2.2. for nomenclature)

SPECIMEN NUMBER	$\log f/\delta$	$\log C$	$f \delta/w$ (N)	C (m) x 10 <sup>2</sup>	$\frac{d(\log f/\delta)}{d(\log C)}$	$\frac{d(f \delta/w)}{d(C)}$	FRACTURE SURFACE WORK, $\gamma$ (Jm <sup>-2</sup> )
17B	4.9435	2.9269	16.9	8.4	1.33	235	78.0
	4.9074	2.9566	20.8	9.0			
	4.8376	1.0086	22.0	10.2			
	4.8082	1.0315	23.6	10.7			
	4.7875	1.0550	25.4	11.3			
	4.7574	1.0792	26.6	12.0			
	4.7388	1.0969	27.6	12.5			
4.7143	1.1139	33.2	13.0				
20A	4.3458	2.3222	9.8	2.1	1.33	900	299
	4.2795	2.3802	12.2	2.4			
	4.1596	2.4771	14.4	3.0			
	4.0433	2.5682	17.7	3.7			
	3.9206	2.6532	18.2	4.5			
	3.8578	2.6990	26.7	5.0			
	3.7024	2.8129	36.3	6.5			
	3.5445	2.9261	54.9	8.45			
3.3720	1.0645	89.3	11.6				

TABLE 3 (Continued) (See section 7.2.2.)

SPECIMEN NUMBER	$\log f/\delta$	$\log C$	$f \delta / w$ (N)	$C^2$ (m) x $10^2$	$\frac{d(\log f/\delta)}{d(\log C)}$	$\frac{d(f \delta / w)}{d(C)}$	FRACTURE SURFACE WORK, ( $Jm^{-2}$ ) $\gamma$
20B	4.2321	2.4314	13.9	2.7	1.33	900	299
	4.0969	2.5315	14.1	3.4			
	4.0174	2.5798	18.9	3.8			
	3.8963	2.6812	24.8	4.8			
	3.7424	2.7853	35.4	6.1			
	3.5775	2.9085	52.6	8.1			
	3.4094	1.0453	86.2	11.1			

TABLE 4 Typical Data for Evaluating  $\gamma$  by Irwin-Kies Equation  
(See section 7.2.3.)

SPECIMEN NUMBER	COMPLIANCE $\left(\frac{R}{mN^{-1}}\right) \times 10^5$	CRACK LENGTH $(m) \times 10^2$	$\frac{dR}{dC}$ $(N^{-1}) \times 10^6$	AVERAGE		FRACTURE SURFACE WORK, $\gamma$ $(Jm^{-2})$
				LOAD f (N)	CRACK WIDTH $w$ $(m) \times 10^3$	
17B	2.28	8.4	338	40.4	2.1	65.8
	2.48	9.0				
	2.9	10.2				
	3.1	10.7				
	3.26	11.3				
	3.5	12.0				
	3.65	12.5				
3.86	13.0					
20A	4.51	2.1	392	63.1	2.0	195
	5.26	2.4				
	6.92	3.0				
	9.05	3.7				
	12.0	4.5				
	13.9	5.0				
	19.8	6.5				
	28.5	8.45				
42.5	11.6					

TABLE 4 (Continued) (See section 7.2.3.)

SPECIMEN NUMBER	COMPLIANCE $R_1$ ( $\text{mN}^{-1}$ ) $\times 10^5$	CRACK LENGTH $C$ (m) $\times 10^2$	$\frac{dR}{dC}$ ( $\text{N}^{-1}$ ) $\times 10^6$	AVERAGE		FRACTURE SURFACE WCRK, $\gamma$ ( $\text{Jm}^{-2}$ )
				LOAD $f$ (N)	CRACK WIDTH $w$ (m) $\times 10^3$	
20B	5.86	4.5	398	64.3	2.04	202
	8.0	3.4				
	9.61	3.8				
	12.7	4.8				
	18.1	6.1				
	26.5	8.1				
	39.0	11.1				

TABLE 5 Typical Data for Evaluating  $\gamma$  by Gurney's Method

SPECIMEN NUMBER	FRACT. SURFACE AREA ( $m^2$ ) $\times 10^5$	AREA OF LOAD/ EXTENSION GRAPH ( $m^2$ ) $\times 10^4$	WORK EQUIV. TO PREVIOUS COLUMN (J) $\times 10^5$	FRACTURE SURFACE WORK FOR EACH EVENT ( $Jm^{-2}$ )	AVERAGE $\gamma$ ( $Jm^{-2}$ )
17B	2.12	13.9	141	66.8	61.6
	2.54	13.9	141	56.0	
	2.54	14.8	151	59.5	
	*2.54	14.4	147	57.7	
	2.12	14.1	144	68.0	
20A	2.8	8.33	340	122	133
	3.2	10.5	429	134	
	6.0	18.6	760	127	
	*7.8	26.6	1085	139	
	12.6	42.8	1748	139	
20B	2.86	9.67	395	138	138
	16.32	5.52	225	137	
	5.3	17.6	718	135	
	8.16	27.8	1135	139	
	12.24	42.6	1738	142	

\* See Appendix A3.3.

TABLE 6

CAST NUMBER	DDM CONTENT (PARTS BY WT)	TENSILE STRENGTH $\times 10^{-6} \text{ (Nm}^{-2}\text{)}$		COMMENTS ON TENSILE STRESS STRAIN BEHAVIOUR	COMPRESSIVE YIELD STRESS $\times 10^{-6} \text{ (Nm}^{-2}\text{)}$	COMPRESSIVE PROOF STRESS $\times 10^{-6} \text{ (Nm}^{-2}\text{)}$
		U.T.S.	FRACTURE STRESS			
15, 21	20	95, 96	-	Deviation from linearity Load drop prior to failure	125	123
17	20	-	73, 80	Almost complete linearity No load drop prior to failure		
14	27	-	78, 67	Some deviation from linearity No load drop prior to failure	-	
13	27	-	73, 66	Deviation not as great as	-	85
12	27	-	71	for 30 parts DDM specimens	-	
16	30	-	83, 81	Deviation from linearity near top of load - extension curve	109	88
18	30	-	83, 78	No load drop prior to failure		
19	35	82, 81	-	Deviation from linearity	105	94
20	40	84, 85	-	Load drop prior to failure	104	98

NOTE: Linearity in this context refers to the major portion of the load-extension curve and does not imply a perfect straight line plot.



TABLE 7

CAST NUMBER	EXCESS CURE TIME AT 448°K (Hrs/ks)	FRACTURE SURFACE WORK, $\gamma$ (Jm <sup>-2</sup> )	TENSILE YOUNG'S MODULUS $E_T$ (x10 <sup>-9</sup> (Nm <sup>-2</sup> ))	FRACTURE TOUGHNESS $K_{IC}$ (x10 <sup>-6</sup> (Nm <sup>-3/2</sup> ))	TRANSITION TEMP. (°C) (TMA)
12, 13, 14	0/0	200	1.97	.9	155-165
22	0.5/1.8	187	*1.99	.86	157-167
23	1.0/3.6	230	*1.96	.95	158-169
28	1.6/5.76	218	*1.97	.93	160-168

\* Single Values

APPENDIX 1

Concepts of Fracture Mechanics

A.1. To provide a background to the detailed description of the technique of fracture testing employed in this work, it is necessary to define certain terms and to explain some concepts of fracture mechanics.

A.1.1. Griffith's Analysis

The original concepts of fracture mechanics were expounded by Griffith<sup>(25)</sup> in 1920. He introduced the term 'fracture surface energy' and was able to deduce from thermodynamic principles an equation relating the fracture stress of a pre-cracked body to the dimensions of the crack, the modulus of elasticity of the material and the fracture surface energy. Essentially he was equating the release of stored strain energy in the whole system during crack growth to the work of creation of new fracture surface (assuming no other energy absorbing agencies were operating). The fracture surface energy,  $\gamma$ , was defined as the work required to create unit area of fracture surface.

Griffith's equation for a sharp crack in an infinite plate of unit thickness and with stresses applied at the external boundaries of the plate is:

$$T_F = \sqrt{\frac{2E\gamma}{\pi C}} \quad \text{for plane stress situations} \quad (A1)$$

$T_F$  = fracture stress (nominal)

E = Young's modulus

C = Crack length

This equation has been superceded by many, more sophisticated analyses (see 31) but the ideas of Griffith still form the basis of many experimental investigations. The interpretation of  $\gamma$  has been changed, but the energy approach to fracture criteria is still very popular.

### A.1.2. Irwin's Analysis

The development of classical fracture mechanics continued with the work of Irwin<sup>(30)</sup> who employed mathematical descriptions of the state of stress in the vicinity of a crack tip (see also (100)) to evolve the concepts of critical stress intensity factor,  $K_C$ , and the critical strain energy release rate,  $G_C$ .  $G_C$  represented the decrease in strain energy of the cracked system (of unit thickness) for a unit increase in crack length.

The dependence of the near-tip stresses on a factor of the form

$$f = T\sqrt{\alpha C} \quad (A2)$$

(where  $T$  = nett section stress,  $\alpha$  is a geometry dependent factor and  $C$  = crack length)

was recognised by Irwin and he coined the term 'stress intensity factor',  $K$  ( $= T\sqrt{\pi C}$  for the infinitely sharp crack in an infinitely wide plate). A critical value of  $K$  ( $= K_C$ ), it was suggested, corresponds to the onset of unstable failure.  $K$ , although proportional to the limiting value of  $K_T$ , the elastic stress concentration factor, should not be confused with  $K_T$ . It should also be noted that the criterion for failure (in terms of failure stress) is not determined by equating the  $G_C$  term to a surface energy term. Irwin pointed out that  $G_C$  contains contributions from all dissipative agencies operating during crack advancement. This aspect is related to the effects of plastic deformation considered in section A.1.4.

A rigorous analysis of many geometries of cracked bodies and different modes of crack propagation<sup>(101)</sup> shows that  $K$  has the general form

$$K = T\sqrt{\alpha \pi C} \quad (A3)$$

where  $\alpha$  is the geometry dependent factor.

The  $G_C$  concept arises as a natural consequence of Irwin's analysis, with  $G$  and  $K$  being related by the equations

$$\begin{aligned} G &= K^2/E \quad \text{in plane stress} \\ G &= K^2(1-\nu^2)/E \quad \text{in plane strain} \end{aligned} \quad (A4)$$

where  $\nu$  = Poisson's ratio

Summarising, at fracture

$$K = K_C \quad \text{and} \quad G = G_C$$

and for the simple case of an 'elastic' crack in an infinitely wide plate we have

$$T_{FI}^2 \pi C = EG_C \quad (A5)$$

(plane stress)

where the subscripts F and I refer to 'fracture' and 'Irwin' respectively.

As previously indicated, the value of  $K_C$  is dependent upon the geometry of the system and the mode of crack displacement as well as the material identity. The three basic modes of crack propagation (Fig. 1) result in the  $K$  term being subscripted  $K_I$ ,  $K_{II}$  and  $K_{III}$ . Reference (101) provides a comprehensive analysis of  $K$  v geometry relationships. Consideration of the geometry - dependence of  $K$  and  $K_C$  has led to the conclusion that there exists a lower limiting value of  $K_C$ , designated  $K_{IC}$  corresponding to a truly plane strain fracture mode. In such circumstances, the deformation across the majority of a crack plane is highly constrained i.e. a tri-axial state of stress exists. The  $K_{IC}$  value is regarded as a material characteristic and can be used for prediction of critical flaw sizes in practical structural situations.

#### A.1.3. The fundamental criterion for fracture

\* It is reasonable to argue that a necessary condition for crack propagation, in the case of a sharp elastic crack, is that the maximum tensile stress level at its tip must be equal

to the cohesive strength of the material. An equation relating fracture strength, the value of  $\gamma$  corresponding to the 'elastic' rupture of atomic bonds ( $\gamma_s$ ),  $E$  and  $C$  can be derived<sup>(32)</sup> and has the form

$$T_f = \sqrt{\frac{2E\gamma_s}{\pi C}} \cdot P/3a_0 \quad (A6)$$

where  $P/a_0$  is the ratio of crack tip radius to equilibrium atomic separation in the unstrained material. The derivation of this equation assumes that the maximum stress at the tip of a crack can be equated to the theoretical cohesive strength of the material and that terms such as 'equilibrium atomic separation' are meaningful (see also section A.2).  $T_f$  in equation (A6) can be regarded as the applied stress (gross) required to cause complete fracture of the specimen provided  $P$  remains constant (or decreases) or if  $C/P$  remains constant during crack propagation.

It is possible to draw some similarities between the above equations, particularly equations (A1) and (A5) and conclude that  $G_C = 2\gamma_G$  (subscript  $G$  referring to Griffith's analysis). The other obvious similarity between equations (A1) and (A6) has been noted<sup>(30,102)</sup> with the implication that  $p = 3a_0$  is a lower limit of the effective radius of an elastic crack tip. This is because  $T_f$  cannot tend to zero as  $P$  tends to zero. Both equations (A1) and (A6) must be satisfied for unstable crack propagation since fracture must involve the severing of atomic bonds and the free energy of the system must be lowered.

\* It should be emphasised that all the above equations arise from the assumption of perfect elasticity up to the point of fracture, which also assumes the yield stress to be greater than the fracture stress.

A.1.4. Plastic deformation during crack propagation

Since materials do not usually fracture in a completely brittle manner, it is necessary to assess the effect of plastic deformation near the crack tip during propagation of a crack. The significance of plastic deformation was first appreciated by Orowan et al<sup>(34,35,36)</sup> and by Irwin<sup>(30)</sup>. It was realised that plastic work is performed in addition to the release of elastic work stored in a stressed system undergoing crack advancement. It is evident that the amount of plastic work is of paramount importance since it may be dependent on strain-rate and environment, as well as the identity or morphological condition of the material.

A simple approach to crack-tip plasticity has been considered by modifying equation (A1) thus (30)

$$T_m = \sqrt{\frac{2E(\gamma_G + \gamma_p)}{\pi C}} \approx \sqrt{\frac{2E\gamma_p}{\pi C}} \quad \text{for } \gamma_p/\gamma_G \gg 1 \quad (A7)$$

$\gamma_p$  represents the energy consumed by plastically deforming material at and around the tip of the moving crack (hence the subscript 'm'). Most measured values of  $\gamma$  are far in excess of those predicted by consideration of interatomic bonding forces. The approximation used in equation (A7) is therefore realistic. As to what constitutes crack movement, there are two ways of considering the problem. Although it is reasonable to expect crack growth to be associated with simple bond rupture, there are situations where the development of a deformed region ahead of the 'true' crack constitutes an effective lengthening of the crack. For example, the formation of crazed regions ahead of crack tips in thermoplastics can be characterised mathematically and related to fracture toughness values. The possibility of strain rate dependence of  $\gamma_p$  is obvious, particularly when dealing with visco-elastic materials.

Plastic deformation may be regarded as a blunting process<sup>(103)</sup>. This effectively relaxes tip stresses (see ref. 32, p. 56) and results in a higher value of fracture toughness. The simple modification of the Griffith equation can, again according to Tetelman and McEvily<sup>(32)</sup> be applied only when the yield stress of the structure exceeds the cohesive strength of the material. The dimension of the deformed region, relative to the overall dimension of the cracked body, is of major importance and provided that gross yielding has not occurred the modified Griffith approach is adequate at least for materials testing and quality assessment purposes.

A more sophisticated approach to the problem (32 p.57) has been suggested. Intrinsically tough materials, or those tested at elevated temperatures have yield strengths less than their cohesive strengths. In the absence of appreciable strain-hardening, the stresses at the tip of a crack cannot greatly exceed the yield stress. Hence, sufficient elastic stress to break atomic bonds cannot be achieved in the initial deformation stages. This immediately rules out the previously considered criterion for failure based on the elastic or elastic/pseudo-plastic concept. It was therefore suggested that localised plastic strains are the cause of crack growth and hence that fracture is plastically induced. Low values of yield stress relative to cohesive strength suggest that relatively large plastic zones should exist at the crack tip.

The characterisation of the plastic zone, in mathematical and geometric terms has been the subject of much research. Most notable treatments are those of Irwin (the crack-border re-positioning concept)<sup>(104, 105)</sup>, Dugdale<sup>(47)</sup> and Bilby, Cottrell and Swinden<sup>(106)</sup>. Out of their and other people's efforts

have come various relationships between the geometric characteristics of the crack tip, the concept of critical crack-opening displacement (C.O.D.) as a material parameter and the demonstration of compatibility between the various models of crack tip plasticity (see 107 for example) and classical fracture mechanics.

A.2. Assessment of classical fracture mechanics

The applicability of the Griffith (purely elastic) concept of fracture surface energy to real situations is, by the nature of its development, somewhat doubtful. This is not simply because real materials are rarely Hookean up to the point of fracture, but because there are aspects of the Griffith theory which can be criticised on a fundamental level. For example, Sih<sup>(108)</sup> has pointed out that Griffith's analysis used an elementary glass surface tension measurement, extrapolated to room temperature, in order to estimate the value of  $\gamma_G$ . The original sharp crack problem considered by Inglis<sup>(26)</sup> (upon which Griffith based his argument) involved non-uniform surface tractions. Thus, Griffith applied a simple, uniform surface tension in a situation which could not accommodate such a concept. Indeed, Sih also points out that the Griffith equation yields very similar fracture strength v. flaw size curves to those predicted by an equation derived purely from considering the equilibrium of an elliptical cavity in a fluid, the boundary of the cavity being subject to uniform surface forces.

The above comments are not meant to imply that the form of the Griffith equation is wrong, but that the concept of fracture surface energy is loosely defined. An apparent explanation for the observed discrepancy between  $\gamma_s$  and  $\gamma_p$  ( $\gamma_s$  being the predicted and  $\gamma_p$  the measured values i.e.),



according to Sih, is that  $\gamma_s$  has been assumed equivalent to  $\gamma_G$  and that one may equate macro tip-stresses with micro-stress at fracture. The question arises whether or not it is valid to make such assumptions of equivalence. Sih has derived an equation which predicts a numerically correct comparison of  $\gamma_s$  and  $\gamma_p$ , without resorting to these assumptions and denounces the 'usual' method of approach as being based upon false reasoning.

Of course, the usefulness or reliability of a parameter must be determined in proper context. Fracture mechanics parameters can be employed in more than one way. Values of fracture toughness are used in design against brittle fracture. Knowing  $K_{IC}$  for the particular geometry and loading condition, failure loads or allowable defect sizes can be predicted. The fracture parameter may also be used as a quality control device. Even in situations where materials break after general yield in a fracture test, crack opening displacement, for example, has been suggested<sup>(109)</sup> as a useful quality control parameter because only small amounts of material may be needed.

The characterisation of the plastic zone by models such as that proposed originally by Dugdale represents an attempt to be more realistic as far as establishing criteria for fracture is concerned. Recent work<sup>(46,48)</sup> has shown that Dugdale type models incorporating the constant C.O.D. criterion can more adequately describe the fracture of some polymeric materials than the constant  $K_C$  criterion can. This view is opposed, to some extent, by Heald et al<sup>(107)</sup> in that  $K_C$  can be shown to be compatible with post-yield fracture mechanics described by the Dugdale model.

Another recent fracture parameter of consequence is an engineering oriented parameter called the critical strain-energy density<sup>(108,112)</sup>. In this case a critical value of the local strain energy density supposedly determines crack instability and the value is regarded as a material constant. Where this concept diverges from that of  $K_C$  or  $G_C$  is that it has a vector property. This enables the criterion to be more readily applied in structural situations.

The extension of fracture mechanics to situations where test pieces have suffered general yielding is currently a topic of considerable interest. Apart from the use of C.O.D. measurements, the J-integral concept has been suggested as an alternative to C.O.D.<sup>(110)</sup>. The J-integral is equivalent to the change in potential energy when a crack extends and is conceptually equivalent to G. The advantage of using J is that non-linear materials can be considered. It may be that J and C.O.D. are closely related, but  $J_{IC}$ , like  $K_{IC}$ , has no physical characteristic which is easily visualised<sup>(111)</sup>. Both C.O.D. and J have their critics, e.g. reference (113). The biggest problem is likely to be the decision as to which of these imperfect parameters will be of most use to the engineer.

## APPENDIX 2

### Machining of Test Specimens

#### A.2.1. Tapered double-cantilever cleavage beam specimens

The TDCB fracture toughness specimens were cut from the cured slabs of resin, using a bandsaw. The loading-pin holes and jig mounting holes were drilled with the aid of a template and the grooves were machined using a 152mm diameter x 1.58mm thick milling cutter on a horizontal milling machine. A special jig (Fig. A1) was used to ensure the correct alignment of the grooves. The swallow-tail lead-in to the fracture plane was produced by the profile of the milling cutter. No post-machining heat treatment of any specimens was carried out. Cutter rpm and table feeds were arranged such that the effective cutter-work surface relative speed was approximately  $4.2 \text{ mm.s}^{-1}$  and all machining was done without lubricant.

#### A.2.2. Tensile test specimens

The tensile test specimens were cut manually on an air-driven router, using a steel former. No post-machining heat treatment was given, and no lubricant applied.

#### A.2.3. Compression test pieces

Specimens were cut to approximately 14mm x 7mm x 6mm (slab thickness) and milled 'square' to nominally 12 x 6 x 6mm. No post-machining heat treatment was given and no lubricant employed.

APPENDIX 3

Statistical Analysis of Fracture Data and Examples of  
Fracture Surface Work Calculation

A.3.1. In order to compare the behaviour of the practical fracture-toughness specimens with theoretical expectations and to compare the three methods of evaluating  $\gamma$ , it was decided that the test data be analysed both statistically and by a manual graphical method. Average values of  $\gamma$  were obtained by treating the test data in the following ways: →

- (a) All fracture test data points from individual specimens were fitted to straight lines (by the least squares method) for the Berry and Irwin-Kies analyses. This allowed a value of  $\gamma$  to be obtained for each test specimen. The results were compared with values of  $\gamma$  obtained by manually plotting the various graphs for each specimen.
- (b) Selected test data points from individual specimens were fitted to straight lines by the least squares method. Selection of data was achieved by ignoring figures apertaining to very short ( $\sim 30\text{mm}$ ) or very long ( $\sim 120\text{mm}$ ) crack lengths where the desired constancy of the  $dR/dC$  term in the Irwin-Kies equation is least likely to be found. The results were compared with those from (a) above. The same criterion of selection was used for the data treated by Berry's equations. (A comparison with manually plotted data from (a) can also be made).
- (c) All fracture test data points from all like-specimens were fitted to 'combined' straight lines by the least squares method. The resulting value of  $\gamma$  for each set of like-specimens was compared with the values obtained by methods outlined in (a) and (b). Manual graph plotting of 'combined' straight lines was also done. The results of analyses (a) and (b) are shown in table A1. The results for the analysis (c)

are summarised in table A2.

A.3.2. It can be argued that it is inherently better to consider individual specimens, so that variations from cast to cast and test to test are realistically included in the result. This is so, provided that adequate data can be generated from a single test. Since most of the resin systems investigated exhibited a stick-slip (unstable) mode of crack propagation, with fairly large crack-jumps (under the prevailing test conditions), it can also be argued that (c) above is likely to provide a more realistic average, if batch and test variations are shown to be small.

The main conclusions from a study of tables A1 and A2 are:

- (1) As specimen  $\gamma$  increases, the error in the result tends to increase. This is most likely to be the result of having fewer crack arrest points per specimen in the case of tough resins, combined with the fact that only two specimens from casts 19 and 20 were considered in the analysis. In fact, only 'combined' results for these casts were considered realistic because of the comparative lack of data.
- (2) Generally, there is little scatter in the results, regardless of the method of plotting, except at the toughest resin compositions (casts 19 and 16 in particular).
- (3) Differences between the resins, based on  $\gamma$  calculations, are significant.

A.3.3. Fracture Surface Work Calculations - Examples

Since data for tapered fracture toughness specimens 17B, 20A and 20B are given in tables 2-5, two of these specimens have been chosen to illustrate the evaluation of fracture surface work,  $\gamma$ . All load values are Newtons and all lengths are expressed as decimal fractions of a metre (area = m<sup>2</sup>).

A.3.3.1. Specimen 17B

by Berry's method

Referring to section 7.2.2. for notation and table 3, we have

$$\begin{aligned} \gamma &= d(\log f/\delta) / d(\log c) \times d(f\delta/w) / d(c) \times .25 \\ &= \frac{1.33 \times 235}{4} = 78 \text{ Jm}^{-2} \end{aligned}$$

by Irwin-Kies equation:

Referring to section 7.2.3. for notation and to table 4, we have

$$\begin{aligned} \gamma &= f^2 / 4w \times dR/dc \\ &= \frac{(40.4)^2 \times 338 \times 10^{-6}}{4 \times 2.1 \times 10^{-5}} \\ &= 65.7 \text{ Jm}^{-2} \end{aligned}$$

by Gurney's method

Referring to section 7.2.4. and table 5, we have

$$\begin{aligned} \gamma &= \Delta(\text{Area under load extension graph}) \text{ m}^2 \\ &\times \text{Work conversion factor} \text{ J per m}^2 \\ &\times \frac{1}{(\text{Area of fracture surface}) \text{ m}^2} \end{aligned}$$

Work conversion factor (per m<sup>2</sup> of test chart)

$$\begin{aligned} &= \text{Newtons (per m of load scale on test chart)} \\ &\times \text{m of crosshead movement (per m of extension scale on test chart)} \\ &= \times \text{J (per m}^2 \text{ of test chart)} \end{aligned}$$

$x$  varies according to the full scale load and the ratio crosshead speed/chart speed.

In this case (17B), for the fracture event marked by an asterisk in table 5,

$$\begin{aligned}\gamma &= \frac{14.4 \times 10^{-4} \times 10.2}{2.54 \times 10^{-5}} \\ &= 57.7 \text{ Jm}^{-2}\end{aligned}$$

(Note that this method provides the lowest value of  $\gamma$ . This point is discussed in Chapter 12).

#### A.3.3.2. Specimen 20A

Repeating the exercise for specimen 20A we have:

for Berry's method,

$$\gamma = \frac{1.33 \times 900}{4} = 299 \text{ Jm}^{-2}$$

for Irwin-Kies' analysis,

$$\gamma = \frac{(63.1)^2 \times 392 \times 10^{-6}}{4 \times 2.0 \times 10^{-3}}$$

$$= 195 \text{ Jm}^{-2}$$

for Gurney's analysis, in this case the work conversion factor is 4.08 J (per m<sup>2</sup> of test chart),

$$\therefore \gamma = \frac{26.6 \times 10^{-4} \times 4.08}{7.8 \times 10^{-5}}$$

$$= 139 \text{ Jm}^{-2}$$

TABLE A1 Statistical Analysis of Fracture Data - Individual Specimens

CAST NUMBER	IRWIN-KIES EQUATION		NUMBER OF SPECS. FOR MEAN CALC. 'N		BERRY'S EQUATION		TEXT PARA. REFERENCE
	MEAN $\bar{Y}$ ( $J_m^{-2}$ )	STANDARD ERROR	(IRWIN-KIES)	(BERRY)	MEAN $\bar{Y}$ ( $J_m^{-2}$ )	STANDARD ERROR	
15,17,21	68.2	2.9(7)	5	5	70.5	4.7	A.3.1.(a)
	67.8	3.0	5	5	65.8	4.1	A.3.1.(b) STATISTICAL
12,13,14	206.1	2.9(5)	5	6	250.3	14.9	A.3.1.(a) LINE
	203.3	2.4(5)	5	6	250.3	14.9	A.3.1.(b) FITTING
16,18	405.2	27.2	4	4	<b>394.0</b>	18.6	A.3.1.(a)
	342.8	8.3	4	4	368.5	32.1	A.3.1.(b)
15,17,21	69.9	2.1	5	5	70.6	2.5	- MANUAL
12,13,14	202.1	2.2	5	6	233.7	16.3	- LINE
16,18	340.3	7.9	4	4	416.5	25.9	- FITTING



TABLE A2 Statistical Analysis of Fracture Data - Combined Specimens

CAST NUMBER	BERRY'S EQUATION			IRWIN-KIES EQUATION		$\gamma$ ( $J_m^{-2}$ )		NUMBER OF SPECIMENS
	CORRELATION COEFF. OF $\log f / \delta$ v. $\log c$	CORRELATION COEFF. OF $f \delta / w$ v. $c$	$\gamma$ ( $J_m^{-2}$ )	CORRELATION COEFF. OF R v. $c$	$\gamma$ ( $J_m^{-2}$ )	BERRY'S METHOD	IRWIN-KIES EQUATION	
15,17,21	.9889	.9654	72.9	.9972	70.5	88.4	61	5
12,13,14	.8598	.9072	197.2	.99	205.6	191.2	200	5
16,18	.9995	.9889	396	.9977	391.9	308-362	344	4
19	.9998	.9455	787	.9981	514.9	880	514	2
20	.9996	.9874	275	.9976	200.4	299	212	2
	STATISTICAL LINE FITTING				MANUAL LINE FITTING			

APPENDIX 4

Notes on the Calculation of Young's Moduli and Compressive Proof Stress

A.4.1. Tensile Young's modulus,  $E_T$

To illustrate the method, a typical example of stoichiometric composition of Epikote 828/Epikure DDM is referred to.

Fig. 16 shows how both the secant modulus on first extension and the linear elastic modulus after relaxation/recovery cycling can be evaluated from the same test result. Since this particular composition of resin was one of the most visco-elastic, the example illustrates a worst case with regard to obtaining a reliable modulus value. It is evident from Fig. 16 that, on first extension, considerable non-linearity exists. A secant modulus is therefore most appropriate. By allowing the material to undergo a relaxation and recovery cycle (as described in section 9.2.2.), a linear load-extension curve could be obtained.

The moduli were evaluated in the following manner;

$$\begin{aligned} \text{Modulus, } E_T, &= \frac{\text{Load/Area of cross section of gauge length}}{\text{Increase in gauge length/original gauge length}} \\ &= \frac{f \cdot l}{A \cdot \Delta l} \end{aligned}$$

when  $f$  is in N,  $l$  and  $\Delta l$  in m,  $A$  in  $m^2$ ,  $E_T$  is in  $N.m^{-2}$ .

For the Instron 0-10% strain gauge extensometer (Type G-51-11-M-A) we have, referring to Fig. 16,

$$E_T = \frac{f \times 25 \times 10^{-3}}{A \times \text{chart length OA} \times \text{extensometer factor}}$$

The extensometer factor varies with the sensitivity level selected for the test and in this case has a value of .002, when chart length is expressed in m.

∴ for the example shown in Fig. 16,

$$\begin{aligned} \text{1st Secant } E_T &= \frac{(200 \times 9.81) \times (25 \times 10^{-3})}{(.624 \times .661 \times 10^{-4}) \times (28 \times 10^{-2}) \times (.002)} \\ &= 2.12 \times 10^9 \text{ N.m}^{-2} \end{aligned}$$

Similarly, the linear  $E_T$  value was,

$$\begin{aligned} \text{Linear or relaxation/recovery } E_T &= \frac{(200 \times 9.81 \times (25 \times 10^{-3}))}{(.624 \times .661 \times 10^{-4}) \times (25 \times 10^{-2}) \times (.002)} \\ &= 2.38 \times 10^9 \text{ N.m}^{-2} \end{aligned}$$

#### A.4.2. Compressive Young's modulus, $E_C$

In these cases, as for the determination of  $E_T$ , two values of Young's modulus were obtained from one specimen, by taking a "first compression" value and a "relaxation/recovery" value. The difference between the compressive and tensile moduli, in terms of the method of evaluation, is that no extensometer device was used for measuring the compressive strain. Instead, a correction for the machine and load cell deflections was applied. The value of the correction was determined by first bringing the two loading plattens into contact. Then the crosshead was driven against the load cell until a specified load was reached while simultaneously recording the load-displacement graph on the chart recorder. In this way the appropriate chart length equivalent to the machine deflection at various loads could be determined and subsequently subtracted from the chart lengths measured in real test situations. In all cases, the correction employed when evaluating a compressive modulus was that appropriate to the full scale load calibration, crosshead speed and chart speed used in the actual test. This ensured that machine characteristics were the same for both the calibration without a specimen and for the test.

In this case we have:

$$\text{Compressive Modulus, } E_C = \frac{f \cdot l}{A \cdot \Delta l}$$

with the same notation as previously. ( $\Delta l$  is a decrease in length, corrected for machine deflection).

Referring to Fig. 17 we have:

$$\begin{aligned} \text{1st Tangent Modulus, } E_C &= \frac{(201 \times 9.81) \times (.0117)}{(.449 \times 10^{-4}) \times (2.1 \times 10^{-4})} \\ &= 2.43 \times 10^9 \text{ Nm}^{-2} \end{aligned}$$

and linear or relaxation/recovery

$$\begin{aligned} \text{modulus, } E_C &= \frac{(201 \times 9.81) \times (.0117)}{(.449 \times 10^{-4}) \times (1.55)} \\ &= 3.3 \times 10^9 \text{ Nm}^{-2} \end{aligned}$$

#### A.4.3. Compressive 1% Proof Stress Calculations

The necessity of correcting for machine deflection also applied to proof stress calculation in a slightly different context than above. In this instance, some estimate of the machine deflection (in terms of chart length) was necessary in order to "offset" the proof stress line by the correct amount. (See Fig. 25). In fact, it was decided to draw the proof stress line at a location corresponding to 2% strain (uncorrected). Because of the variability of the machine correction with applied load, the actual proof strains vary from about 1.3 to 1.5%.

APPENDIX 5

Tabulated Data for Cross-Reference with  
Graphical Figures

TABLE A3 Effect of DDM Content on, and Comparison of Gurney's, Berry's and  
Irwin-Kies' Analyses for Evaluation of Fracture Surface Work

	DDM CONTENT (PARTS/100 RESIN)	20	27	30	32	33.4	35	40
FRACTURE SURFACE WORK  ( $J_m^{-2}$ )	GURNEY'S METHOD	64	102	162	-	-	204	130
	BERRY'S METHOD	72.9	197.2	396	-	-	787	275
	IRWIN-KIES' METHOD	70.5	205.6	391.9	399	604	514.9	200.4

STATISTICAL LINE  
FITTING,  
'COMBINED'  
SPECIMENS

All cured 3.6 Ks at 373°K and 7.2 Ks at 373 / 448°K

0.1mm.min<sup>-1</sup> crosshead speed Room Temperature.  
See also Appendix 3 and Fig 15.

TABLE A4 Tensile and Compressive Young's Moduli v. DDM Content

	DDM CONTENT (PARTS/100 RESIN)	20	27	30	35	40
TENSILE YOUNG'S MODULUS $\times 10^{-9}(\text{Nm}^{-2})$	NORMAL METHOD	3.56	2.10	*1.99	*2.18	*2.58
	RELAXATION/ RECOVERY METHOD	3.51	2.38	-	2.57	2.79
COMPRESSIVE YOUNG'S MODULUS $\times 10^{-9}(\text{Nm}^{-2})$	NORMAL METHOD	4.18	2.82	2.81	3.06	3.19
	RELAXATION/ RECOVERY METHOD	5.26	3.35	3.52	3.68	3.6

All cured 3.6 Ks at 373°K and 7.2 Ks 373 / 448°K

\* .0017 mms<sup>-1</sup> crosshead speed  
Others at .017 mms<sup>-1</sup> Room Temperature  
See Figs. 18 and 19.

TABLE A5 Fracture Toughness,  $K_{IC}$ , Compressive Yield and  
1% Proof Stress v. DDM Content

DDM CONTENT (PARTS/100 RESIN)	20	27	30	35	40
* $K_{IC}$ $\times 10^{-6} (Nm^{-3/2})$	.66	0.9	1.25	1.47	0.9
COMPRESSIVE YIELD STRESS $\times 10^{-6} (Nm^{-2})$	125	-	109.5	105	104
COMPRESSIVE 1% PROOF STRESS $\times 10^{-6} (Nm^{-2})$	123.5	85	88	94	97.5

All cured 3.6 Ks at 373°K and 7.2 Ks at 373 / 448°K

\* .0017mms<sup>-1</sup> crosshead speed  
Others at .017mms<sup>-1</sup> Room Temperature  
See Figs. 21 and 22.



TABLE A6 Compressive Characteristics v. DDM Content

DDM CONTENTS (PARTS/100 RESIN)	20	27	30	35	40
YIELD DROP (N)	510	0	0	3.5	15
RELAXATION FROM 1800 N (N)	23	112.5	95	75	15
POST-YIELD COMPRESSIBILITY (mm CHART)	530	345	360	445	478

All cured 3.6 Ks at 373°K and 7.2 Ks at 373 / 448°K

.0017 mms<sup>-1</sup> crosshead speed Room Temperature.  
See Fig. 24.

TABLE A7 Fracture Surface Work,  $\gamma$ , v. Gel Temperature for Three DDM Contents

INITIAL GEL TEMPERATURE (°K)		323	333	348	373
Values for various DDM contents (Parts/100 Resin) ( $\gamma$ in $\text{Jm}^{-2}$ )	20 PARTS DDM	72.3	85*	89.4	69.9
	27 PARTS DDM	225.5	239	274	202
	40 PARTS DDM	255.5	280.5	282*	218.5

\* Single values. All others are averages of at least two figures, obtained by Irwin-Kies' equation, manual line-fitting of individual specimens. (See Appendix 3).  
.0017  $\text{mms}^{-1}$  crosshead speed.  
See Fig. 26.

TABLE A8 Compressive Characteristics v. Gel Temperature

INITIAL GEL TEMPERATURE ( $^{\circ}$ K)		323	333	348	373
YIELD DROP (N)	20 PARTS DDM	407	627	663	510
	27 PARTS DDM	0	0	0	0
	40 PARTS DDM	165	180	165	150
RELAXATION FROM 1800 N (N)	20 PARTS DDM	20-40	40	40-60	23
	27 PARTS DDM	170	119	115	112.5
	40 PARTS DDM	42.5	43.5	36.5	39
POST-YIELD COMPRESSIBILITY (mm CHART)	20 PARTS DDM	548	545	566	530
	27 PARTS DDM	255	283	297	345
	40 PARTS DDM	485	492	498	478

.017mm $s^{-1}$  crosshead speed.  
See Fig. 27.

TABLE A9 Compressive and Tensile Young's Moduli v. Gel Temperature

INITIAL GEL TEMPERATURE (°K)		323	333	348	373
Tensile Young's Modulus $\times 10^{-9} (\text{Nm}^{-2})$	20 PARTS DDM	3.5	3.49	3.52	3.37
	27 PARTS DDM	2.0	2.12	2.13	2.10
	40 PARTS DDM	2.58	2.41	2.56	2.58*
	20 PARTS DDM	3.59	3.56	3.74	3.55
	27 PARTS DDM	2.37	2.36	2.35	2.38
	40 PARTS DDM	2.72	2.65	2.79	2.79
Compressive Young's Modulus $\times 10^{-9} (\text{Nm}^{-2})$	20 PARTS DDM	3.81	4.17	3.94	4.18
	27 PARTS DDM	2.58	2.88	2.88	2.82
	40 PARTS DDM	3.22	3.28	3.20	3.12
	20 PARTS DDM	4.12	4.35	4.03	5.26
	27 PARTS DDM	3.21	3.15	3.16	3.35
	40 PARTS DDM	3.45	3.49	3.46	4.14

\*  $.0017\text{mms}^{-1}$  crosshead speed.  
Others at  $.017\text{mms}^{-1}$  See Fig. 28

TABLE A10 Fracture Surface Work,  $\gamma$ , and Fracture Toughness,  $K_{IC}$ , v. Crosshead Speed

CROSSHEAD SPEED (mm.s <sup>-1</sup> )		.017	.17	1.7
$\gamma$ (Jm <sup>-2</sup> )	20 PARTS DDM	61	-	36*
	27 PARTS DDM	200	156	126
	30 PARTS DDM	308-362	368*	313*
	32 PARTS DDM	399	-	325*
	35 PARTS DDM	514		320-370*
$K_{IC}$ (Nm <sup>-3/2</sup> ) x10 <sup>-5</sup>	27 PARTS DDM	9.0	8.1	7.3

All cured 3.6 Ks at 373°K and 7.2 Ks at 373 / 448°K  
(See Figs. 29 and 31).

\* Single values.

TABLE A11 Tensile Young's Modulus,  $E_T$ , and Tensile Strength v. Crosshead Speed

CROSSHEAD SPEED (mm.s <sup>-1</sup> )	.017	.17	1.7
$E_T$ $\times 10^{-9}$ (Nm <sup>-2</sup> )	1.9-2.05	2.06-2.14	2.08-2.22
TENSILE STRENGTH $\times 10^{-7}$ (Nm <sup>-2</sup> )	7.1	7.2	7.25

All cured 3.6 Ks at 373°K and 7.2 Ks at 373 / 448°K

All 27 parts DDM.  
See Figs. 30 and 32.

Table A12 Fracture Test Primary Data

CAST AND SPECIMEN NO.	LOAD f (N)	DEFLECTION (m) x 10 <sup>4</sup>	CRACK PLANE WIDTH w (m) <sup>3</sup> x 10 <sup>3</sup>	CRACK LENGTH C (m) x 10 <sup>3</sup>
12A	63.0	5.2	2.08	32.5
	59.0	9.0		50.6
	60.0	16.9		79.0
	62.0	33.4		13.31
13A	63.0	6.6	2.16	36.5
	61.0	11.4		57.0
	62.0	22.0		92.0
13B	74.5	3.4	2.13	18.2
	66.5	5.6		29.9
	61.5	9.8		48.9
	61.0	19.0		83.2
	55.5	36.0		155.0
14A	63.0	6.6	2.16	39.0
	61.0	11.2		59.0
	62.5	22.0		93.0
14B	66.5	6.8	2.18	36.8
	61.5	12.6		62.3
	64.5	25.0		102.5
15A	47.5	2.0	2.03	20.0
	43.5	3.0		30.0
	40.5	4.0		40.0
	38.5	5.0		50.0
	37.5	6.0		60.0
	37.5	7.2		70.0
	37.5	8.4		80.0
	40.5	9.6		-
	42.0	11.2		92.0
	39.3	11.7		102.0
	40.8	12.7		106.0
	40.3	13.5		113.0
	40.3	14.3		119.0
	40.0	15.0		125.0
40.0	16.0	132.0		
40.0	17.2	141.0		
15B	42.0	3.5	1.96	38.0
	41.0	4.6		51.0
	41.0	5.1		55.0
	40.0	5.4		59.0
	39.0	5.7		61.0
	40.0	6.1		65.0
	39.0	6.4		67.0
	40.0	7.2		69.0

Table A12 (Cont.)

CAST AND SPECIMEN NO.	LOAD $f$ (N)	DEFLECTION (m) $\times 10^4$	CRACK PLANE WIDTH $w$ (m) $\times 10^3$	CRACK LENGTH $C$ (m) $\times 10^3$
16A	101.1	2.5	2.05	1.25
	85.6	5.3		2.5
	80.0	12.7		4.95
	82.5	34.3		10.65
16B	106.2	3.0	2.05	14.0
	84.4	6.4		30.0
	76.3	14.8		61.0
	80.0	40.0		128.0
17A	75.0	5.0	2.13	33.0
	41.0	6.8		62.0
	42.0	7.4		67.0
	42.0	8.4		75.0
	42.0	9.2		80.0
	41.0	10.4		90.0
	40.5	11.4		96.0
	42.0	12.4		100.0
	41.0	13.2		108.0
	41.5	14.0		114.0
	41.0	15.2		122.0
	41.5	16.4		130.0
38.5	17.2	144.0		
17B	39.5	9.0	2.1	84.5
	42.0	10.4		90.5
	39.5	10.8		-
	40.0	11.6		102.0
	40.0	12.4		107.5
	40.5	13.2		113.5
	40.0	14.0		120.0
	40.0	14.6		125.0
	42.5	16.4		130.0
18A	107.5	2.6	2.21	12.0
	90.0	5.2		25.0
	77.5	11.6		50.0
	80.0	29.8		100.0
18B	110.6	2.8	2.12	13.0
	83.8	6.0		28.5
	76.9	14.2		55.5
	79.4	36.6		116.0
19A	137.5	6.2	2.12	20.0
	110.0	21.4		58.5
19B	86.0	3.2	2.13	17.0
	78.0	5.0		26.0
	123.0	15.2		41.5



Table A12 (Cont.)

CAST AND SPECIMEN NO.	LOAD $f$ (N)	DEFLECTION (m) $\times 10^4$	CRACK PLANE WIDTH $w$ (m) $\times 10^3$	CRACK LENGTH $C$ (m) $\times 10^3$
20A	66.5	3.0	2.0	21.0
	68.5	3.6		24.0
	65.0	4.5		30.0
	63.0	5.7		37.0
	55.0	6.6		45.0
	62.0	8.6		50.0
	60.5	12.0		65.0
	62.0	17.7		84.5
	65.0	27.6		116.0
20B	70.0	4.1	2.04	27.0
	60.0	4.8		34.0
	63.5	6.1		38.0
	63.0	8.0		48.0
	63.0	11.4		61.0
	63.5	16.8		81.0
	67.5	26.3		111.0
21A	52.5	3.3	2.03	28.0
	47.0	4.0		34.0
	44.0	4.5		41.0
	40.0	5.3		51.0
	40.0	5.9		56.0
	40.0	6.5		60.0
	41.0	7.3		65.0
	41.0	7.9		70.0
	41.0	8.6		75.0
	41.0	9.2		80.0
	41.0	10.0		85.0
	42.0	10.9		90.0
	43.5	12.0		95.0
	43.0	12.5		100.0
	44.0	13.3		-
	42.5	14.9		118.0
	41.5	16.3		130.0
38.5	17.1	146.0		
22A	75.0	2.7	2.19	18.0
	69.0	4.5		29.0
	62.5	8.0		46.5
	61.5	15.3		75.0
	66.0	31.6		126.5
22B	73.5	2.9	2.13	20.5
	66.0	4.9		32.0
	62.0	8.9		50.5
	62.0	17.1		81.0
23A	81.0	2.2	2.1	14.0
	70.0	3.4		23.0
	64.0	5.8		35.0
	59.0	13.0		56.5
	62.0	26.0		91.0

Table A12 (Cont.)

CAST AND SPECIMEN NO.	LOAD $f$ (N)	DEFLECTION (m) $\times 10^4$	CRACK PLANE WIDTH $w$ (m) $\times 10^3$	CRACK LENGTH $C$ (m) $\times 10^3$
23B	70.0	4.4	2.08	27.0
	61.0	7.7		45.0
	62.0	14.8		70.5
	59.0	27.5		12.2
24A	70.5	3.0	2.22	19.5
	64.0	4.5		29.0
	57.0	7.05		44.0
	56.5	11.6		64.0
	56.5	19.9		97.0
24B	64.5	2.8	2.19	21.0
	60.5	3.8		28.5
	58.0	5.6		39.0
	54.5	8.2		53.5
	53.5	12.3		74.5
	54.0	18.9		104.5
25A	70.5	3.0	2.05	20.5
	58.5	4.7		33.0
	56.0	7.8		48.5
	54.5	13.2		72.5
	55.0	23.2		112.5
25B	58.0	3.0	2.07	21.0
	55.0	4.3		31.0
	52.5	6.3		42.5
	52.0	9.4		58.0
	52.0	14.8		82.5
	53.0	23.6		119.5
26A	77.5	2.1	2.17	15.5
	69.5	3.2		23.0
	64.0	5.1		34.5
	57.5	8.3		52.5
	58.0	14.1		78.0
	62.5	26.8		120.5
26B	69.0	1.8	2.16	15.0
	63.0	2.4		21.5
	59.0	3.6		29.5
	55.0	5.4		41.0
	53.0	8.3		57.0
	53.0	13.0		79.5
	54.0	20.8		113.5
27A	80.8	2.1	2.21	14.0
	68.7	3.2		22.0
	62.5	5.0		33.0
	59.3	8.3		49.5
	57.5	14.1		76.0
	61.0	25.8		117.5

Table A12 (Cont.)

CAST AND SPECIMEN NO.	LOAD $f$ (N)	DEFLECTION (m) $\times 10^4$	CRACK PLANE WIDTH $w$ (m) $\times 10^3$	CRACK LENGTH $C$ (m) $\times 10^3$
27B	62.0	3.0	2.18	23.5
	56.5	4.2		32.0
	54.0	6.0		42.5
	54.0	8.9		57.0
	53.5	13.7		79.5
	54.5	21.2		113.5
28A	75.5	2.4	1.95	15.5
	65.5	3.8		26.0
	62.0	7.1		41.0
	60.5	7.1		68.0
	64.0	31.5		12.0
28B	76.0	2.5	2.1	18.0
	69.0	4.2		28.0
	63.0	7.8		45.0
	64.0	15.8		74.0
	59.5	30.7		13.3
29A	164.0	5.1	2.12	16.0
	137.0	20.5		53.0
29B	133.0	11.4	2.12	36.0
	142.0	56.4		111.0
30A	103.0	7.0	2.03	30.0
	103.0	21.0		68.0
30B	112.0	13.3	2.06	45.0
31A	115.0	5.9	1.97	25.0
	110.0	20.0		60.0
31B	103.0	14.0	1.95	48.0
	104.0	49.8		130.0
32A	78.0	9.1	2.0	45.0
	66.0	14.3		72.0
	70.0	22.5		97.0
	67.0	36.7		153.0
32B	69.0	7.5	2.01	45.0
	69.0	11.2		59.0
	62.0	15.4		81.0
	63.0	20.7		99.0
	79.0	34.6		128.0
33-40	NO FRACTURE TOUGHNESS TESTS PERFORMED			

Table A12 (Cont.)

CAST AND SPECIMEN NO.	LOAD $f$ (N)	DEFLECTION $(m) \times 10^4$	CRACK PLANE WIDTH $w$ (m) $\times 10^3$	CRACK LENGTH $C$ (m) $\times 10^3$
41A	70.0	3.5	2.07	24.0
	48.0	5.0		44.0
	44.0	6.6		48.0
	43.0	7.1		55.0
	41.0	8.1		65.0
	42.0	10.3		80.0
	42.0	11.2		86.0
	42.0	11.8		90.0
	43.0	13.4		98.0
	45.0	16.3		115.0
41B	44.5	4.8	2.14	50.0
	43.5	6.1		60.0
	42.0	7.3		70.0
	42.0	8.5		80.0
	42.5	10.3		92.0
	42.5	11.5		100.0
	44.5	12.3		102.0
	44.5	14.7		128.0
42A	48.0	3.2	2.01	28.0
	46.0	3.6		32.0
	45.0	4.2		36.5
	47.5	5.2		42.0
	44.0	6.5		52.0
	47.5	8.2		59.0
	44.0	9.9		75.0
	40.0	11.2		91.0
	41.0	13.0		102.0
	42.0	14.1		108.0
	43.0	15.7		117.0
	44.0	20.6		138.0
42B	NO TEST			
43A	54.0	3.7	2.26	30.0
	52.5	4.2		35.0
	51.0	4.8		40.0
	48.5	7.0		65.0
	46.0	12.3		86.0
	43.0	15.3		115.0
43B	52.0	6.5	2.34	49.0
	55.0	9.3		60.0
	51.0	11.9		80.0
	47.0	14.7		99.0
	43.0	16.0		121.0
	43.0	17.6		133.0

Table A12 (Cont.)

CAST AND SPECIMEN NO.	LOAD $f$ (N)	DEFLECTION (m) $\times 10^4$	CRACK PLANE WIDTH $w$ (m) $\times 10^3$	CRACK LENGTH $C$ (m) $\times 10^3$
44A	54.5	6.3	1.95	36.0
	58.5	10.5		53.0
	63.0	19.1		78.0
	58.5	33.0		131.0
44B	83.5	2.3	1.9	13.0
	71.0	3.2		22.0
	64.0	5.5		34.0
	60.0	9.9		53.0
	58.5	18.2		84.0
59.5	35.9	146.0		
45A	72.0	3.0	1.99	21.0
	64.5	4.9		31.0
	60.0	8.4		47.0
	59.0	14.8		71.5
	63.0	26.9		109.0
45B	95.0	3.0	1.98	14.0
	69.0	4.5		26.5
	64.5	8.0		42.0
	61.0	15.0		71.0
	65.0	30.6		119.0
46A	70.0	3.7	1.94	23.0
	69.5	6.5		35.0
	63.5	12.1		57.5
	67.5	23.8		92.0
46B	83.5	3.3	1.96	17.5
	69.0	4.6		28.5
	66.0	8.0		43.0
	63.5	15.5		71.0
	66.0	34.2		121.5
47A	85.0	3.2	2.05	18.0
	74.0	3.9		24.5
	71.5	4.9		30.5
	68.5	7.1		39.5
	68.0	10.1		52.0
	70.0	16.2		71.0
73.5	27.9	105.0		
47B	93.5	9.0	2.08	37.5
	69.5	15.2		68.5
	75.0	26.6		99.0

Table A12 (Cont.)

CAST AND SPECIMEN NO.	LOAD $f$ (N)	DEFLECTION (m) $\times 10^4$	CRACK PLANE WIDTH $w$ (m) $\times 10^3$	CRACK LENGTH $C$ (m) $\times 10^3$
48A	75.5 68.0 69.0 75.0	7.2 10.1 15.8 26.8	2.04	36.0 51.5 70.0 100.0
48B	93.5 72.5 76.5 76.5 69.5	6.7 9.3 14.1 24.4 40.0	2.20	30.0 47.0 61.0 94.0 159.0
49A	87.5 71.5 73.0 75.0	6.5 9.4 15.0 25.7	2.18	31.0 48.0 66.0 98.0
49B	NO TEST			

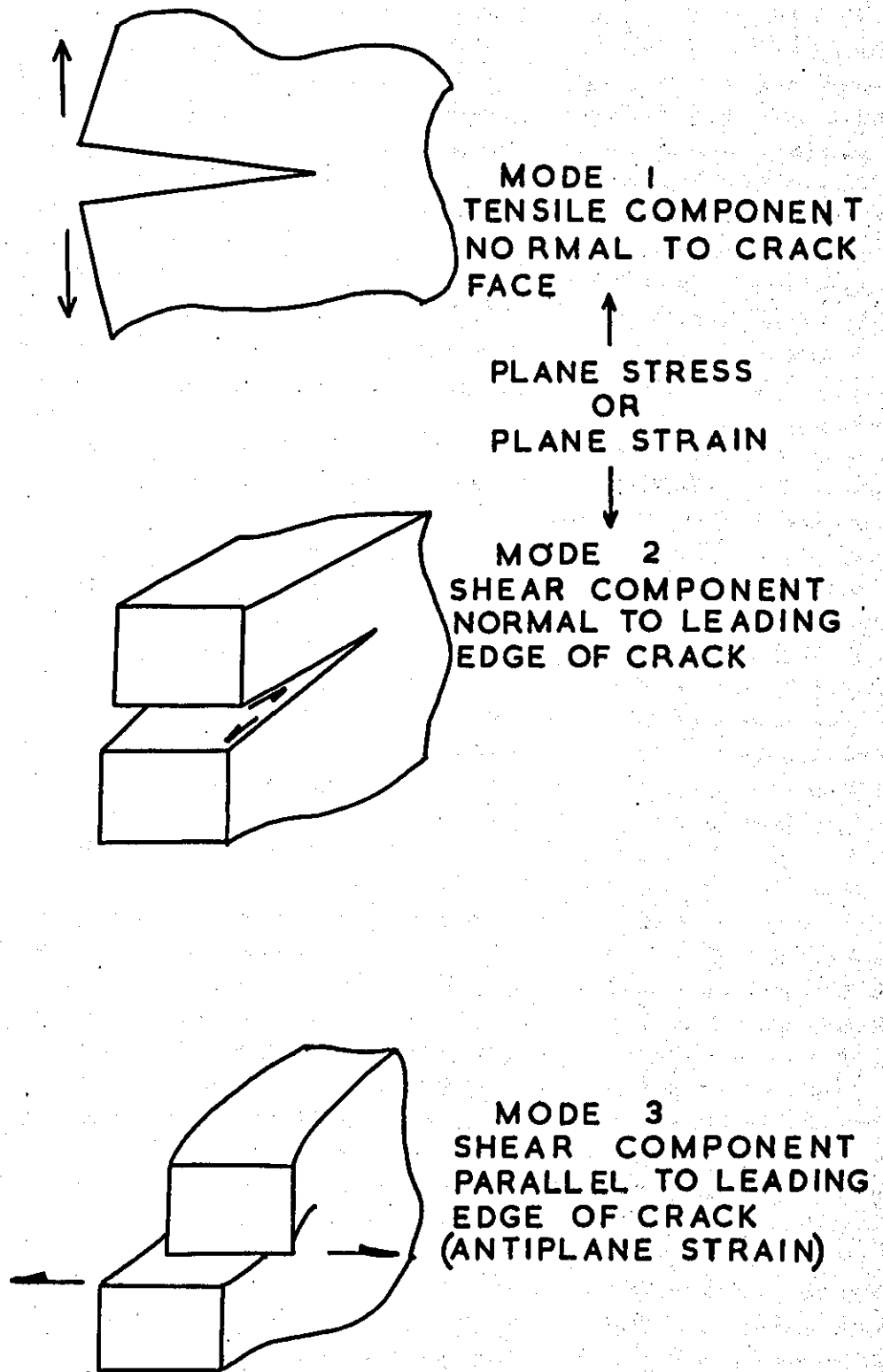


FIG. 1

MODES OF CRACK ADVANCE

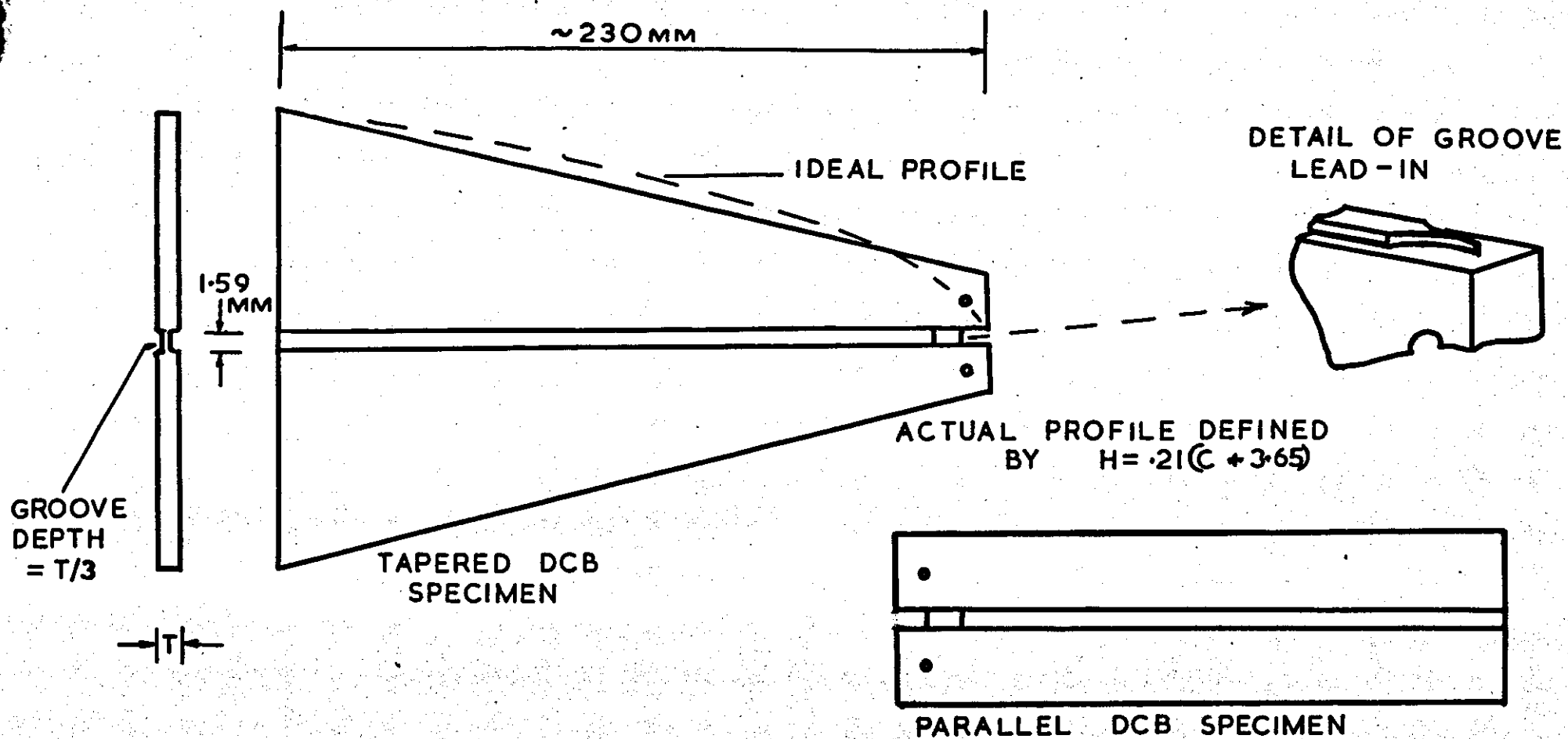
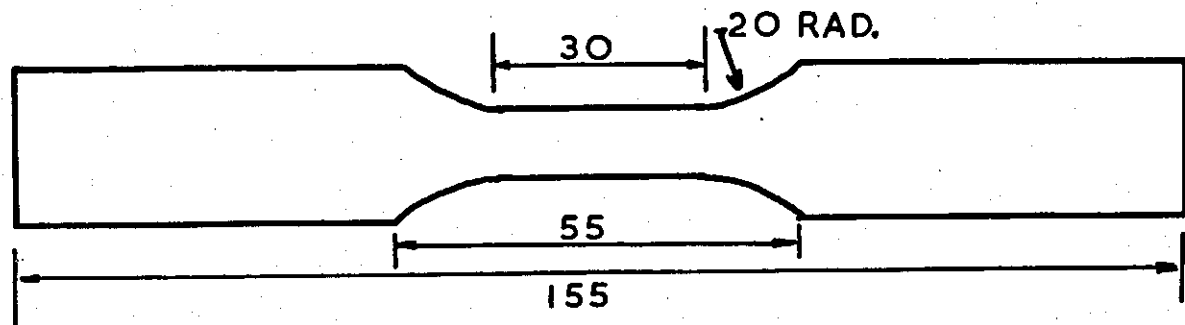


FIG. 2  
 TYPICAL DCB CLEAVAGE SPECIMENS



ALL DIMENSIONS IN MM.

TENSILE TEST SPECIMEN



COMPRESSION TEST SPECIMEN

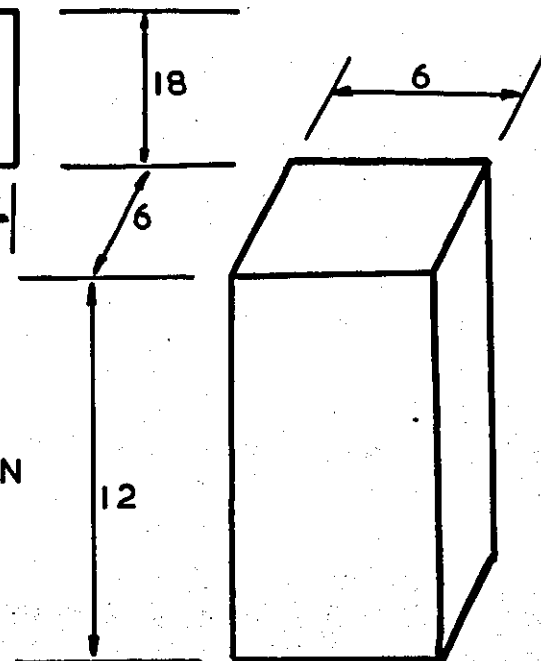
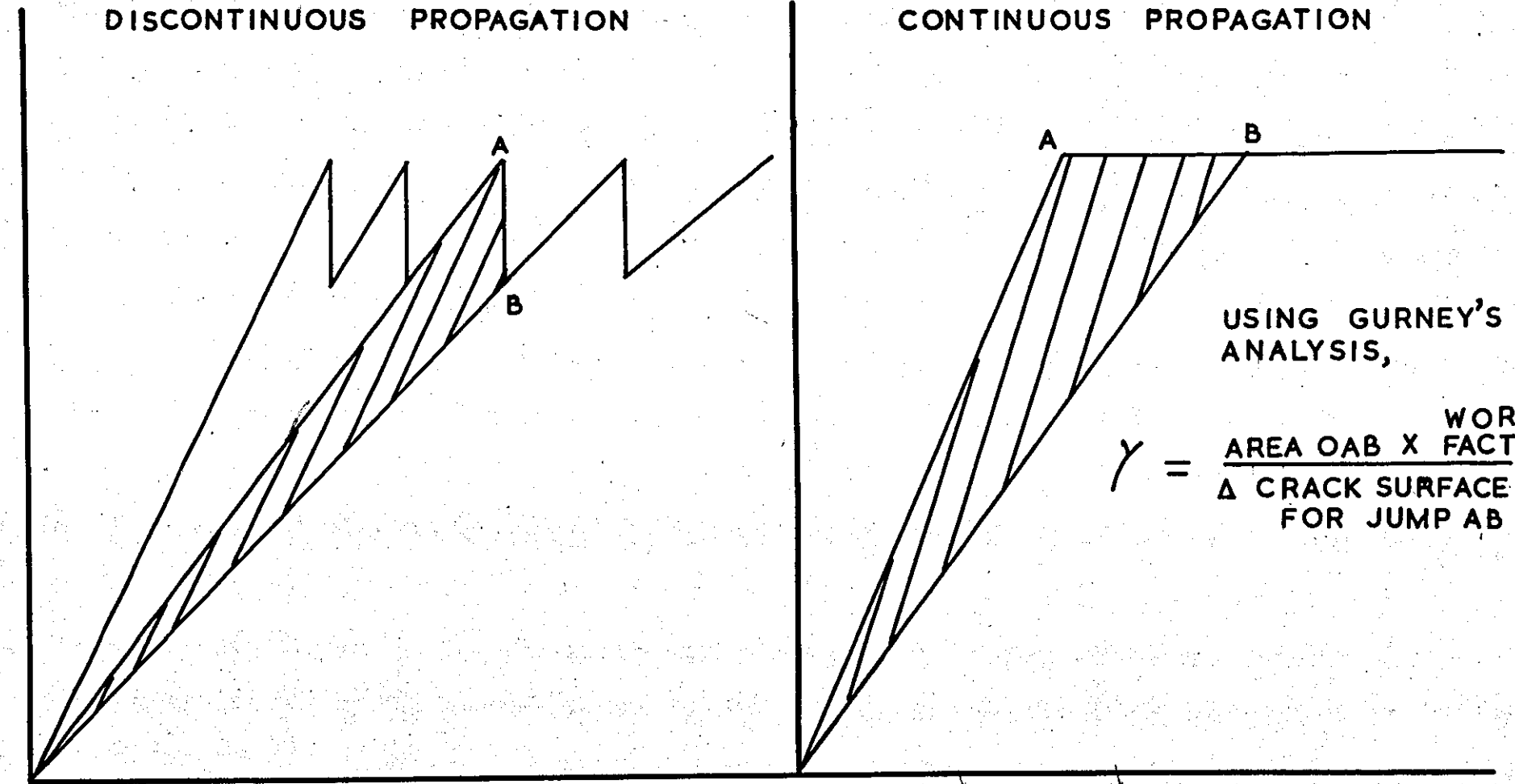


FIG. 3  
TENSION & COMPRESSION SPECIMENS

LOAD

DISCONTINUOUS PROPAGATION

CONTINUOUS PROPAGATION



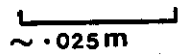
USING GURNEY'S ANALYSIS,

$$\gamma = \frac{\text{AREA OAB} \times \text{WORK FACTOR}}{\Delta \text{ CRACK SURFACE AREA FOR JUMP AB}}$$

FIG. 4

EXTENSION

IDEALISED FORMS OF LOAD-EXTENSION CURVE FOR THE TDCB SPECIMEN



~ 0.025 m

Fig. 5  
Cleavage apparatus for crack tip  
micro-examination

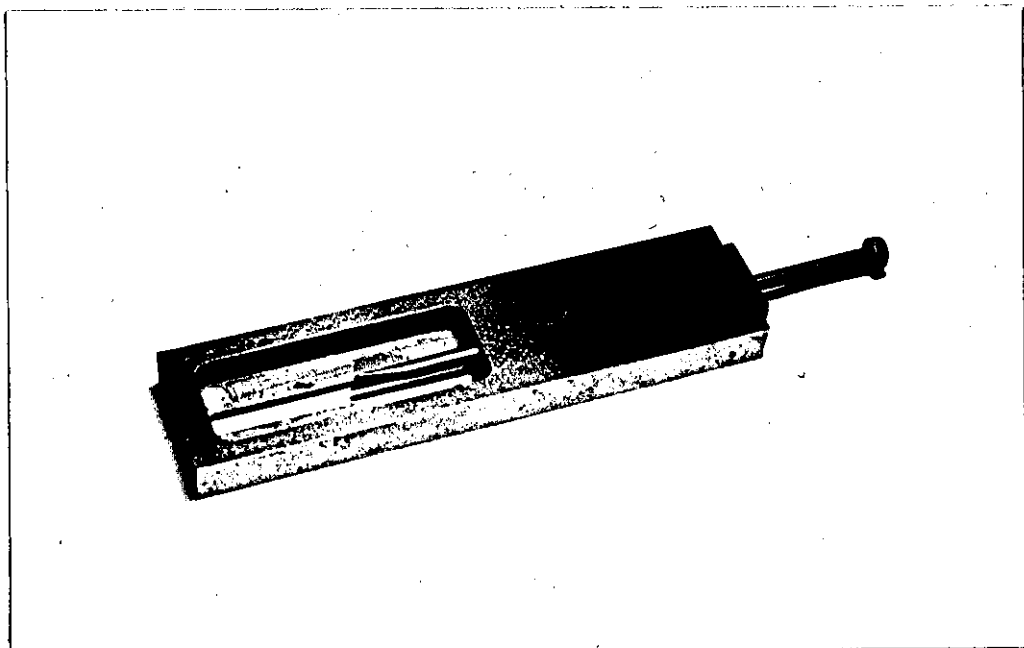
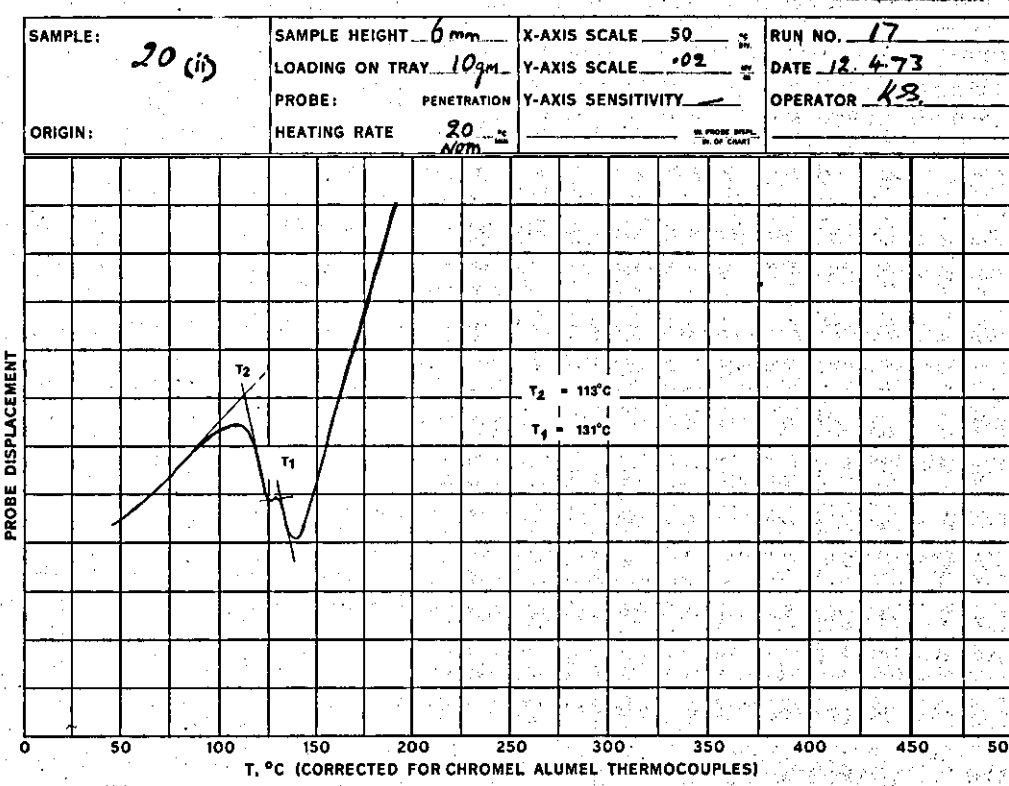
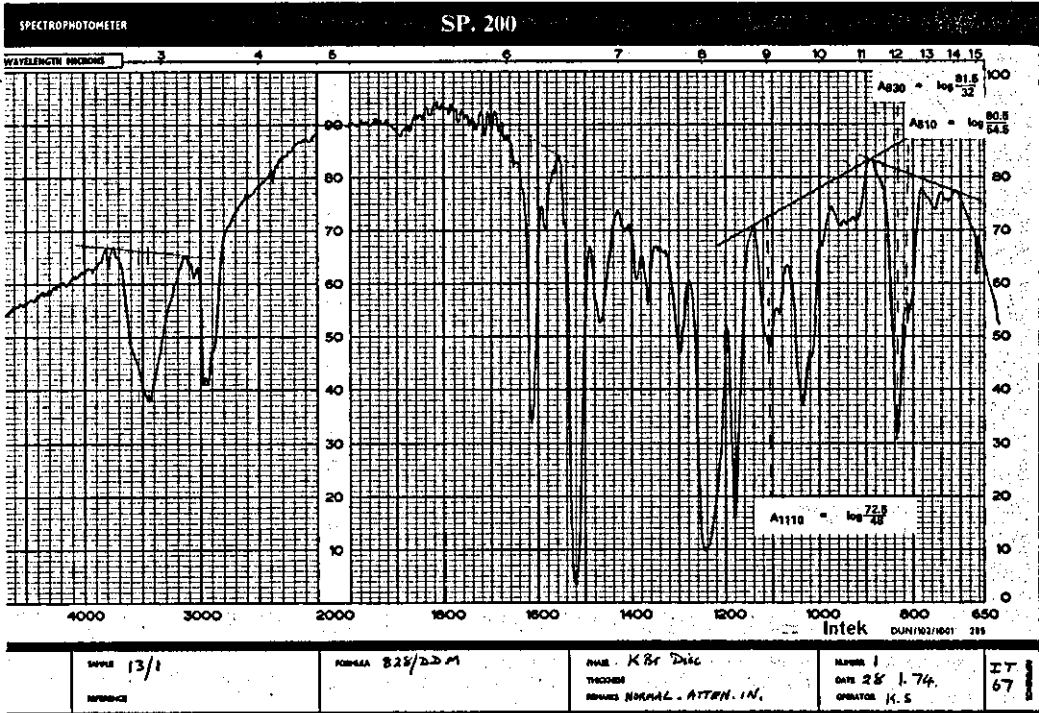


Fig. 6  
Typical Infra Red Spectrogram  
of Epikote 828/Epikure DDM

Fig. 7  
Typical TMA Penetrometer curve  
for Epikote 828/Epikure DDM  
(40 parts DDM)



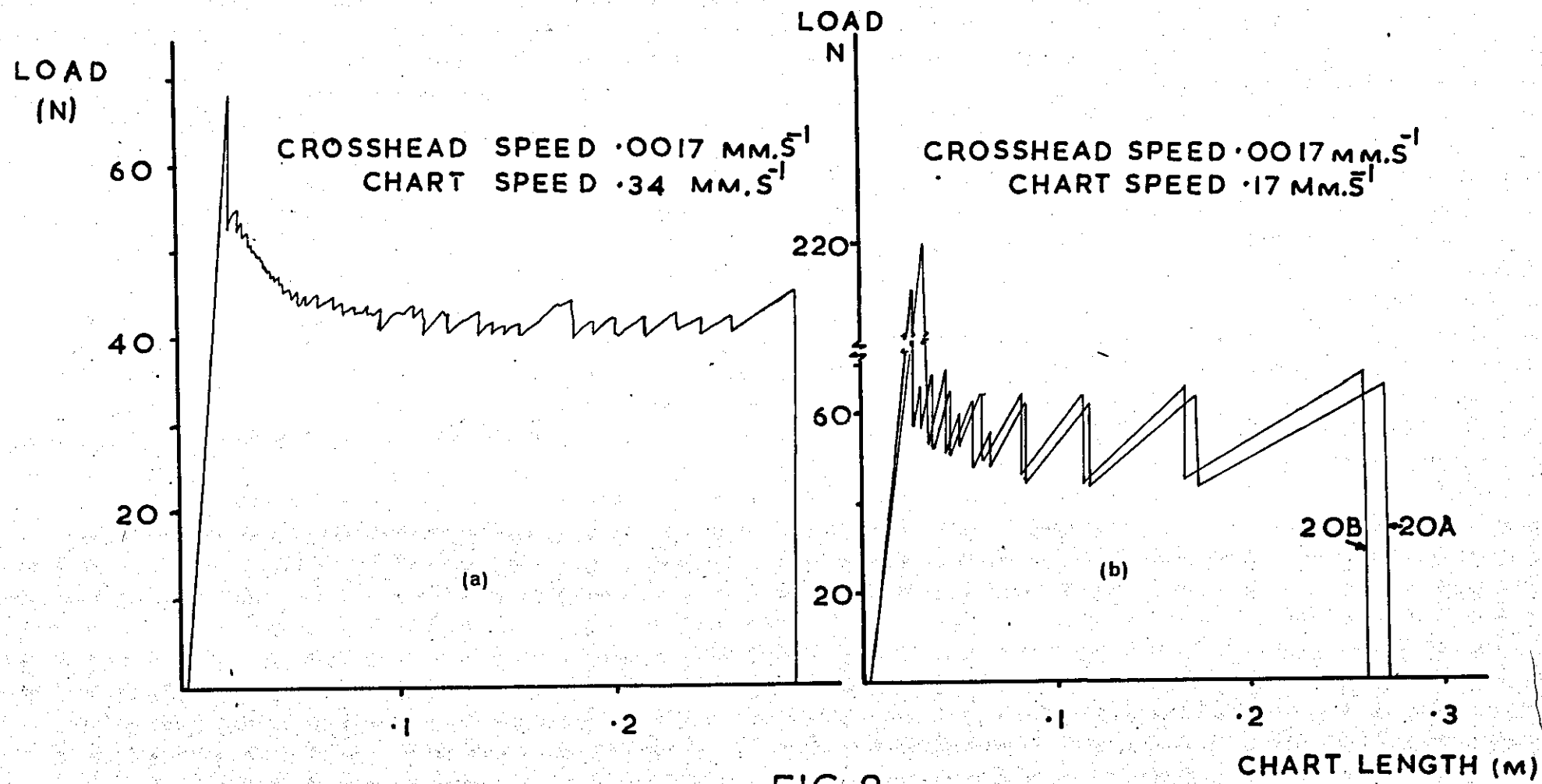


FIG. 8  
LOAD EXTENSION CURVES FOR TDCB SPECIMENS 17B, 20A & B

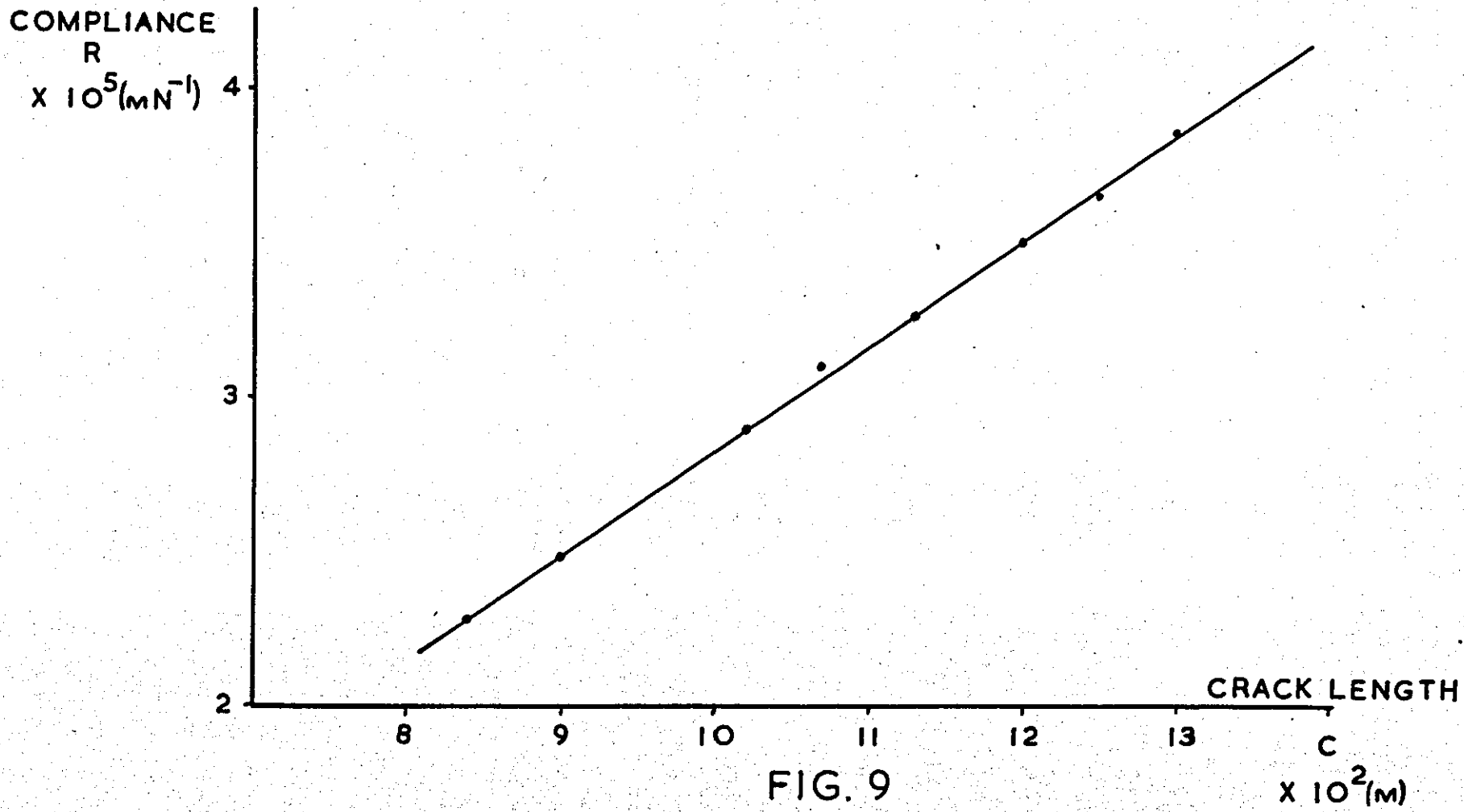


FIG. 9

R<sub>v</sub>C FOR TDCB SPECIMEN 17B



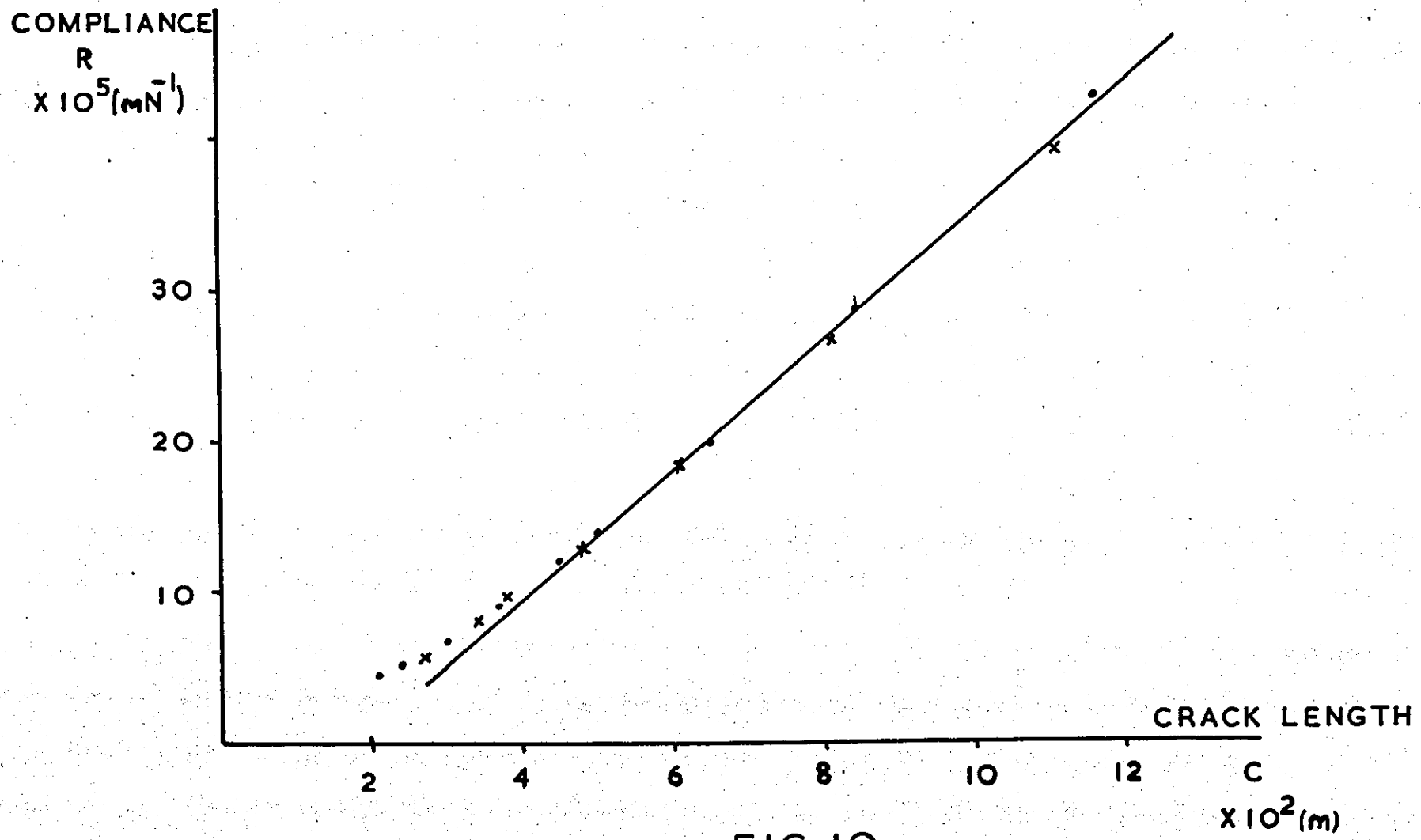


FIG. 10

R v C FOR TDCB SPECIMENS 20A & 20B

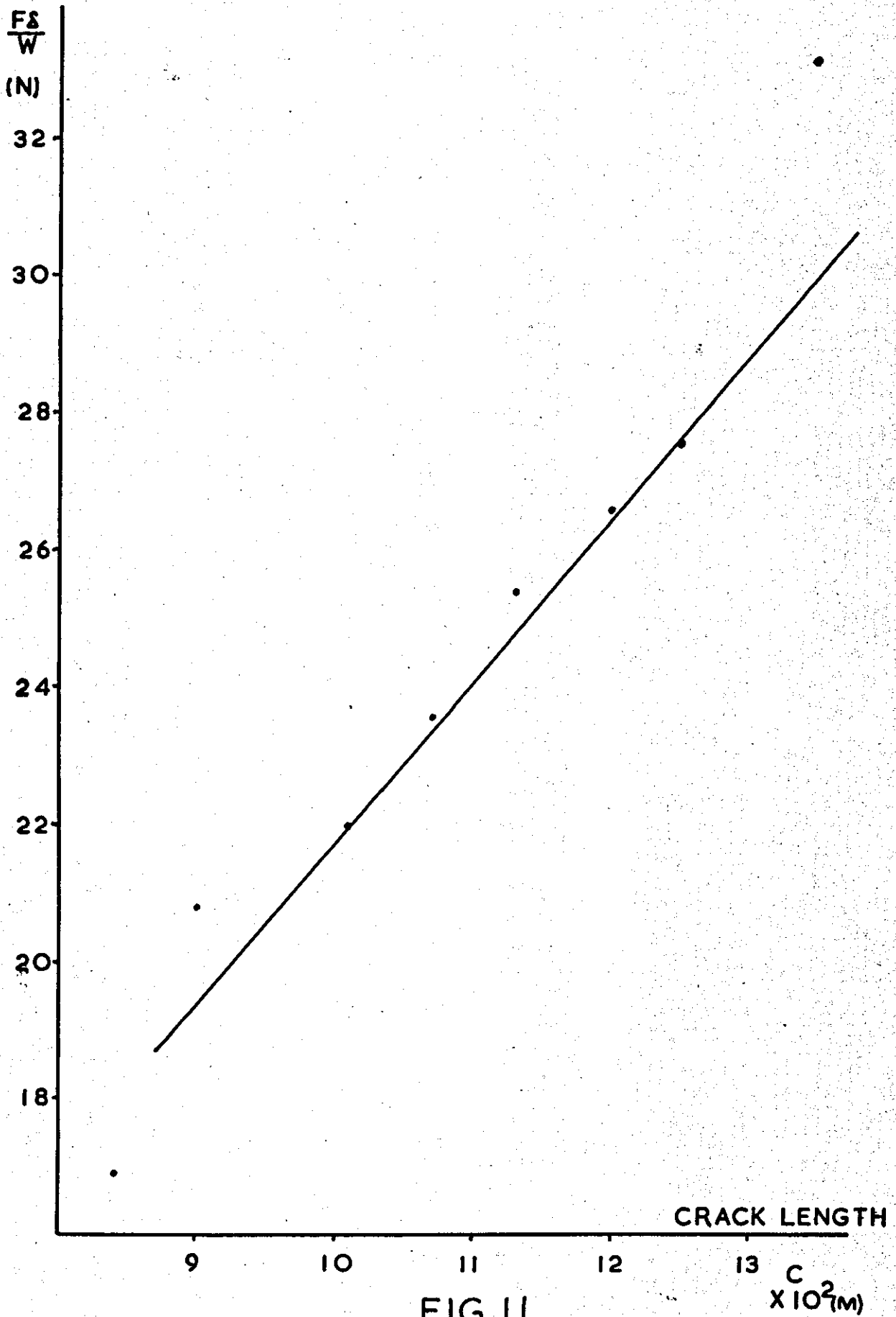


FIG. II

$F\Delta/W$  v  $C$  FOR TDCB SPECIMEN 17B

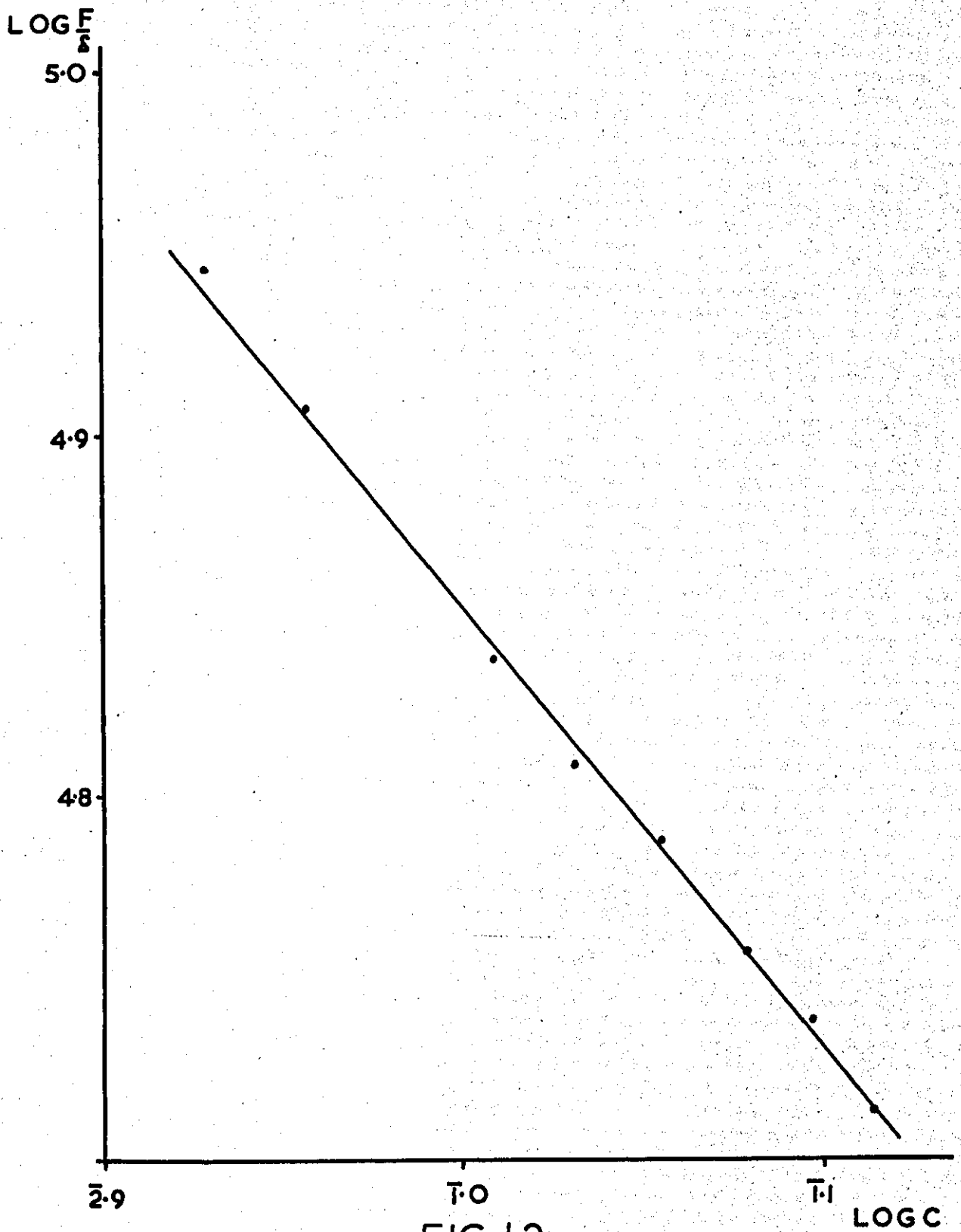


FIG. 12

LOG  $\frac{F_v}{S}$  LOG C FOR TDCB SPECIMEN 17B

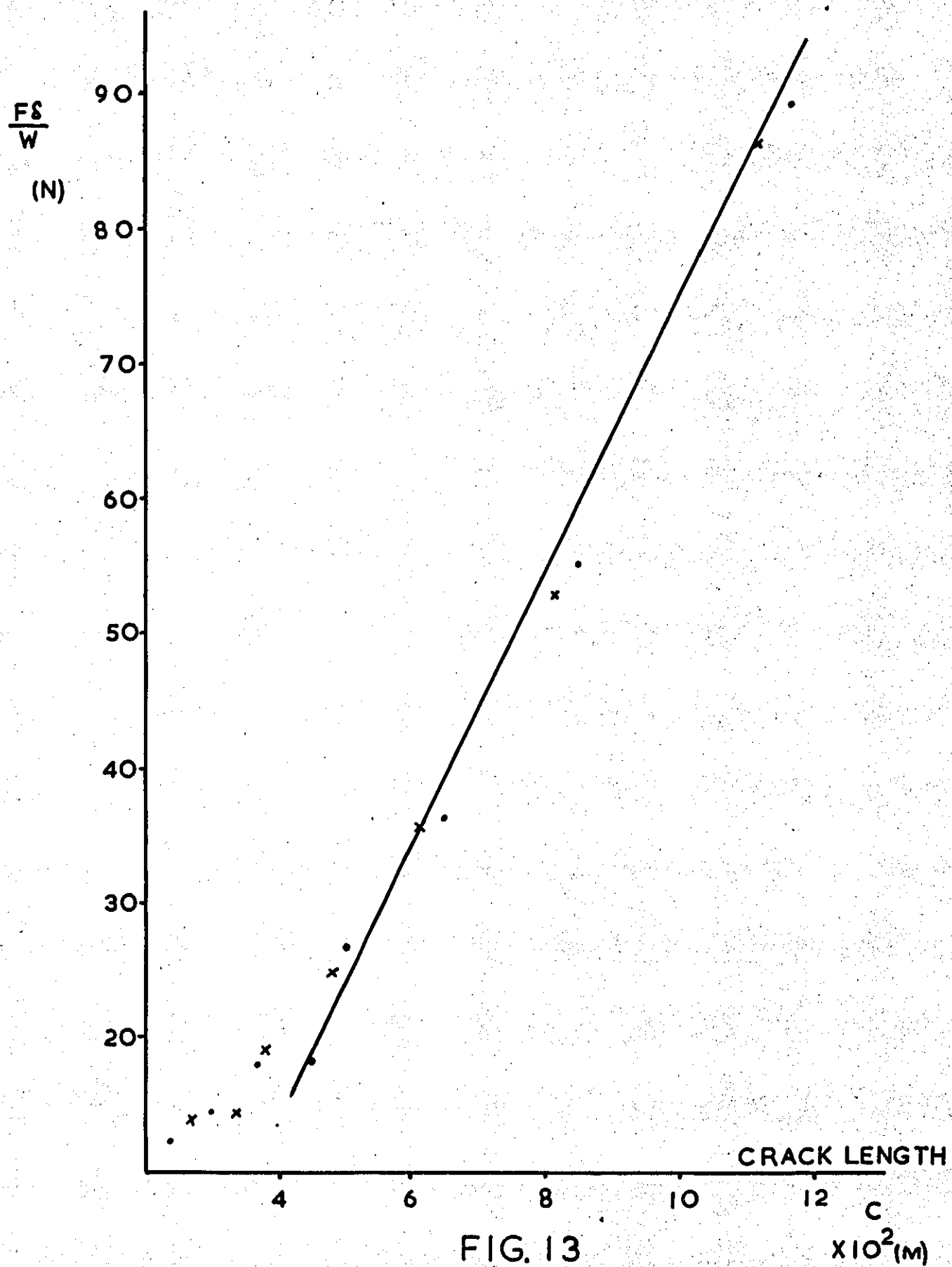


FIG. 13  
 $FS/W$  v  $C$  FOR TDCB SPECIMENS 20A&B  
 (COMBINED PLOT)

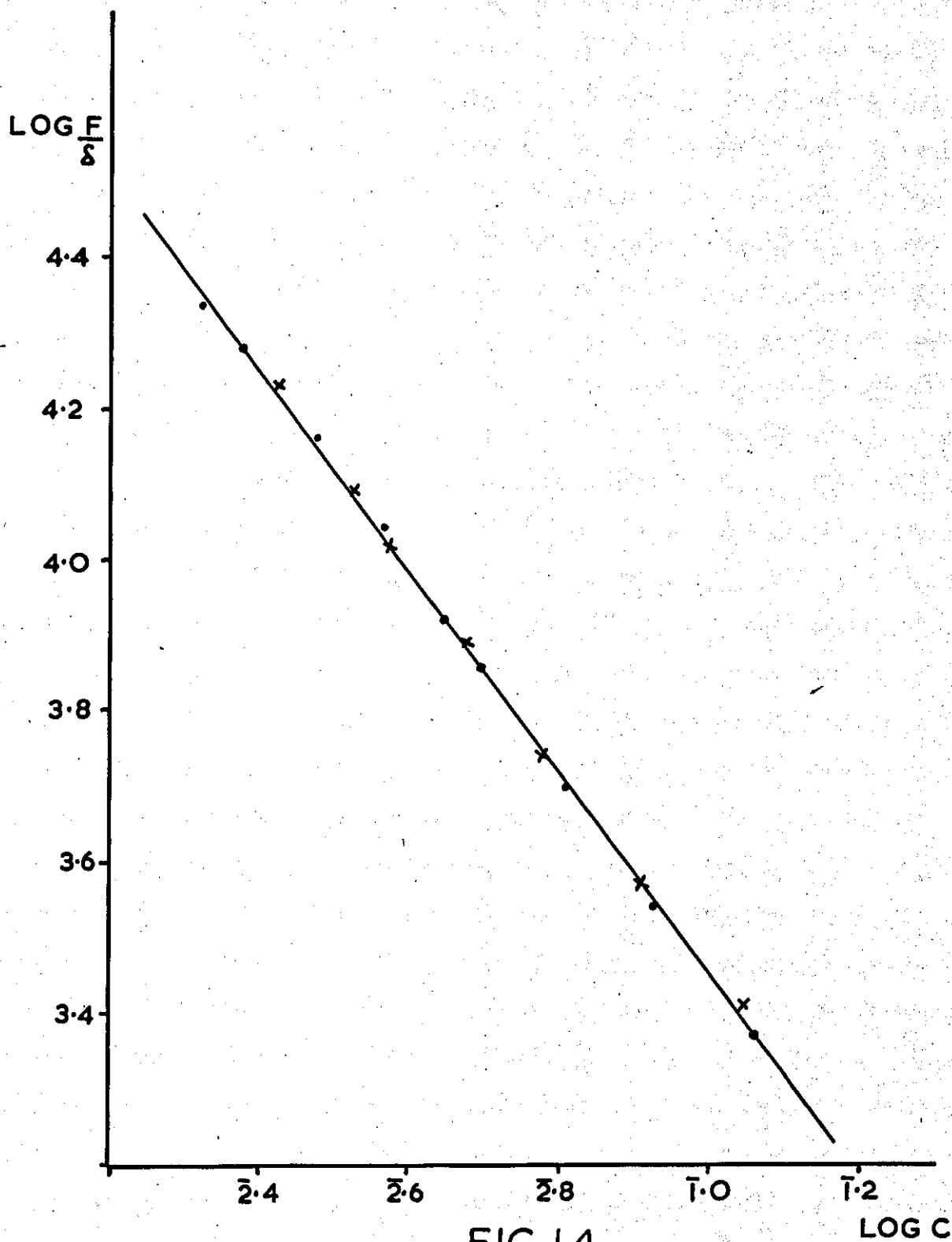


FIG. 14

$\text{LOG } \frac{E}{\delta}$  v  $\text{LOG } C$  FOR TDCB SPECIMENS 20A & B  
(COMBINED PLOT)

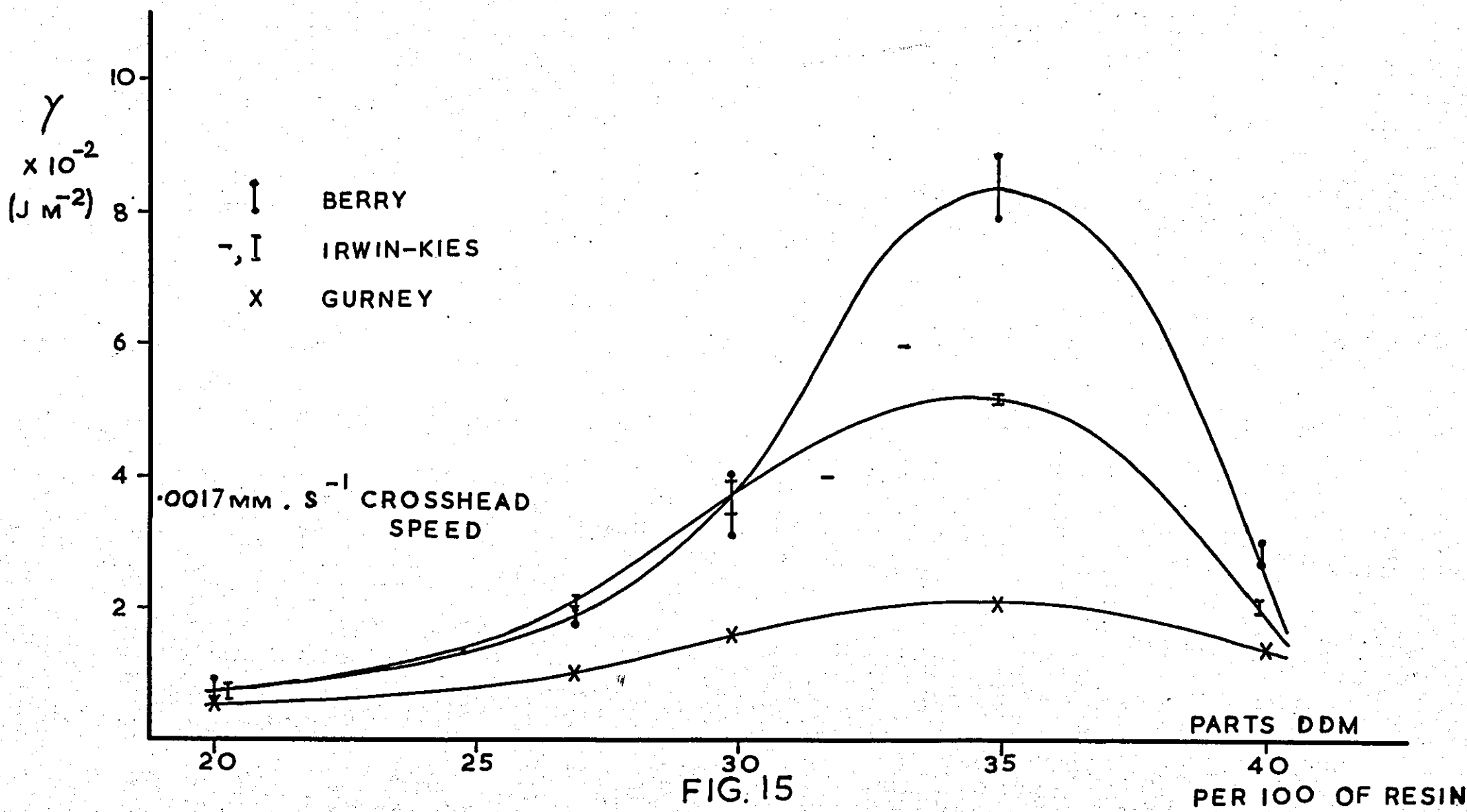


FIG. 15

FRACTURE SURFACE WORK,  $\gamma$ , v DDM CONTENT

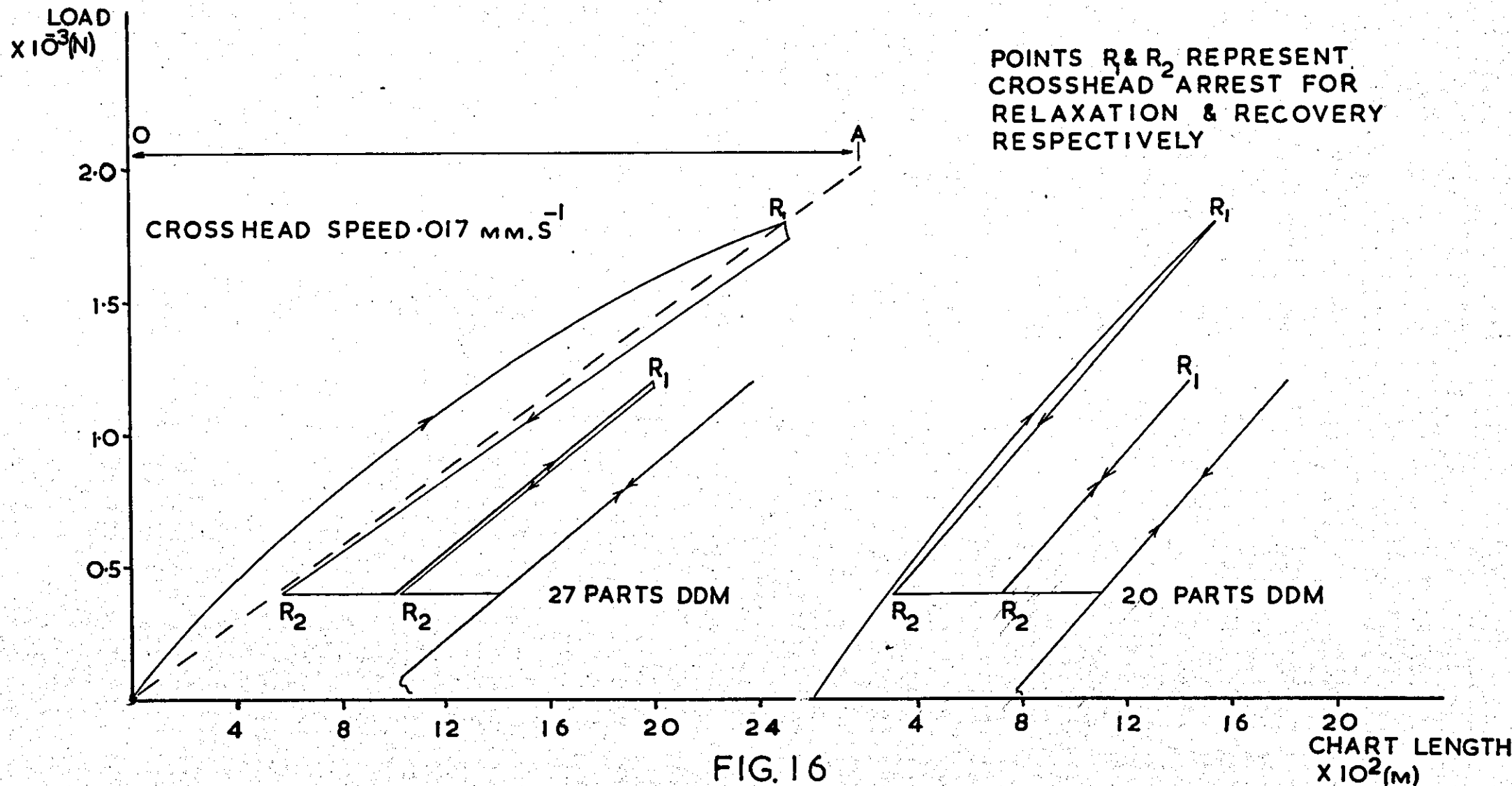


FIG. 16

TYPICAL LOAD-EXTENSION CURVES OBTAINED DURING TENSILE MODULUS TESTING OF EPI.828/DDM

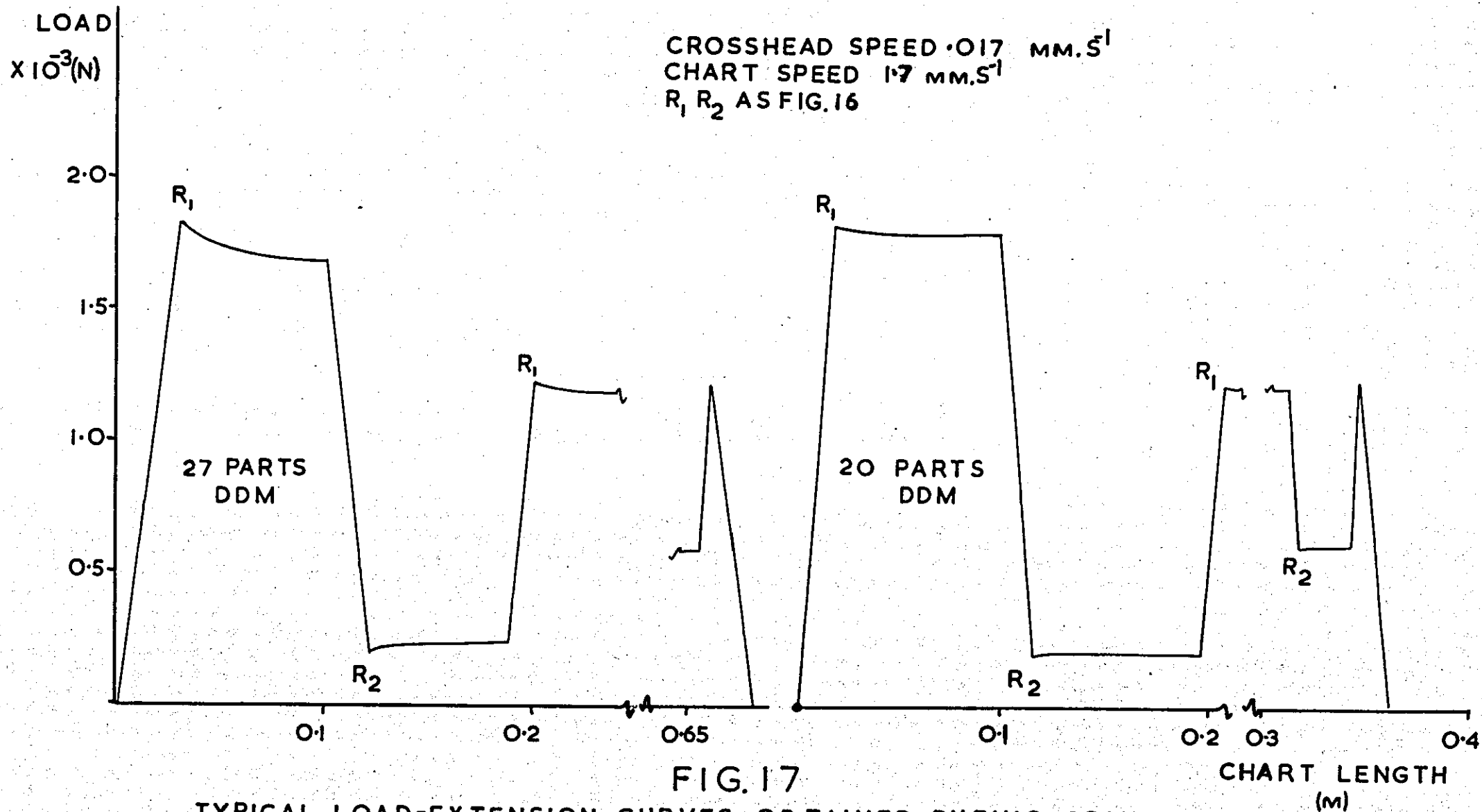


FIG. 17  
 TYPICAL LOAD-EXTENSION CURVES OBTAINED DURING COMPRESSIVE  
 MODULUS TESTING OF EPI,828/DDM



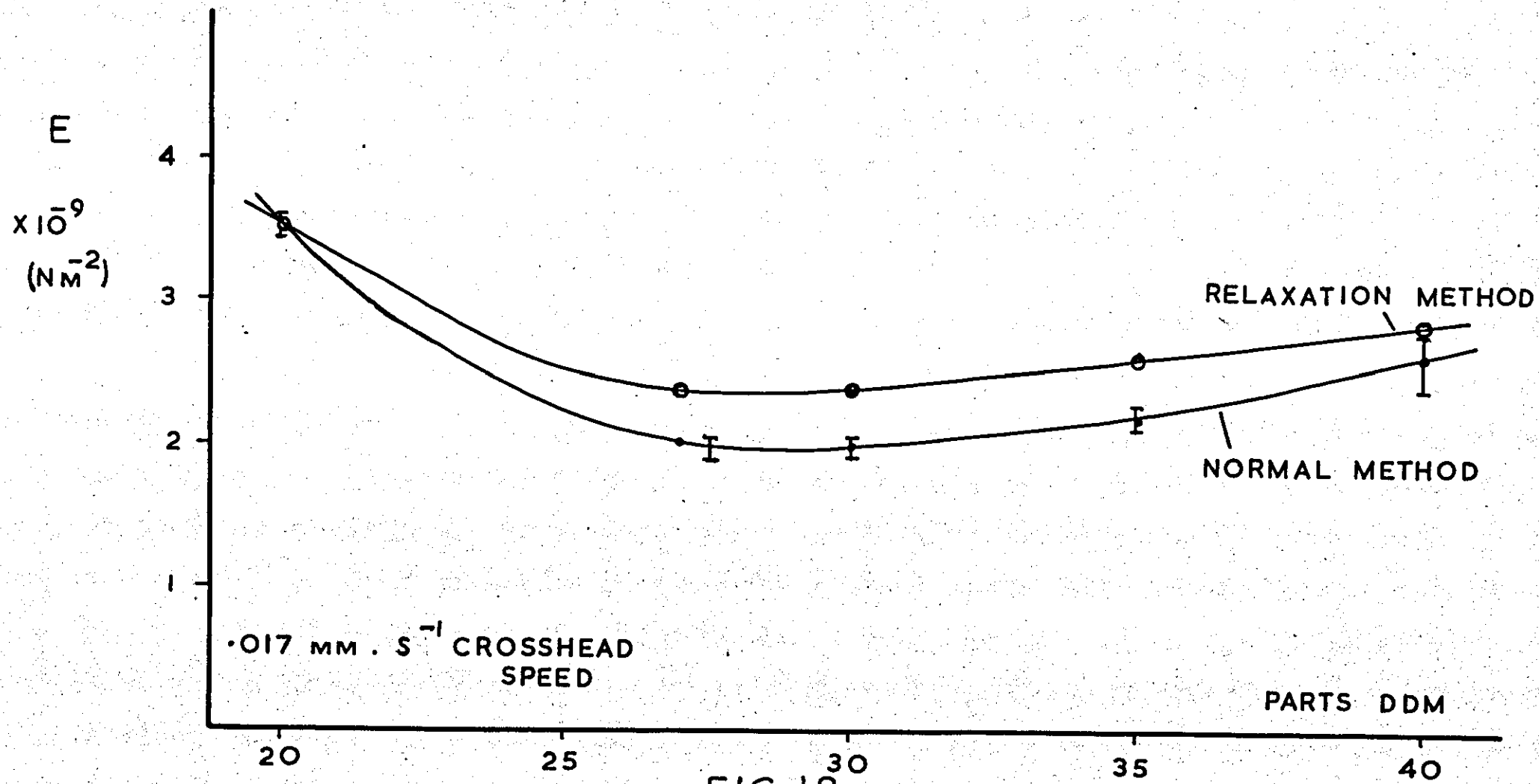


FIG. 18

TENSILE E v DDM CONTENT

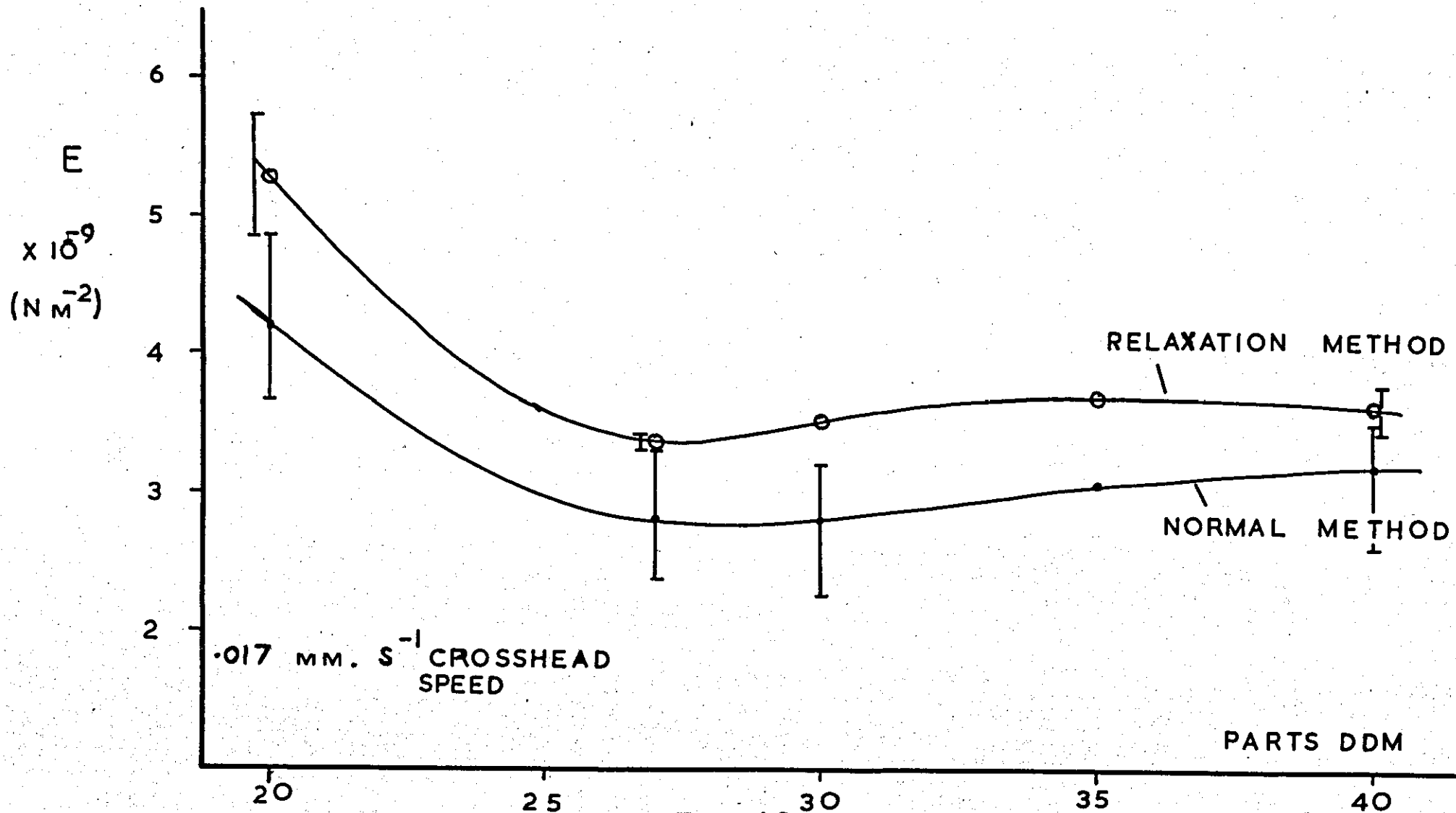


FIG. 19

COMPRESSIVE  $E$  v DDM CONTENT

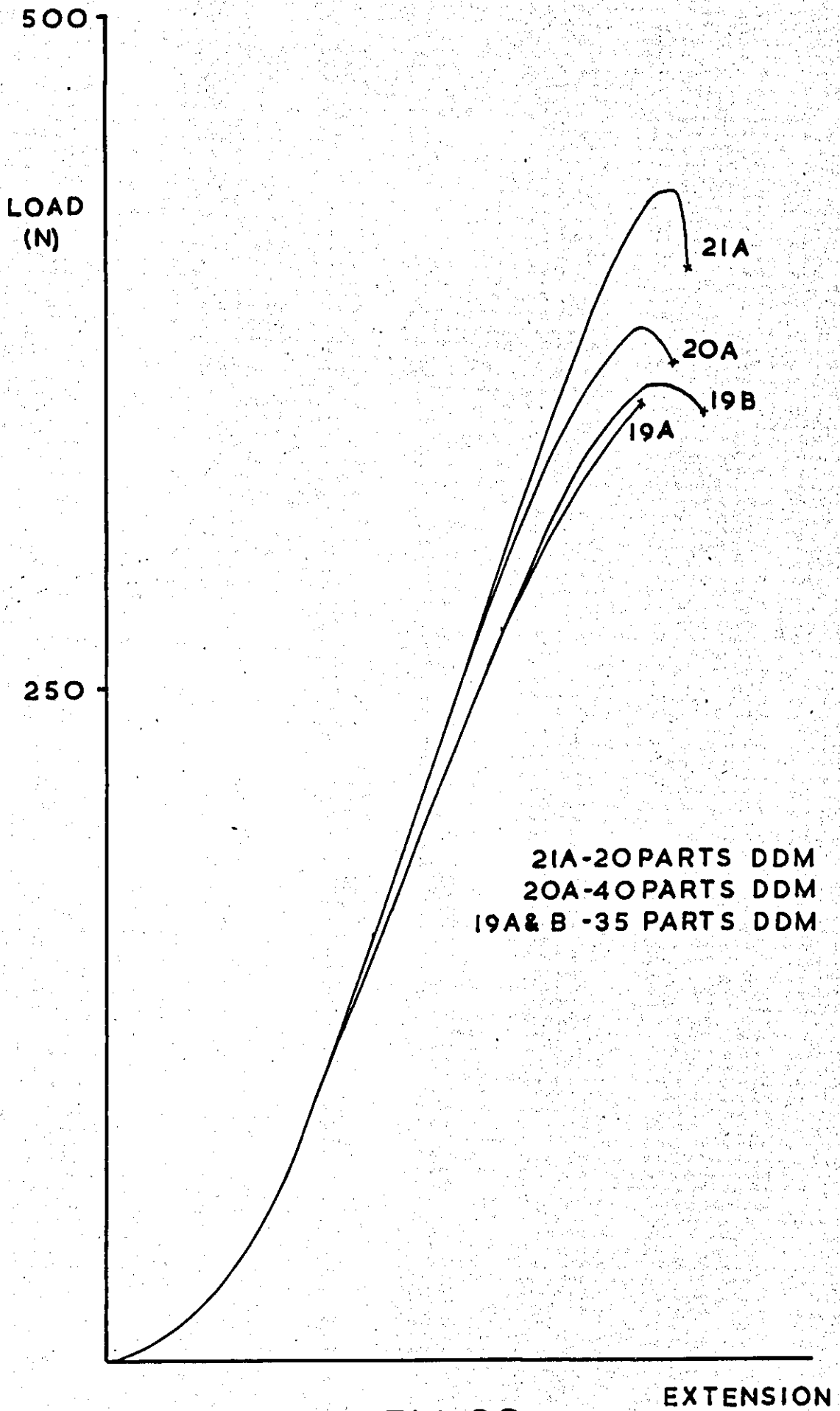


FIG. 20  
TYPICAL TENSILE LOAD EXTENSION CURVES

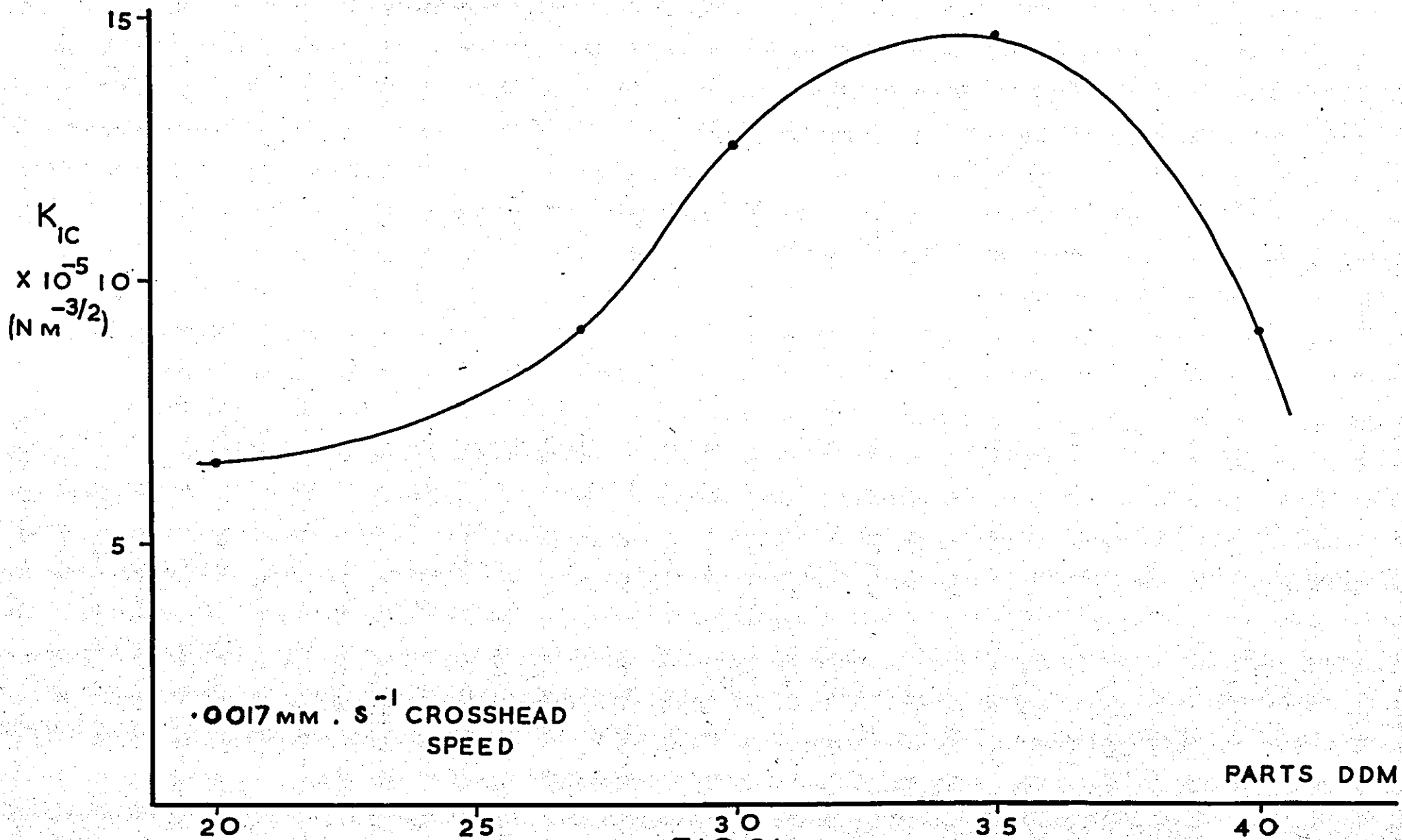


FIG.21  
 PLANE STRAIN FRACTURE TOUGHNESS,  $K_{IC}$ , v DDM CONTENT

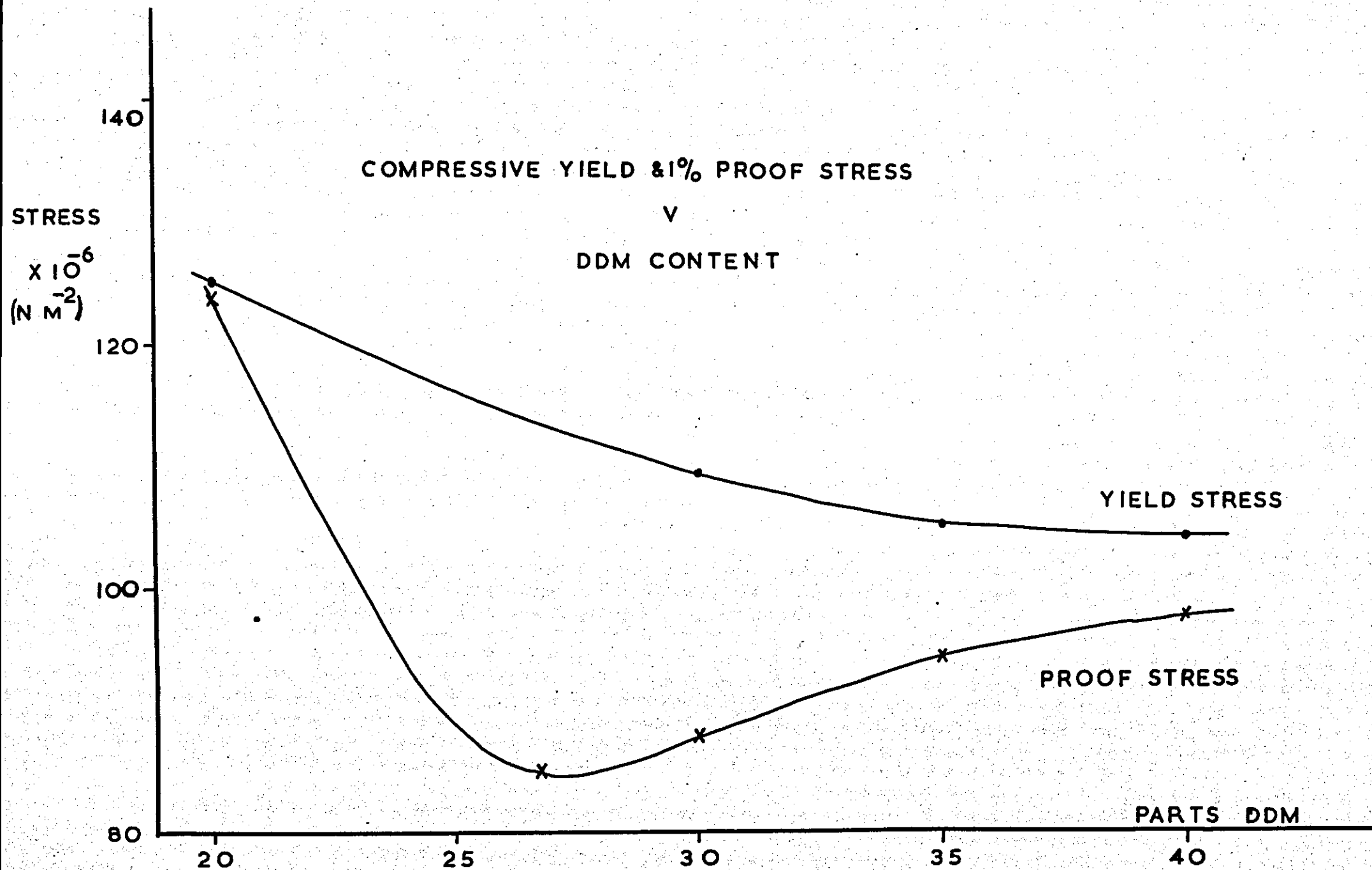


FIG 22

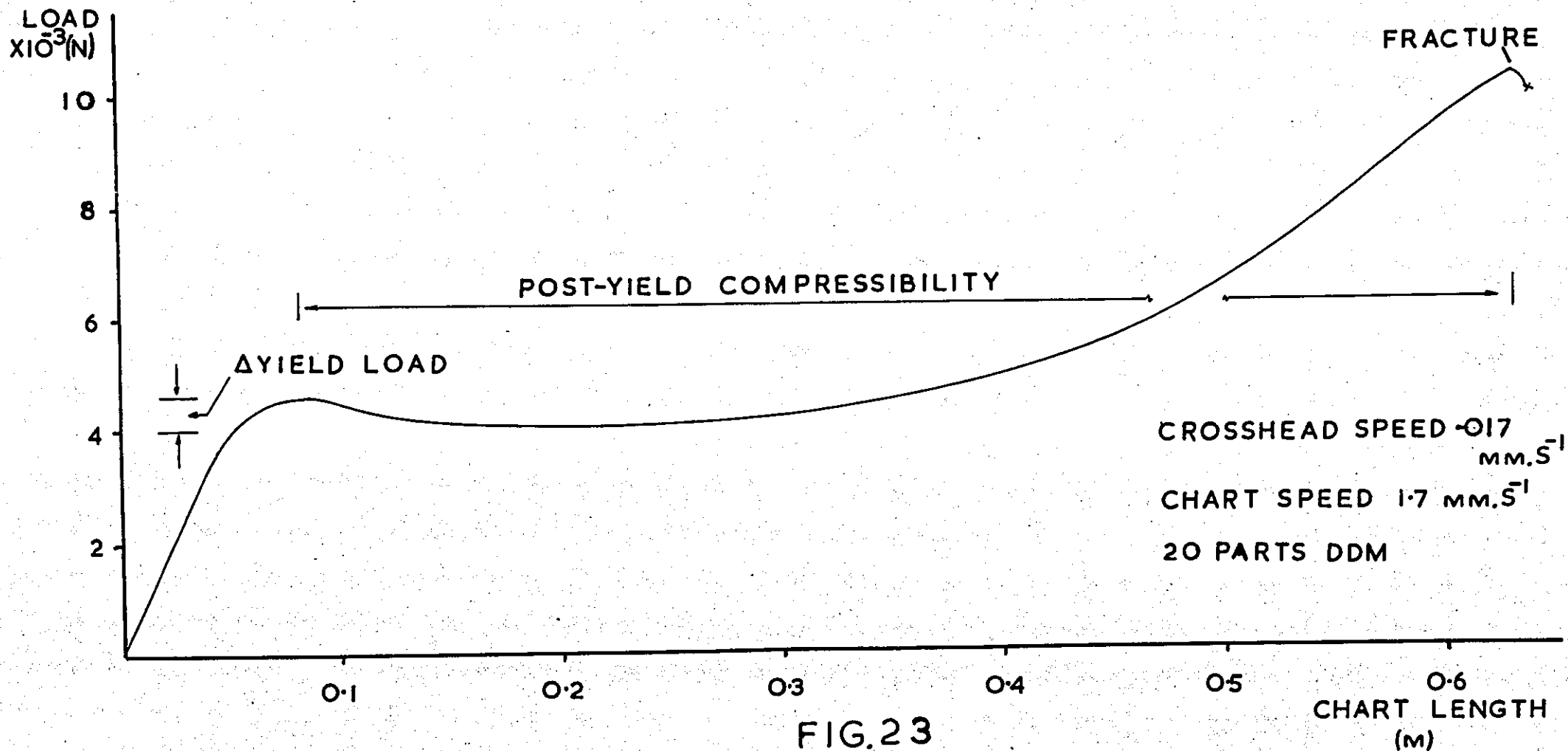


FIG.23

TYPICAL LOAD-EXTENSION CURVE TO FRACTURE FOR EPI,828/DDM  
IN COMPRESSION - LOW DDM CONTENT

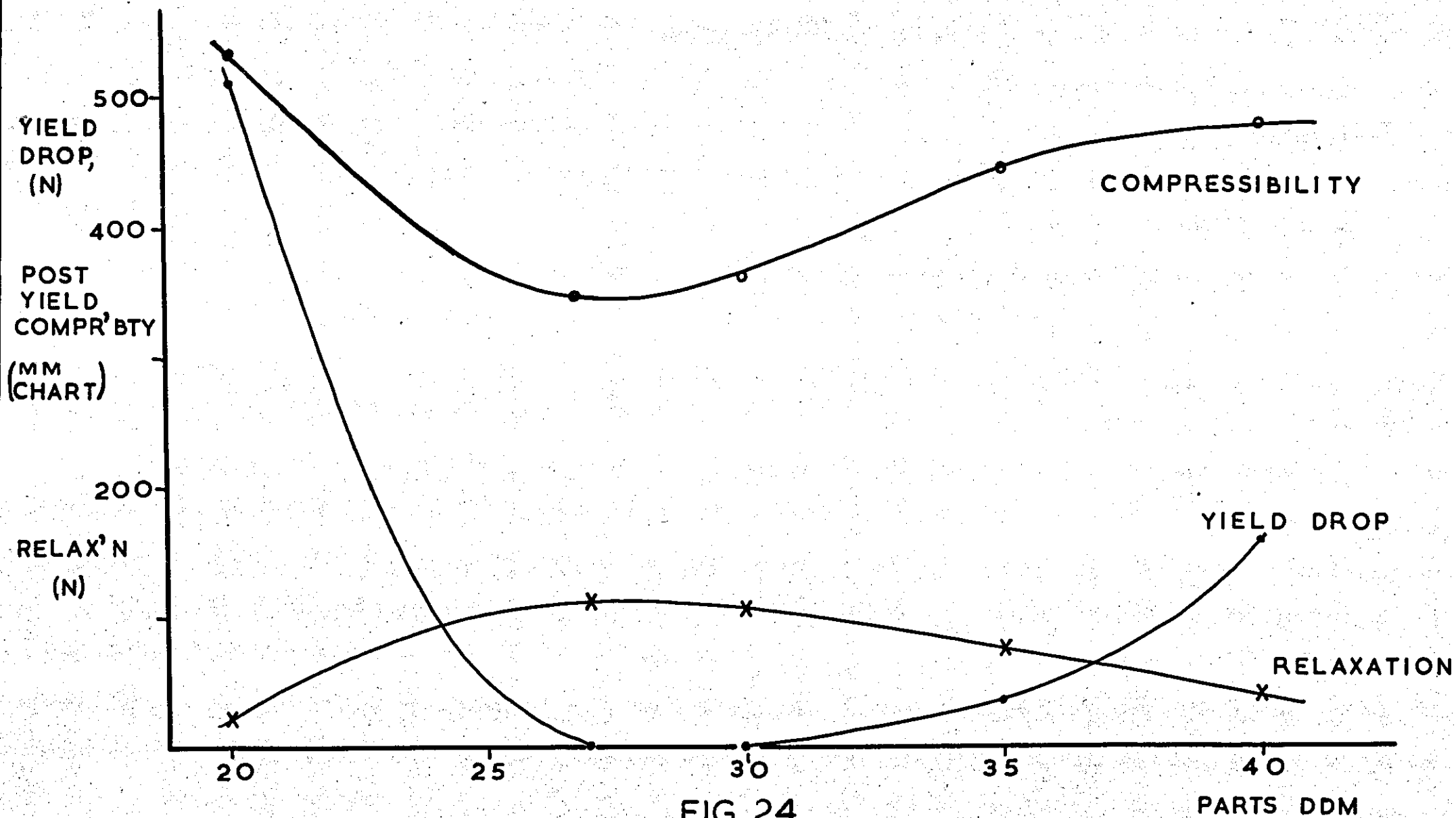


FIG. 24

RELAXATION, YIELD-DROP & POST-YIELD COMPRESSIBILITY  
 v  
 DDM CONTENT

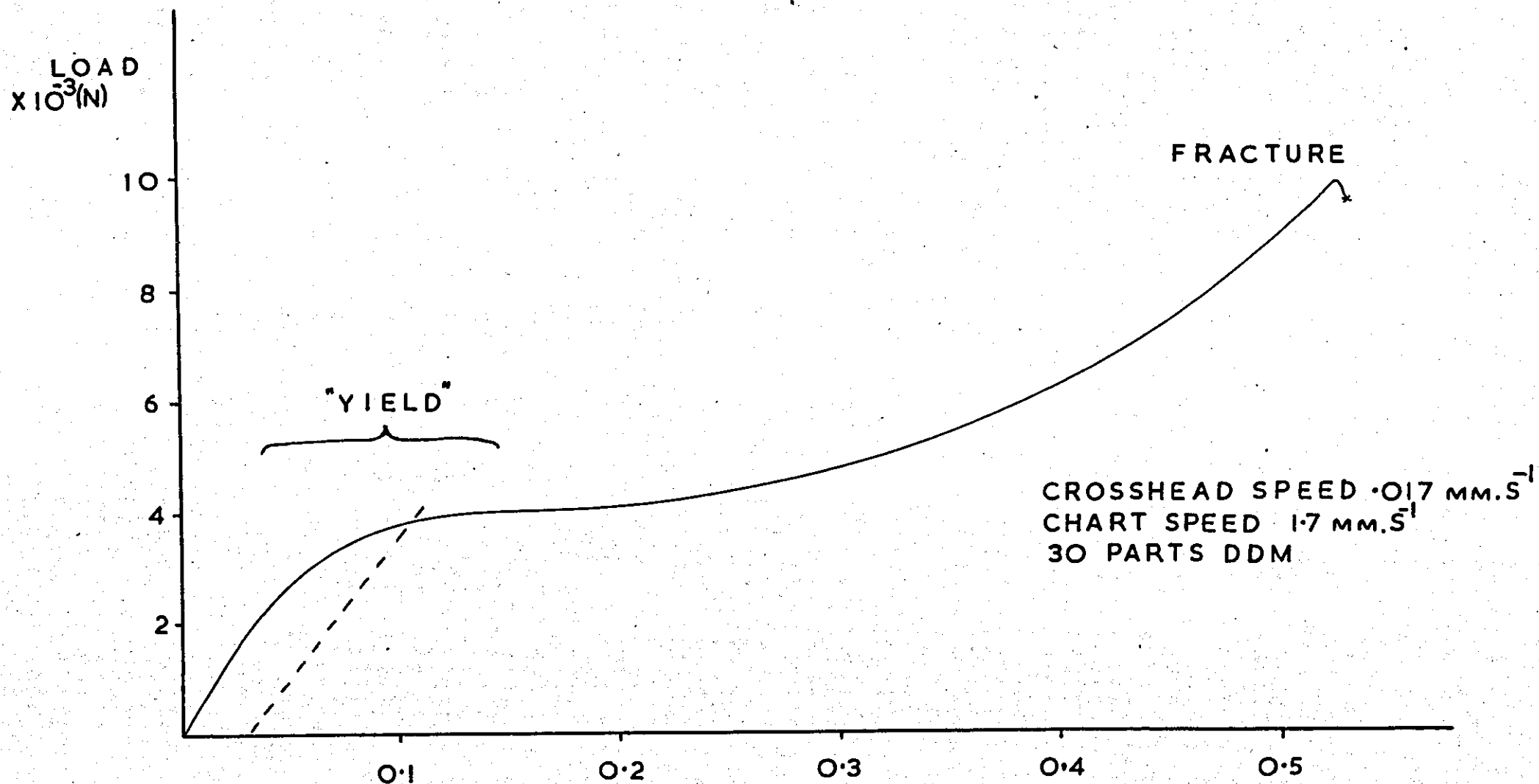
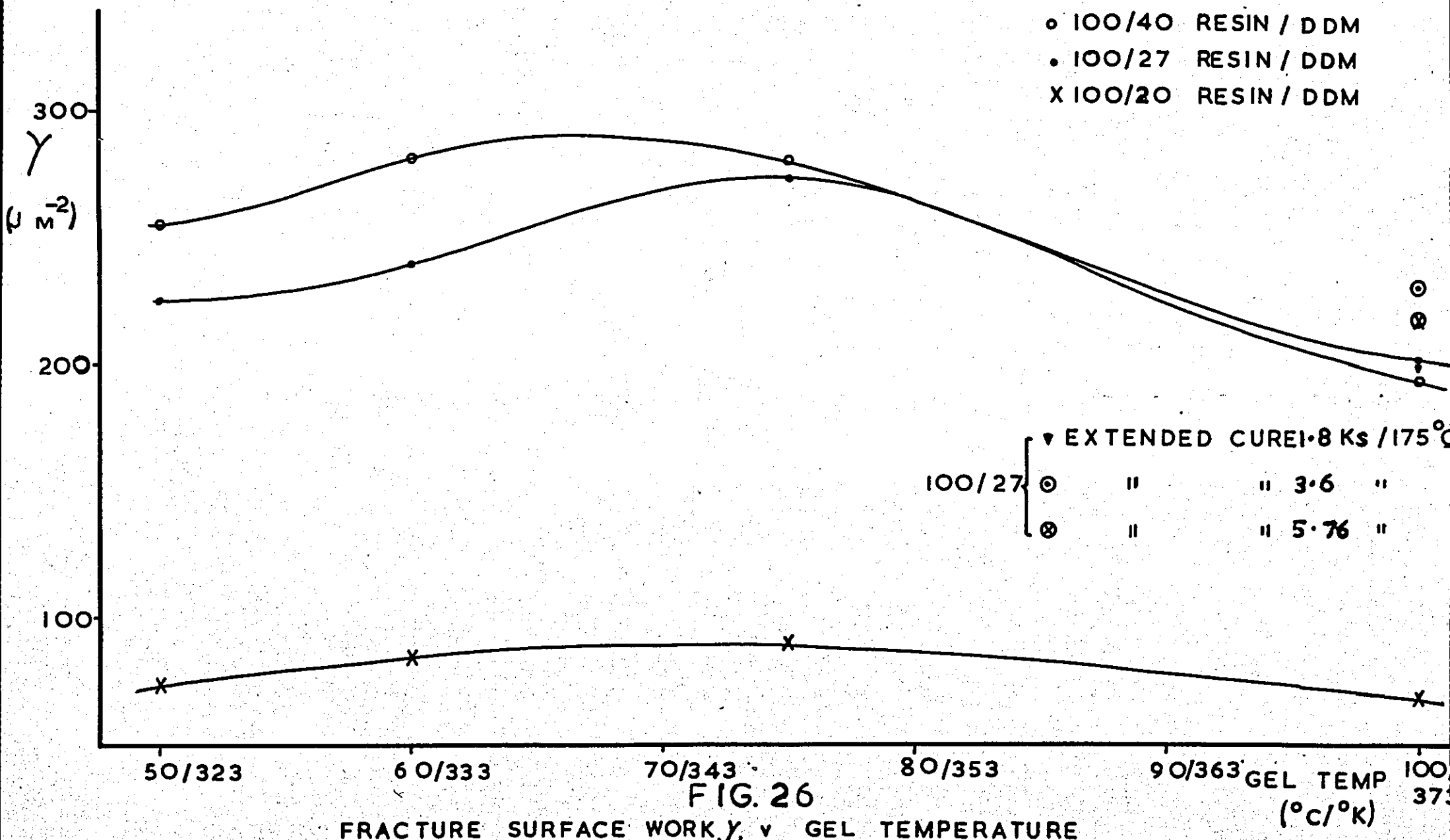


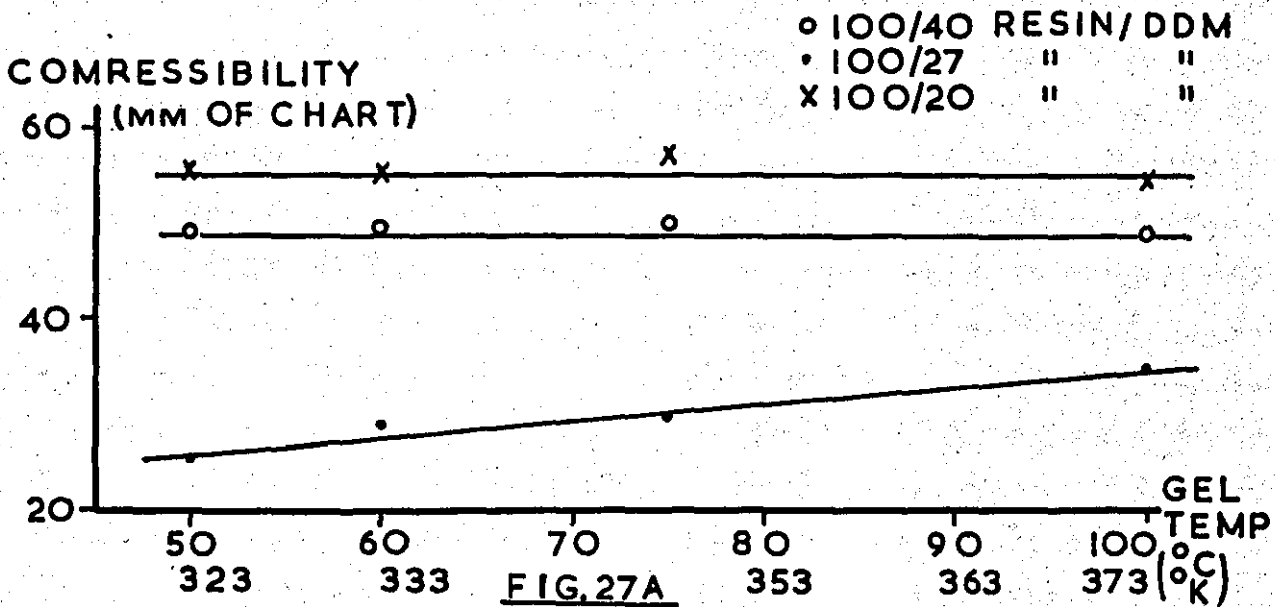
FIG 25

TYPICAL LOAD-EXTENSION CURVE TO FRACTURE FOR EPI828/DDM  
IN COMPRESSION - INTERMEDIATE DDM CONTENT

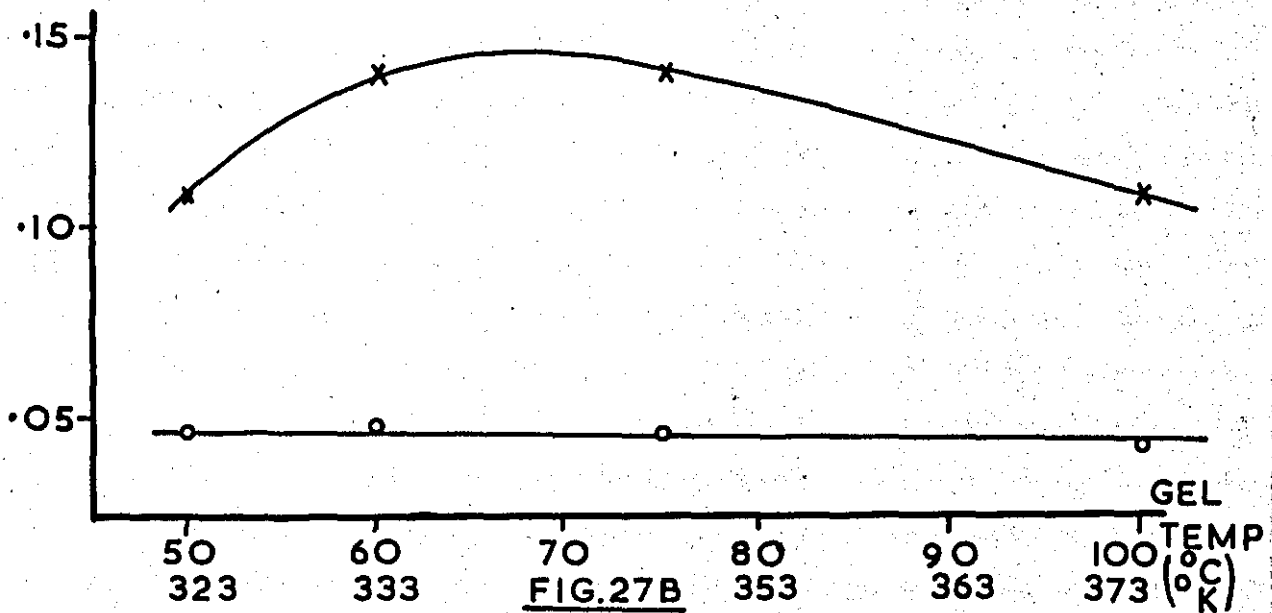




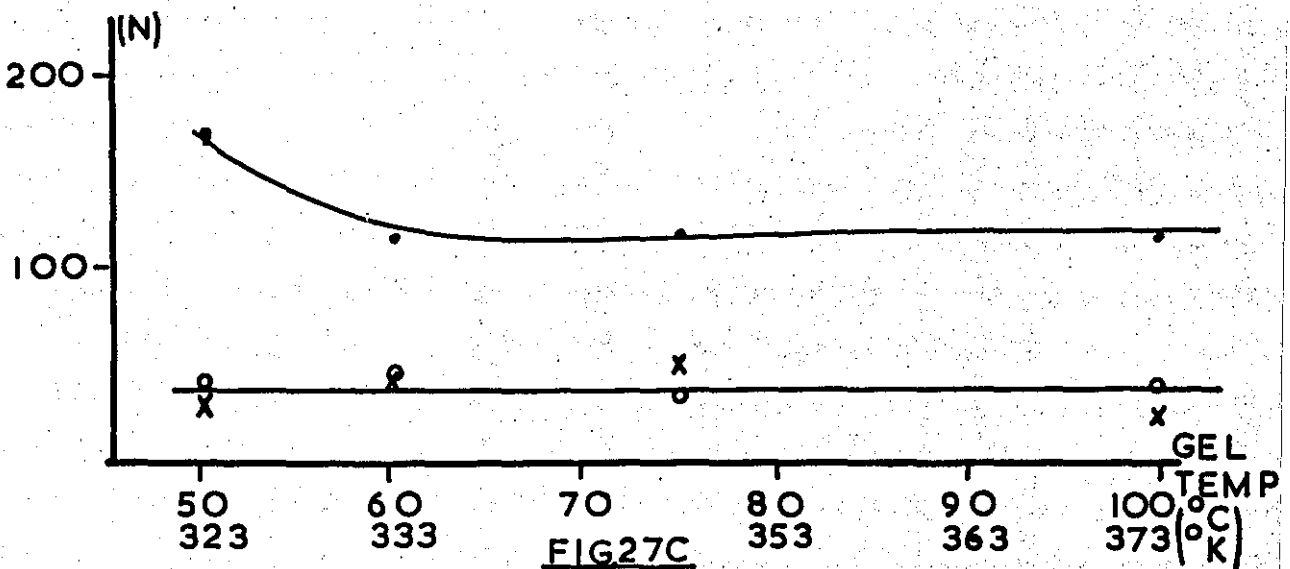
# COMPRESSION CHARACTERISTICS v GEL TEMPERATURE



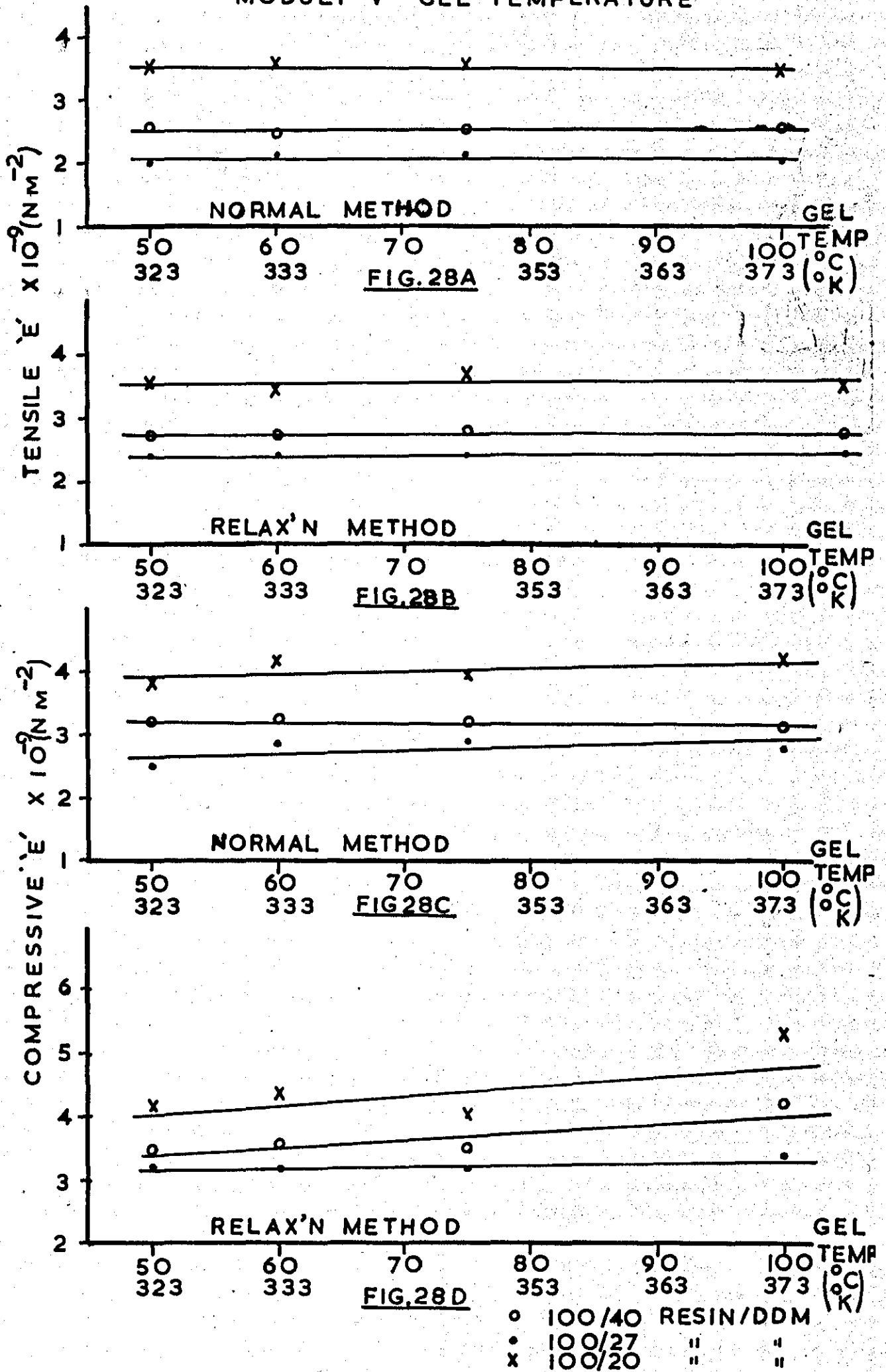
## Δ YIELD LOAD UPPER YIELD LOAD



## RELAXATION



# TENSILE AND COMPRESSIVE YOUNG'S MODULI v GEL TEMPERATURE



○ 100/40 RESIN/DDM  
 ● 100/27 " "  
 × 100/20 " "

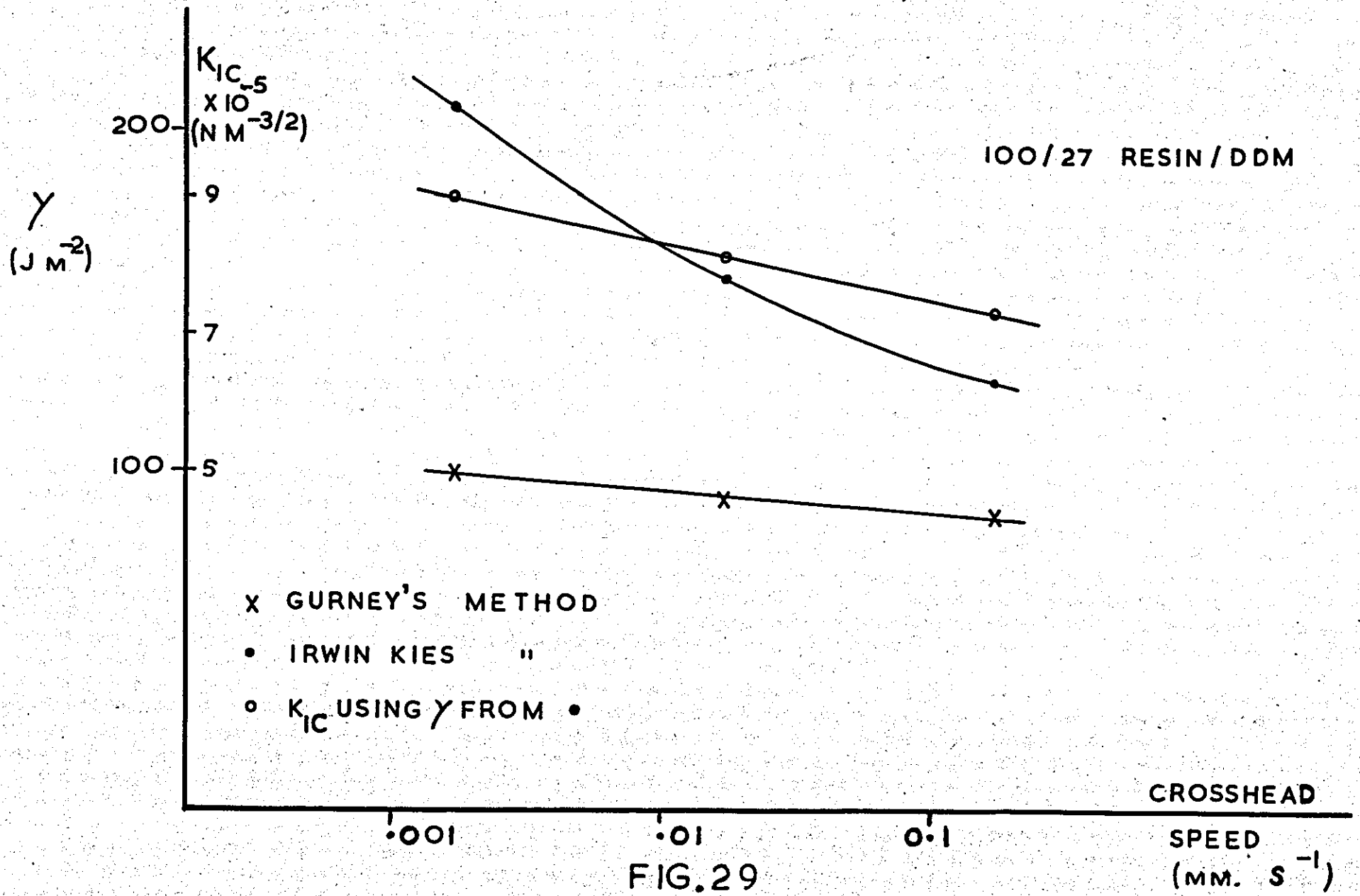


FIG.29

K<sub>IC</sub> & γ v CROSSHEAD SPEED

TENSILE YOUNG'S MODULUS  
v TEST SPEED

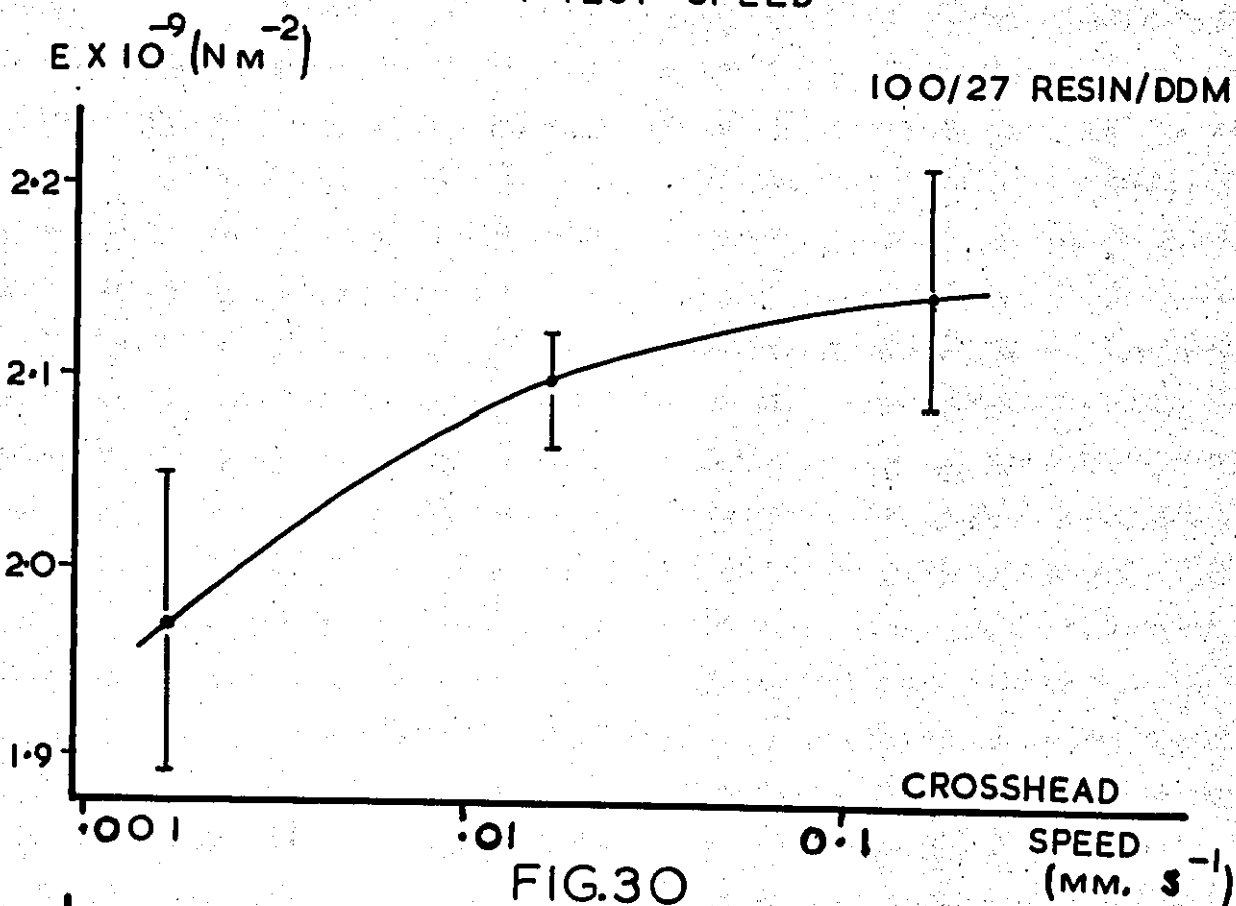


FIG. 30

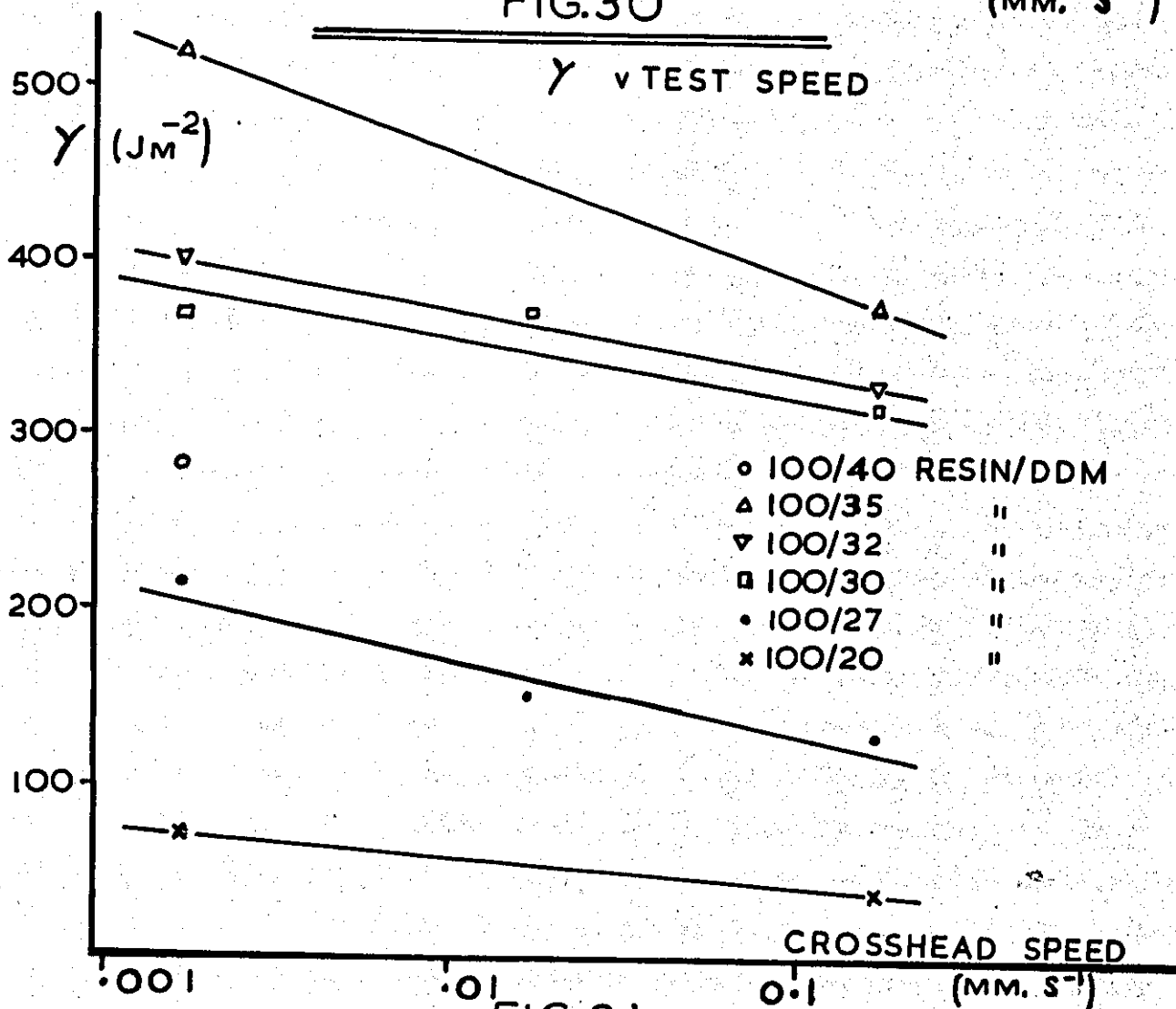
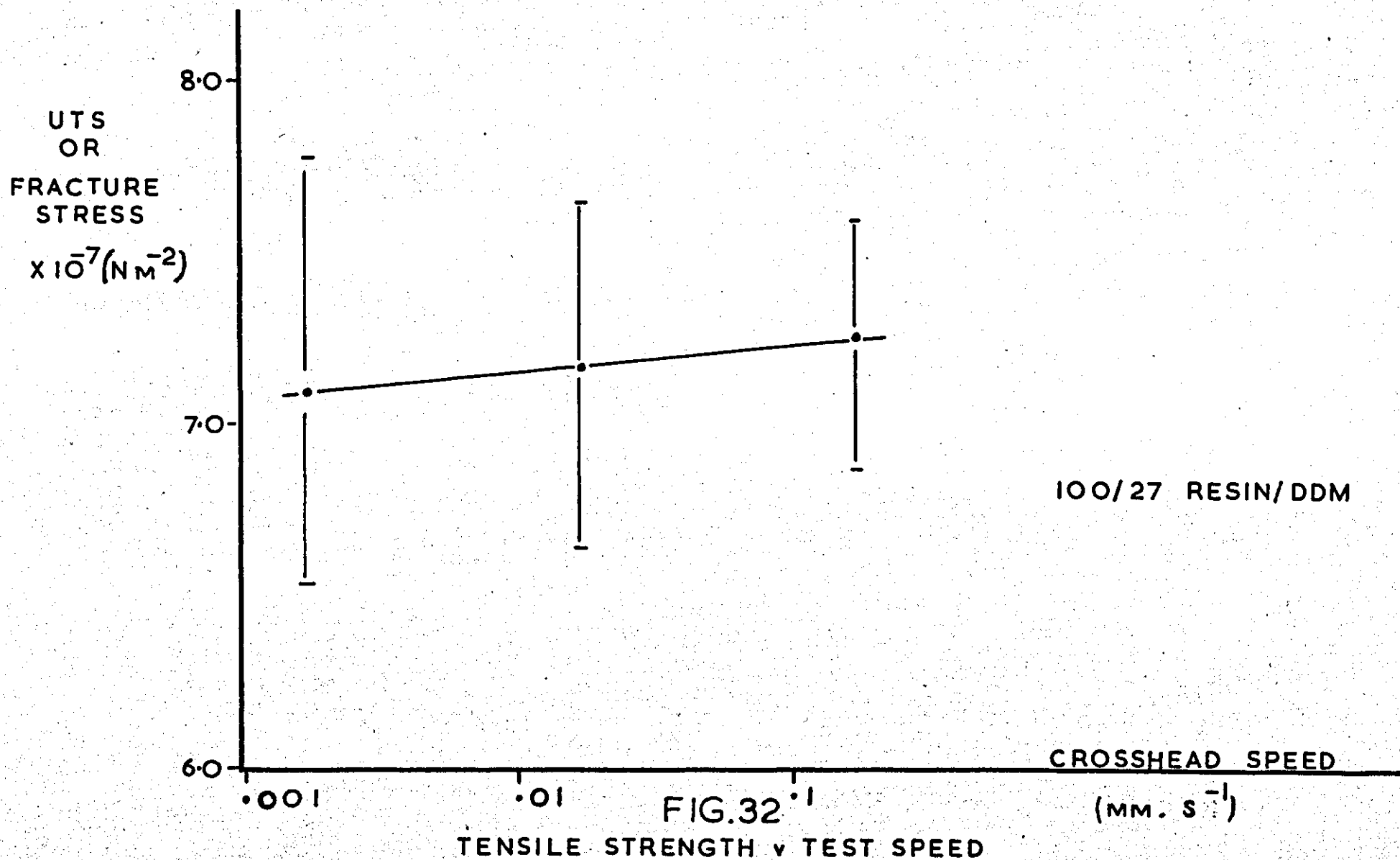


FIG. 31



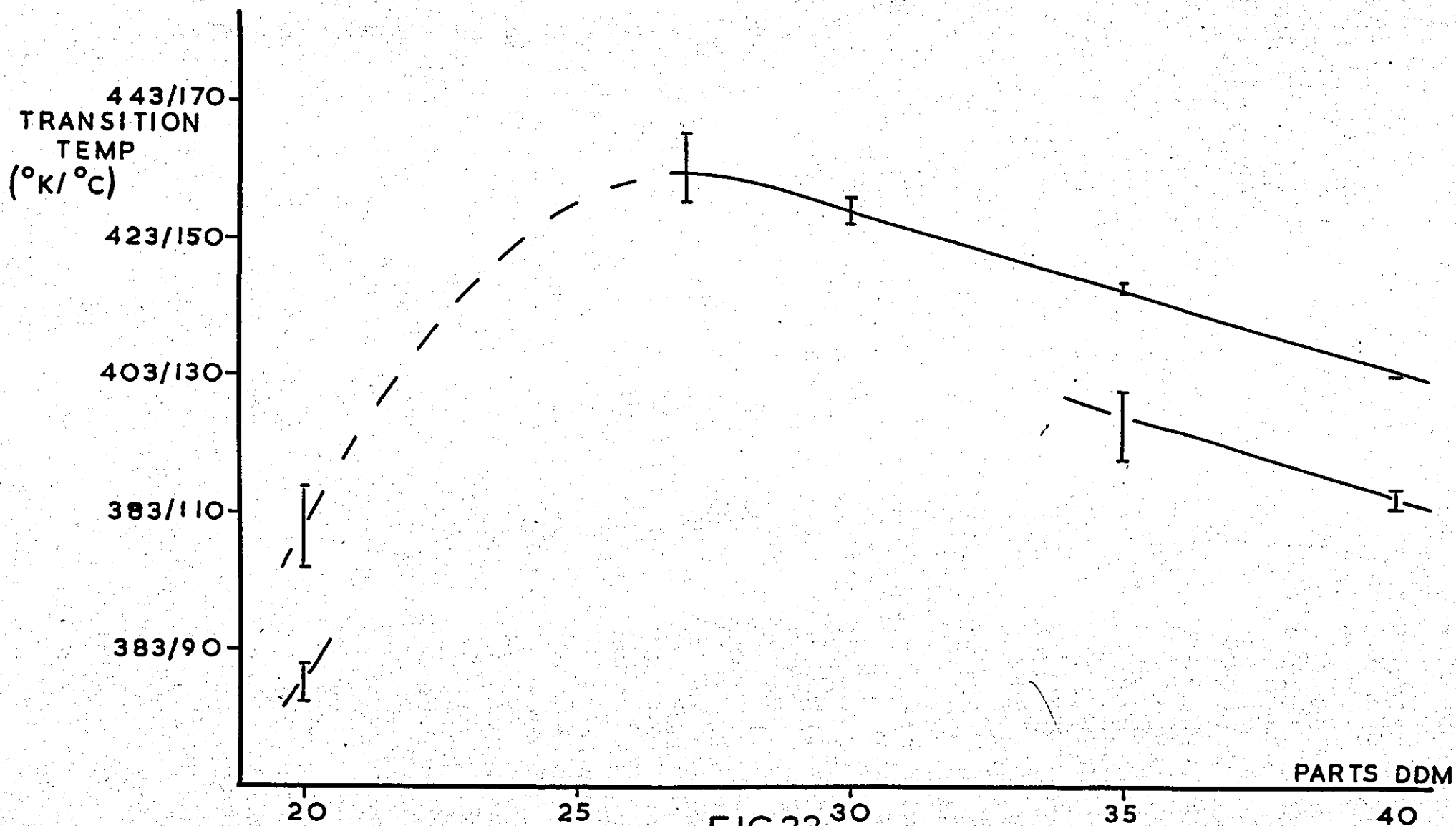


FIG.33  
THERMO-MECHANICAL TRANSITIONS v DDM CONTENT

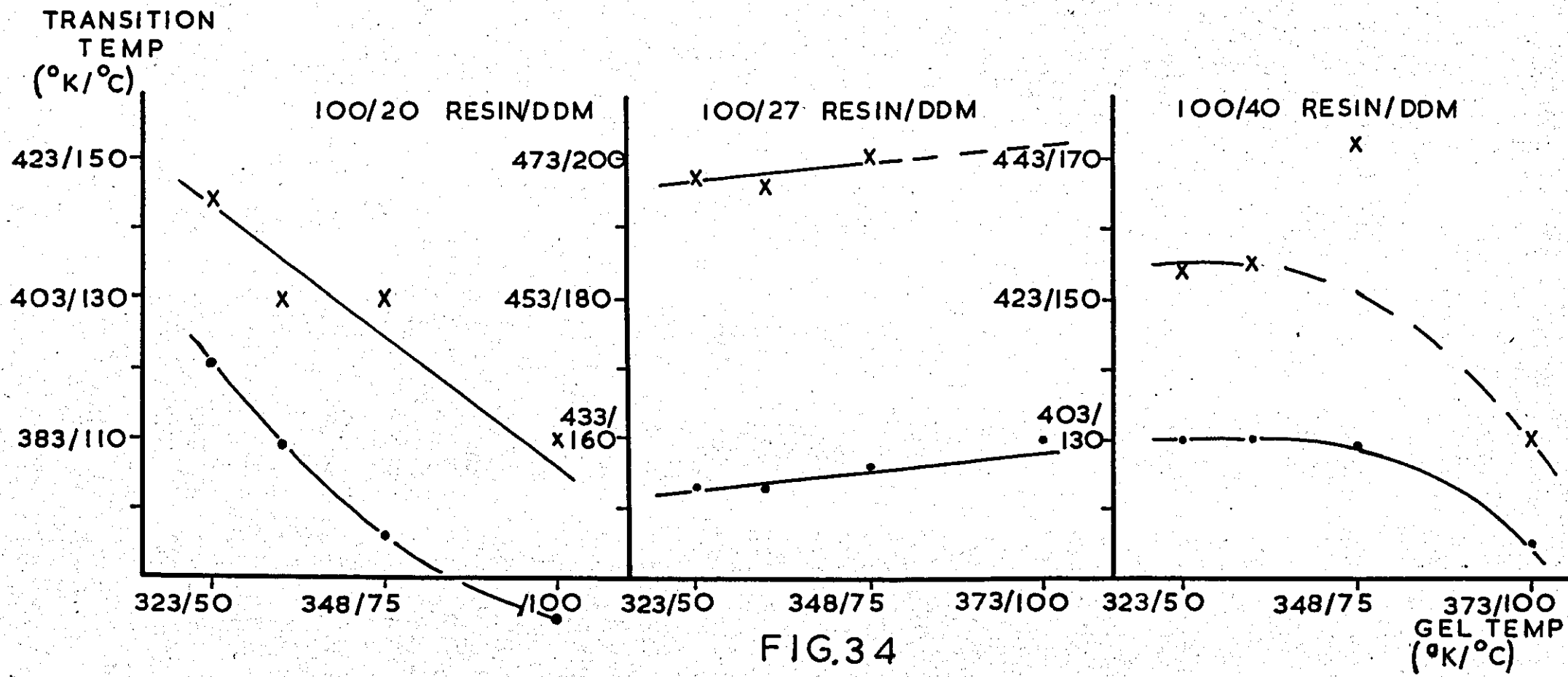


FIG.34

THERMO MECHANICAL TRANSITIONS  
 v GEL TEMPERATURE



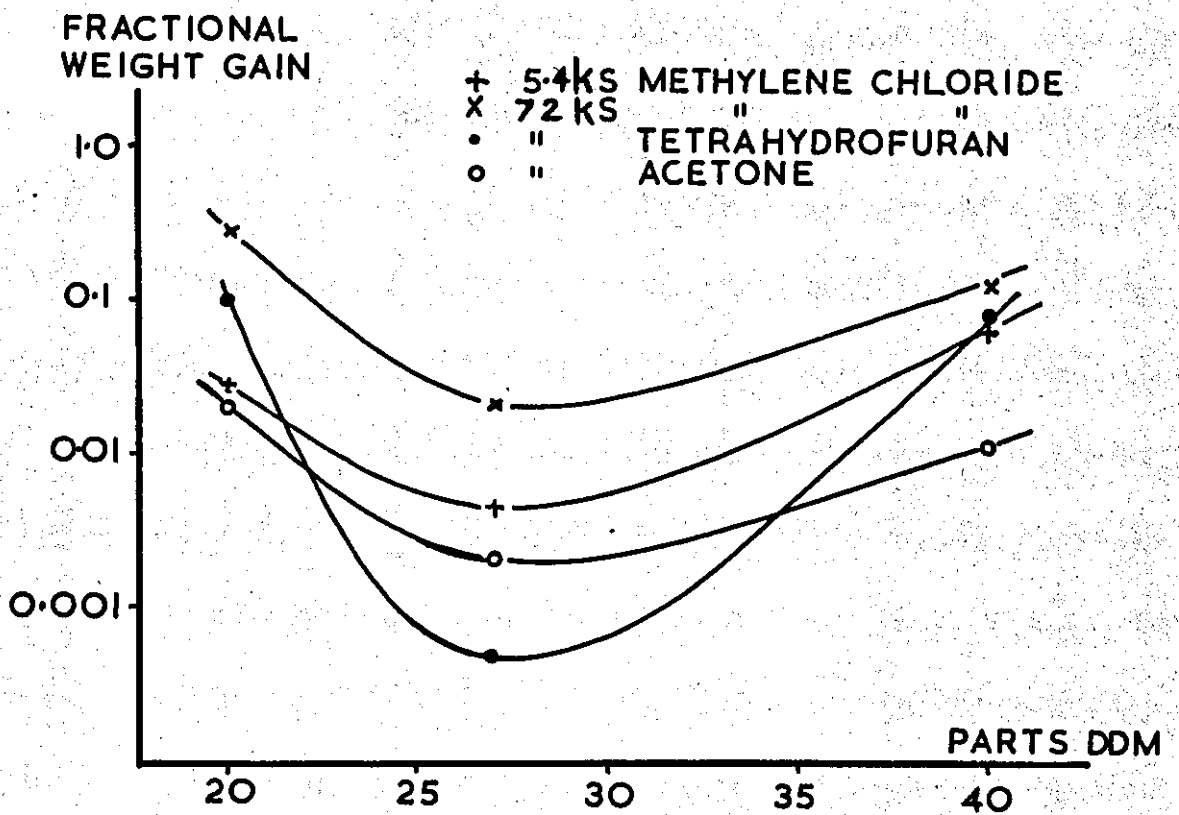


FIG.35  
SOLVENT UPTAKE v DDM CONTENT

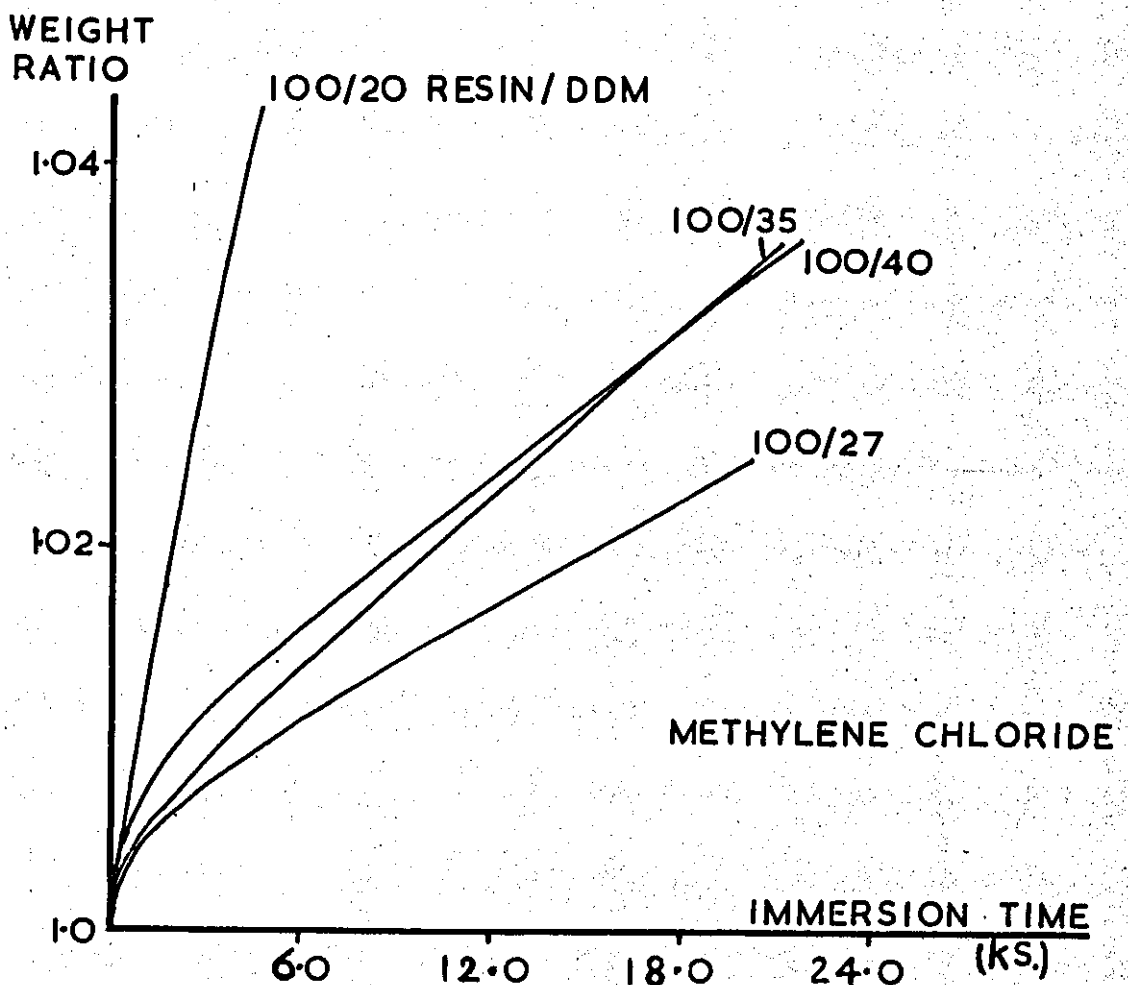


FIG.36  
SOLVENT UPTAKE v IMMERSION TIME  
& DDM CONTENT

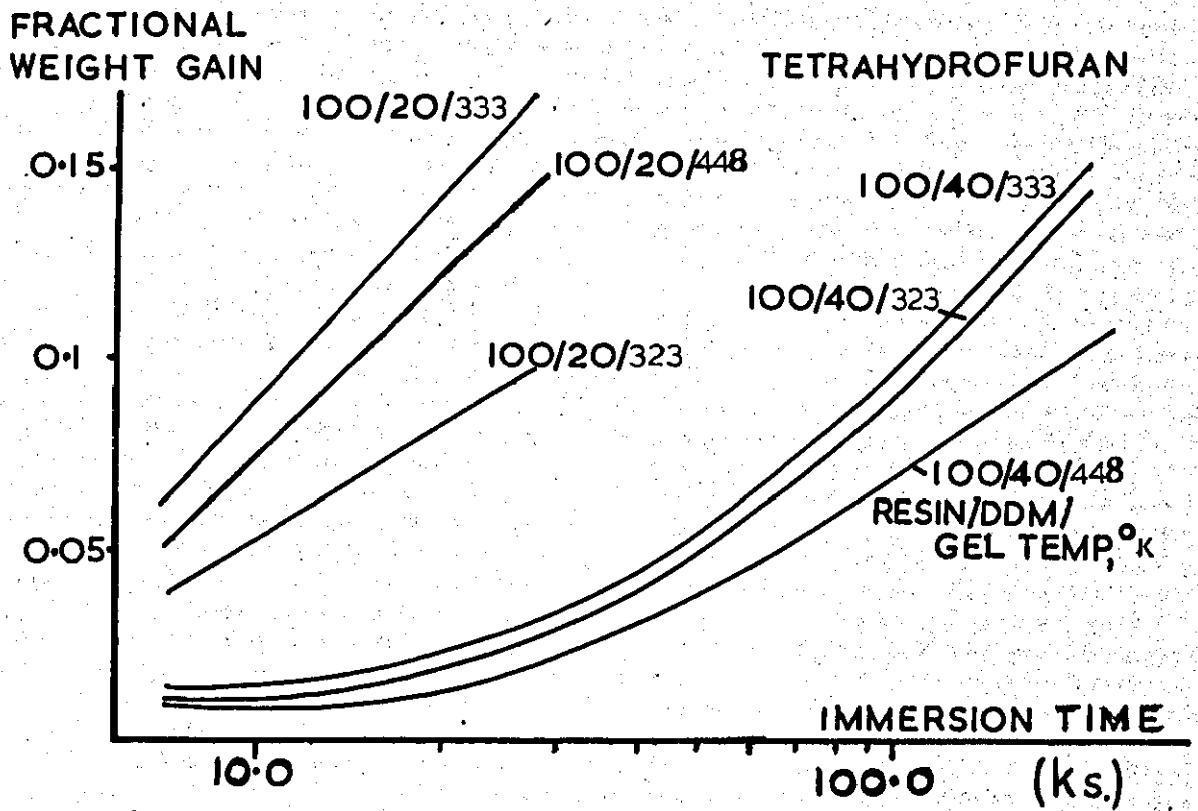


FIG. 37  
SOLVENT UPTAKE v IMMERSION TIME,  
DDM CONTENT & GEL TEMPERATURE

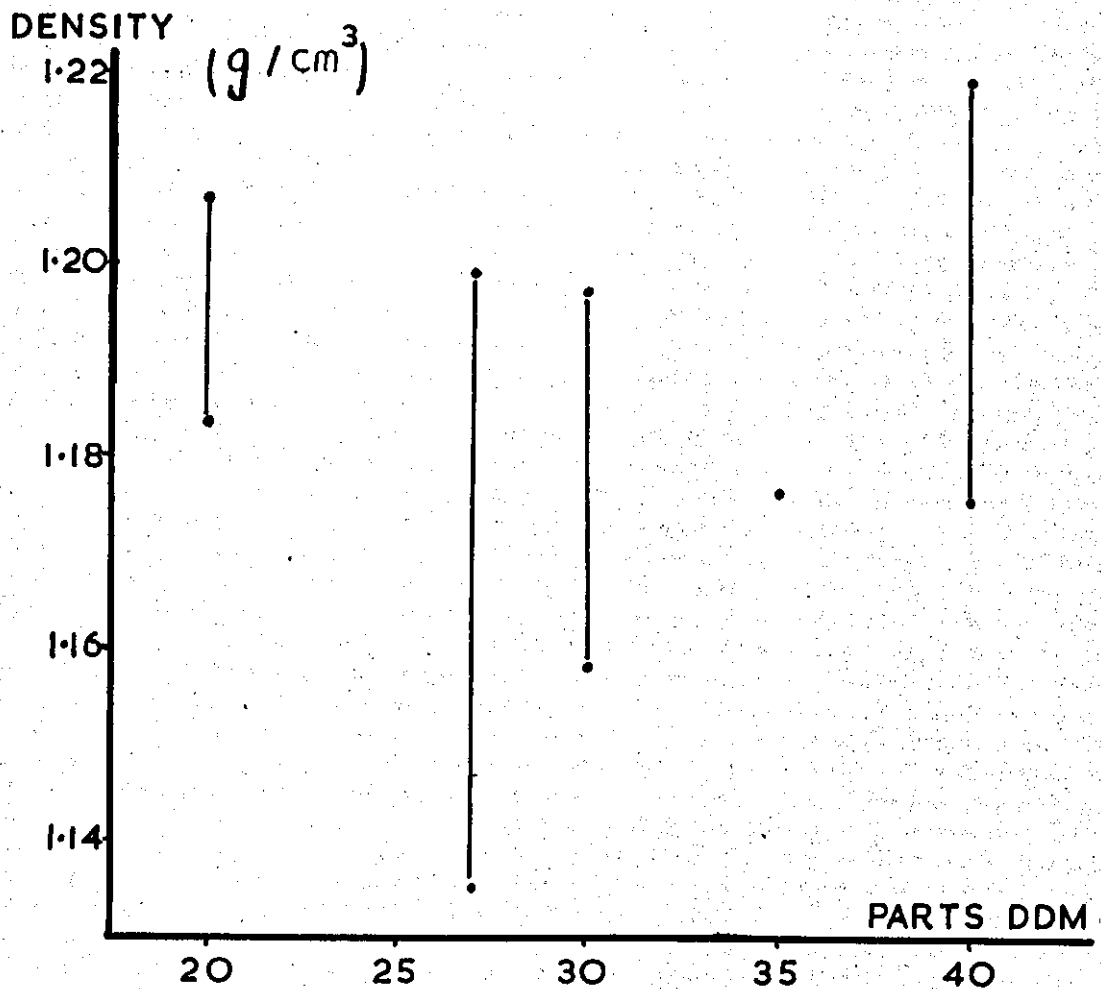


FIG. 38  
DENSITY v DDM CONTENT

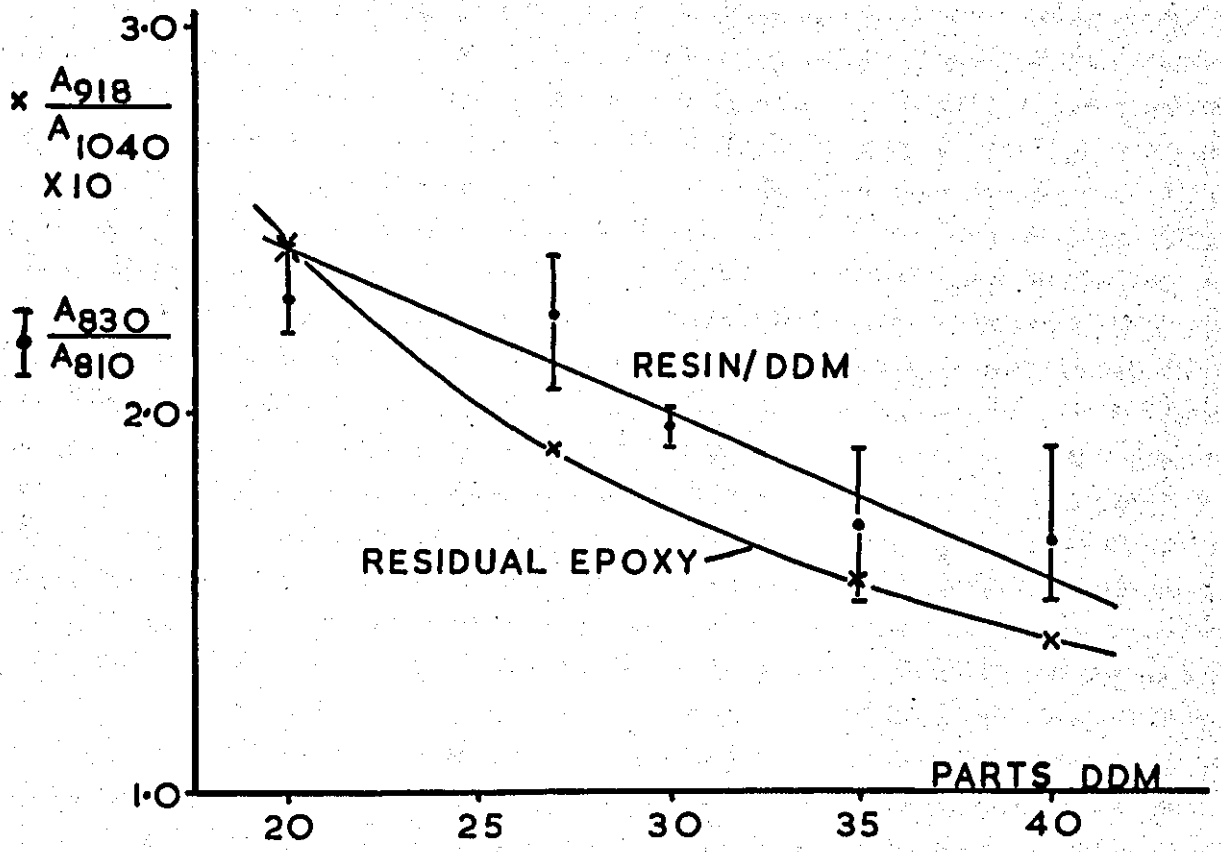


FIG.39  
INFRA RED DATA ON EPOXY/DDM CONTENTS

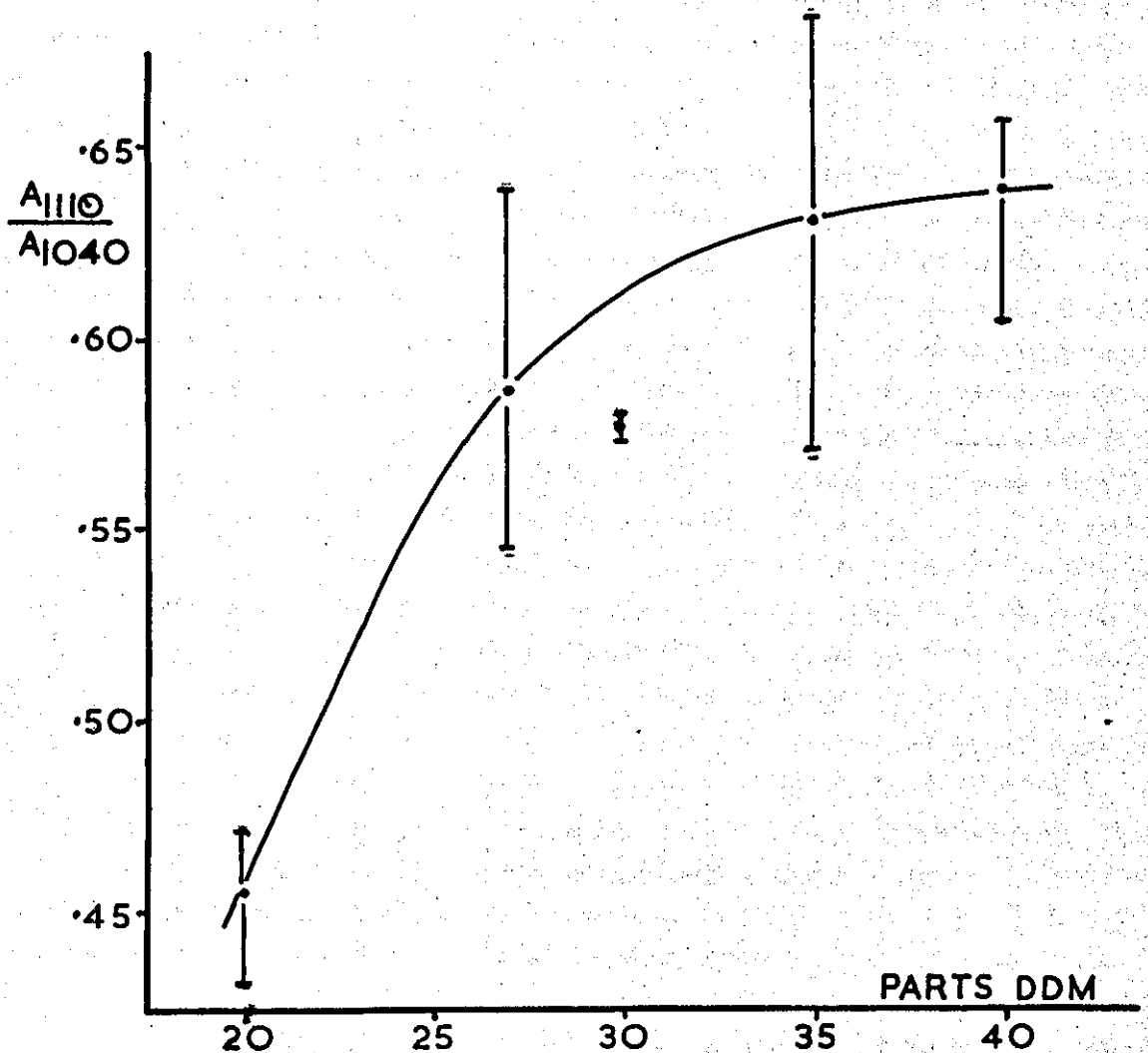
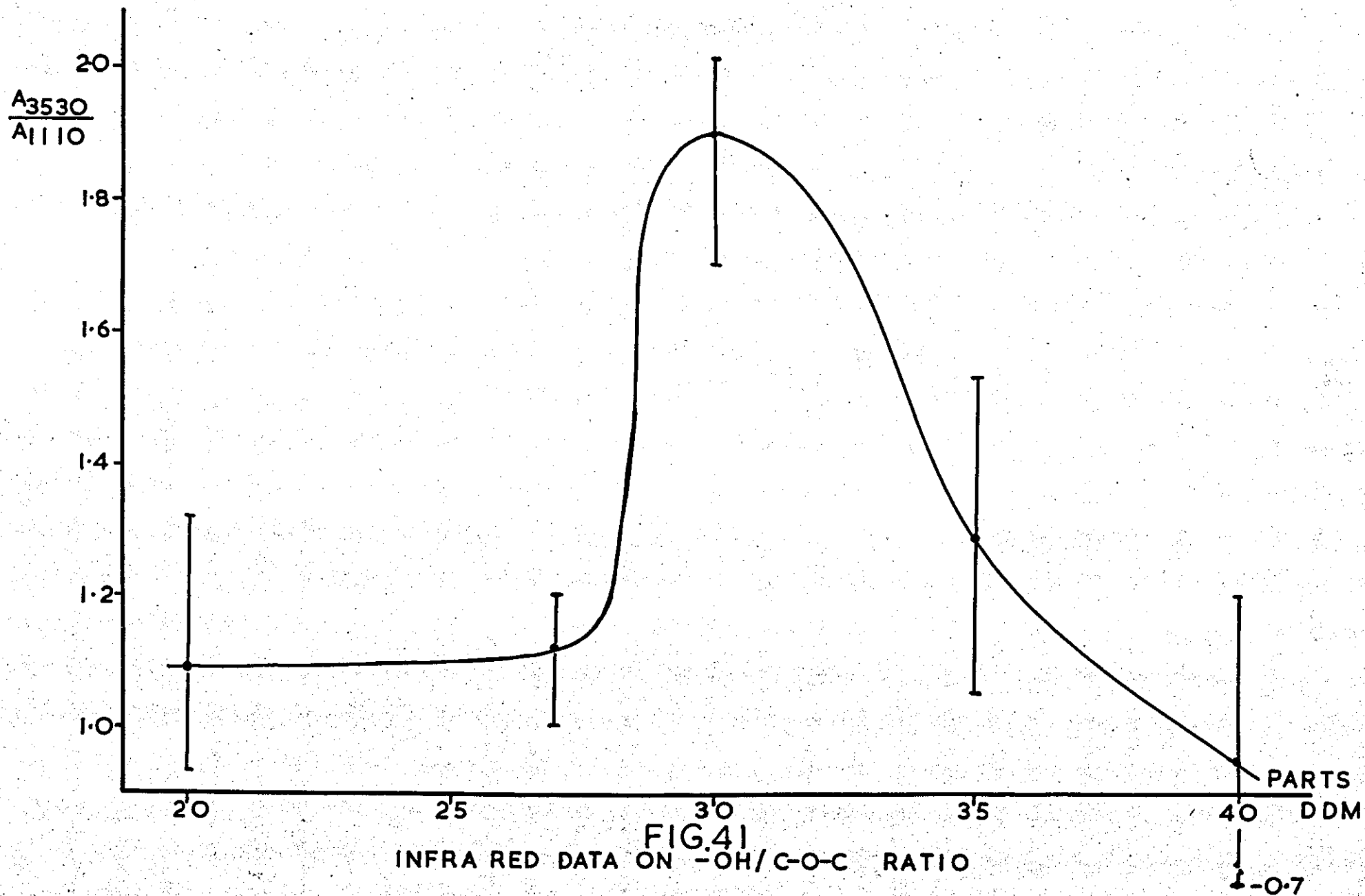


FIG.40  
INFRA RED DATA ON ETHER CROSS-LINKS

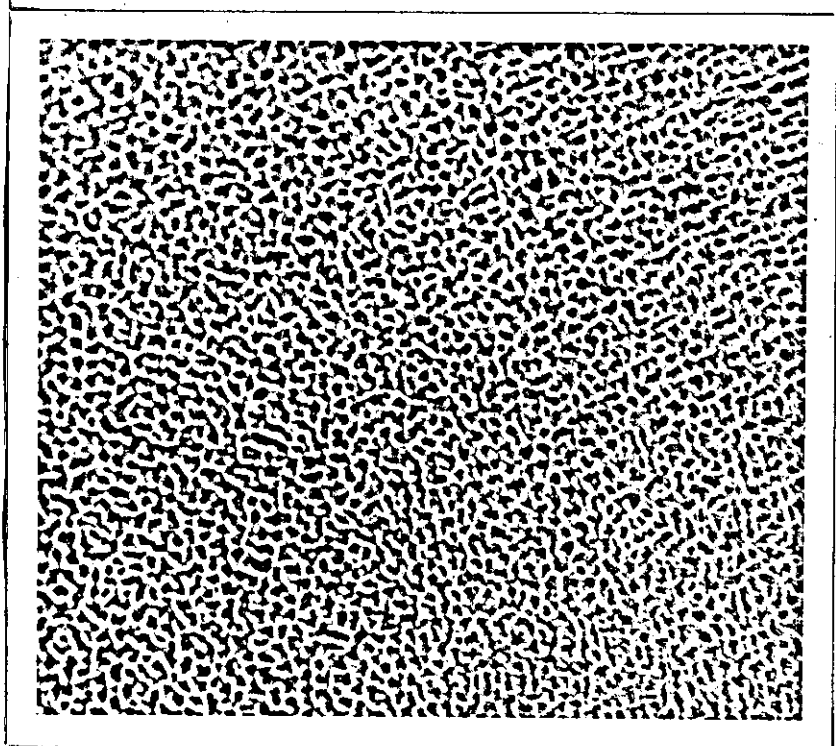
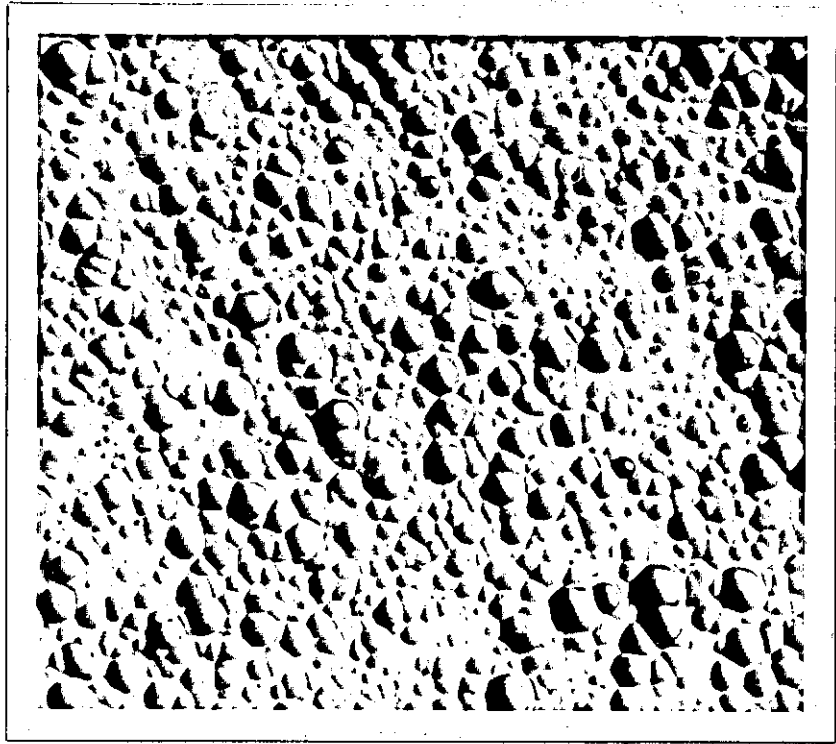


10  $\mu$ m

Fig. 42  
Typical feature revealed by  
etching epoxy in  $\text{CrO}_3/\text{H}_2\text{O}$

10  $\mu$ m

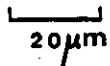
Fig. 43  
Typical feature revealed by  
etching epoxy in  $\text{CrO}_3/\text{H}_2\text{O}/$   
 $\text{H}_3\text{PO}_4/\text{H}_2\text{SO}_4$





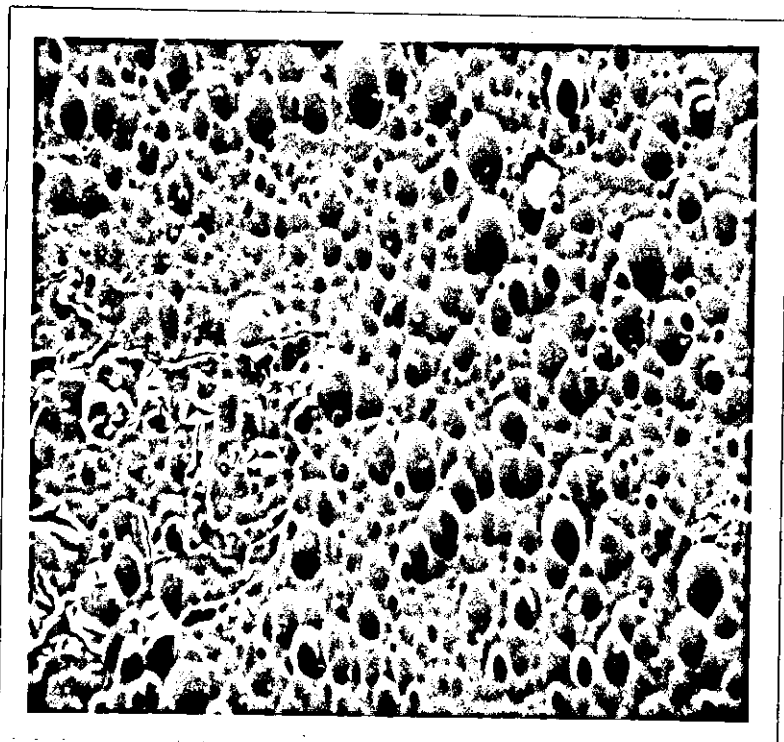
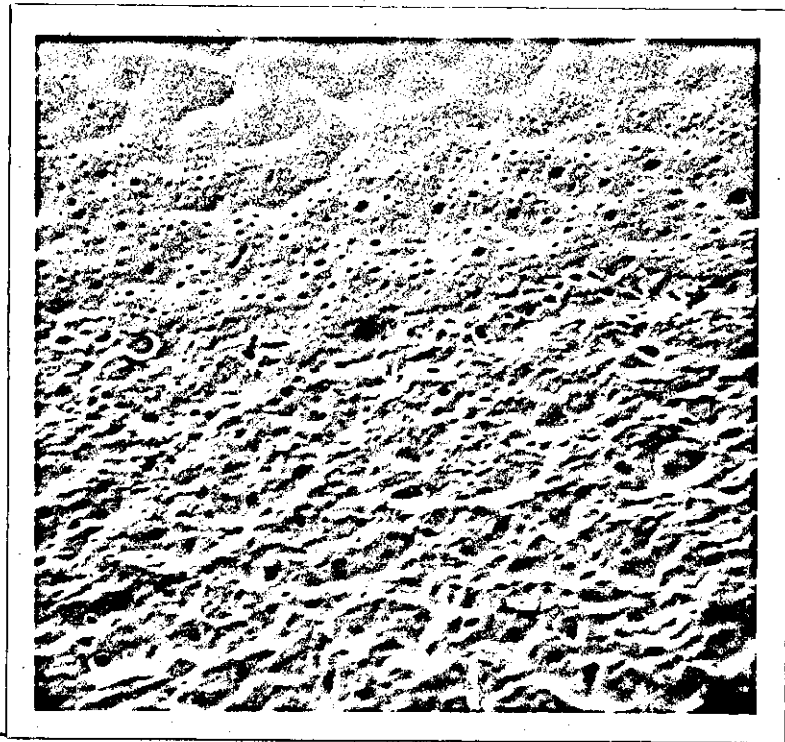
1µm

Fig. 44  
Scanning-electron micrograph of  
etched resin shown in Fig. 43

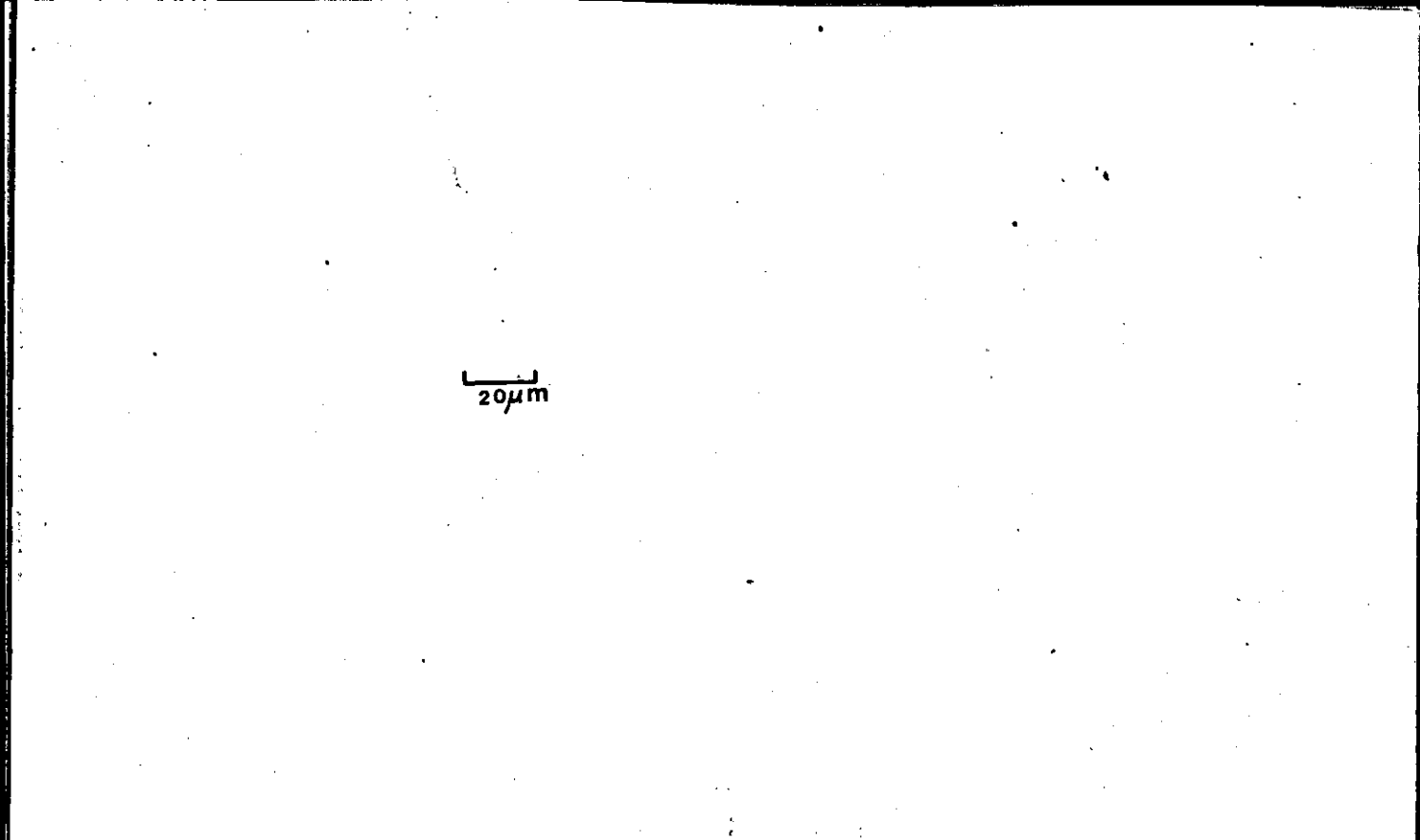


20µm

Fig. 45  
Distortion of resin revealed by  
chromic acid etching







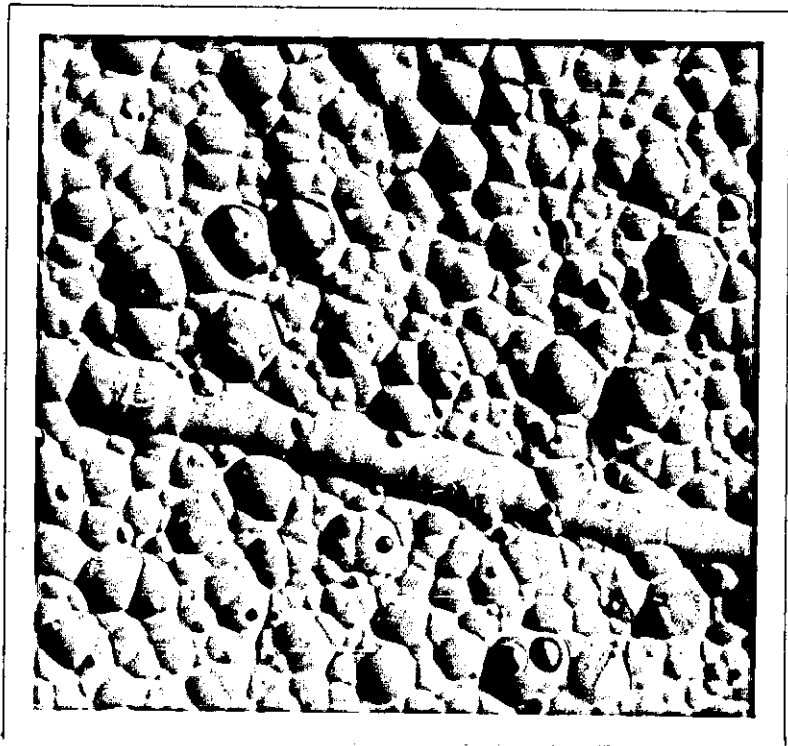
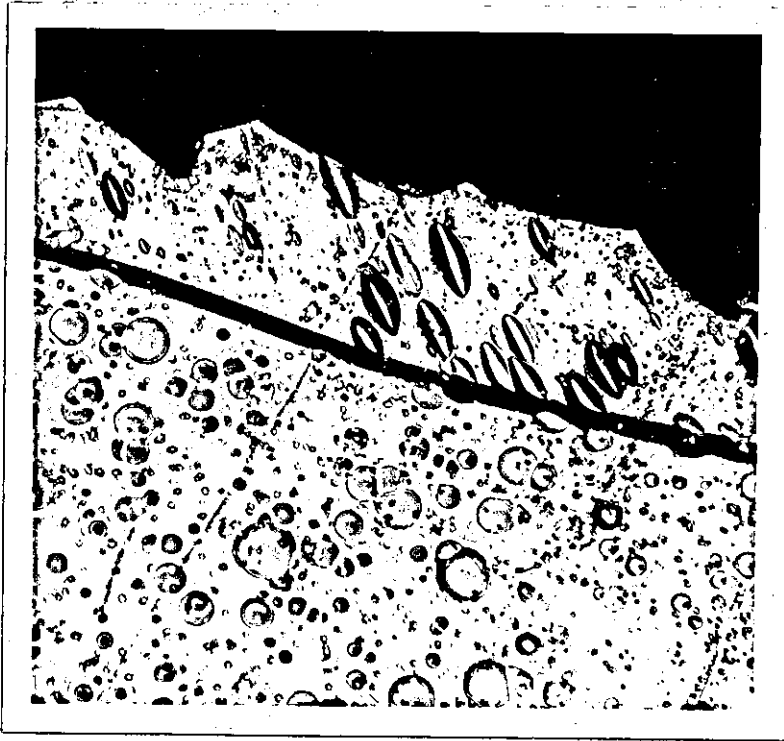
20 $\mu$ m

Fig. 46  
Cleavage fracture surface etched  
in chromic acid



10 $\mu$ m

Fig. 47  
Scratch marks on chemically etched  
epoxy

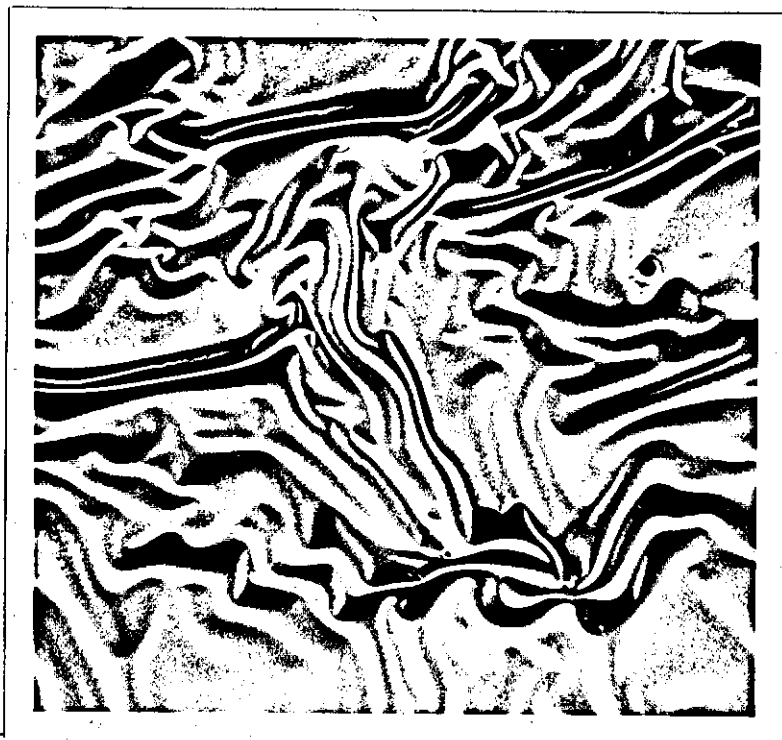
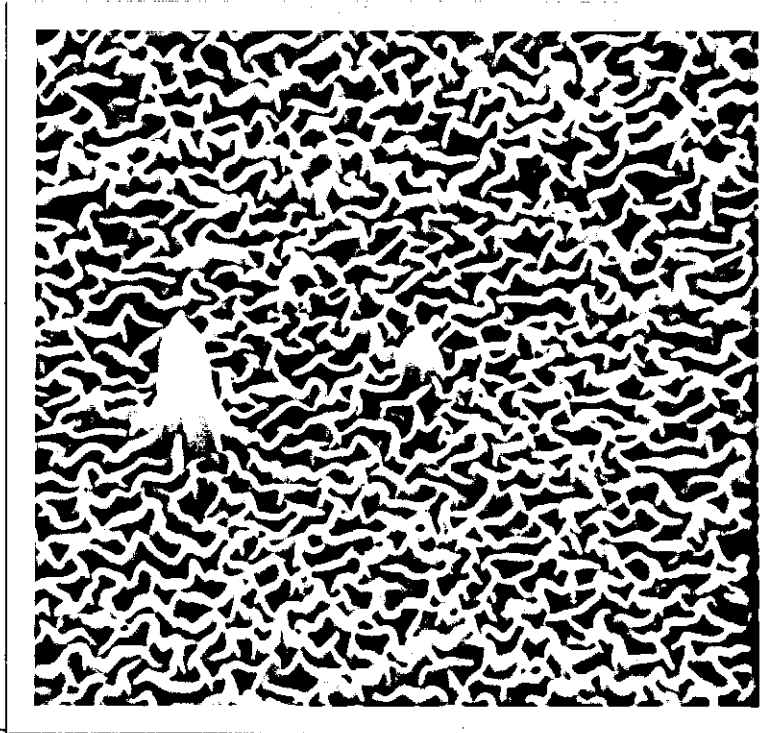


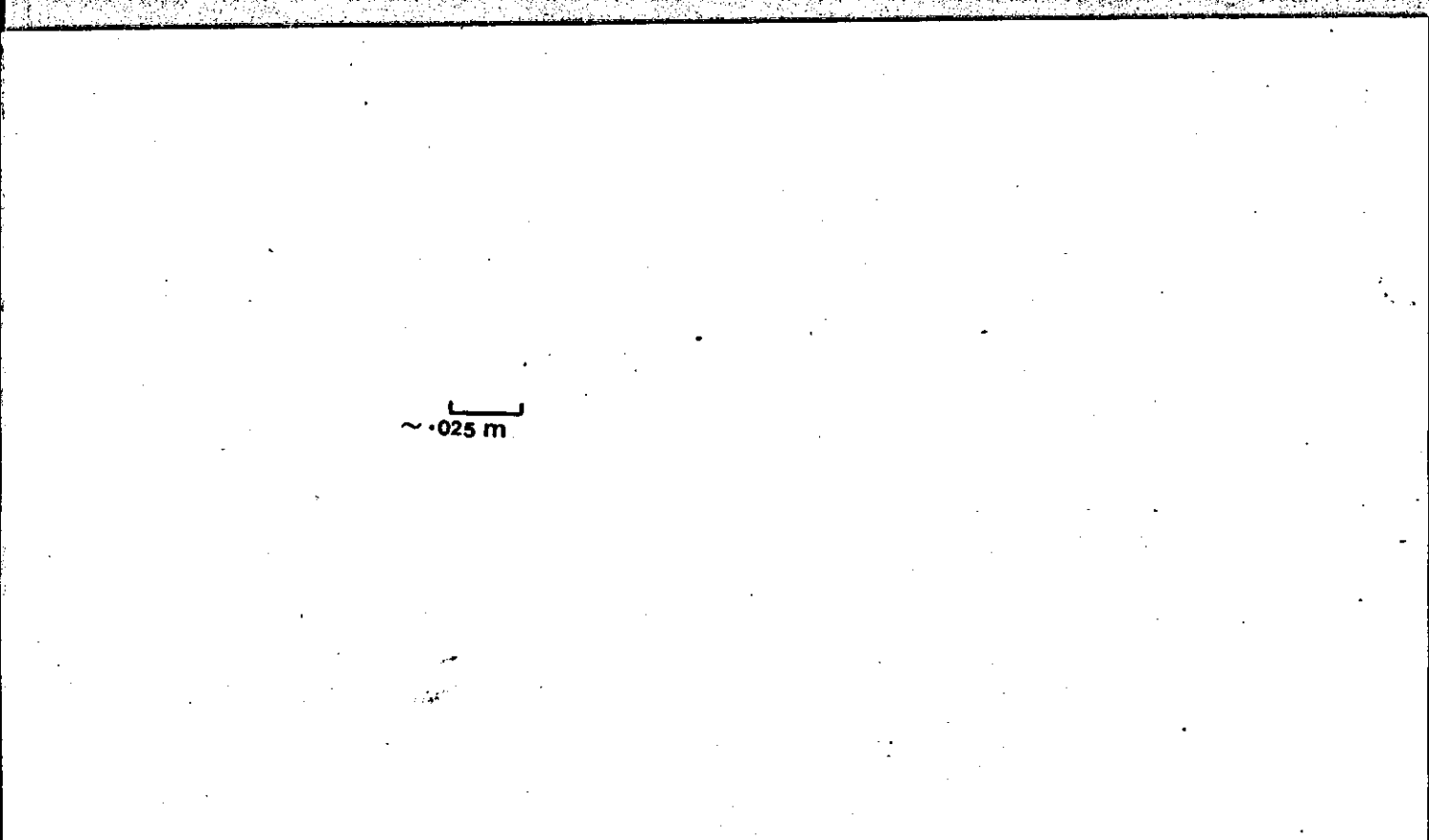
16  $\mu$ m

Fig. 48  
Wrinkled surface of ion bombarded epoxy

18  $\mu$ m

Fig. 49  
Flash heated epoxy surface





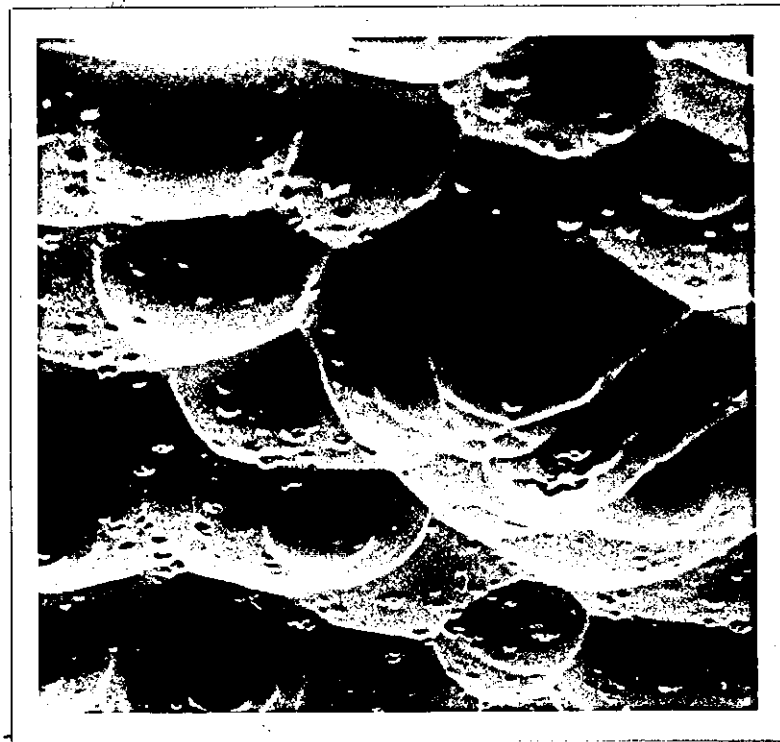
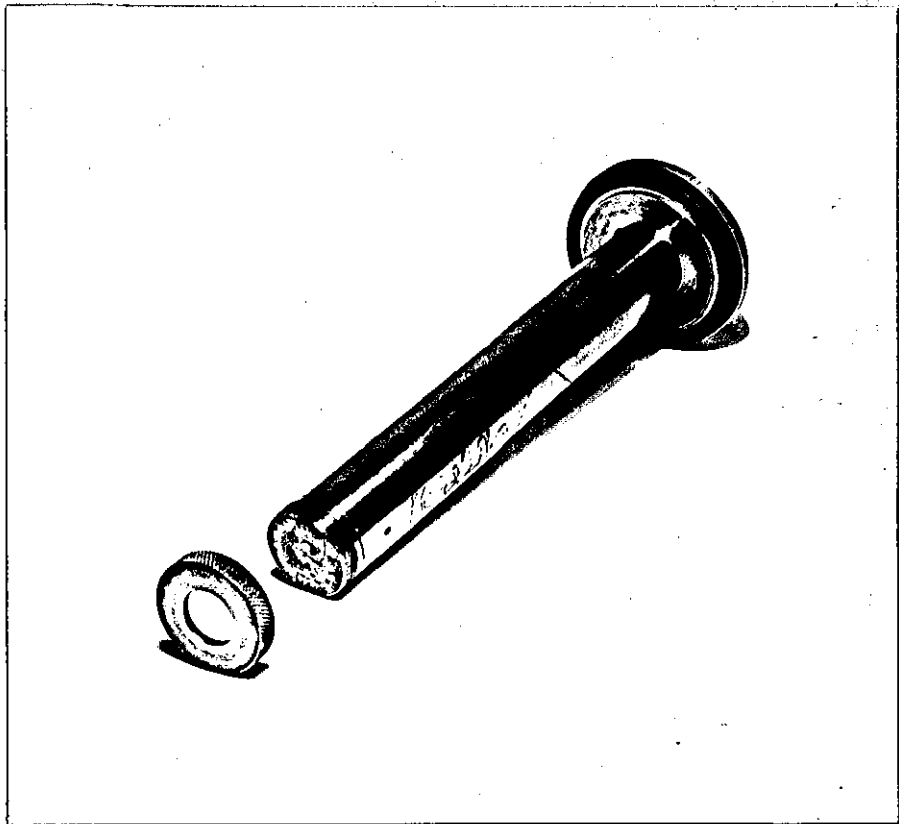
~.025 m

Fig. 50  
Specimen mount for cryogenic ion  
bombardment



5 $\mu$ m

Fig. 51  
Surface of low DDM content resin  
after cryogenic ion bombardment





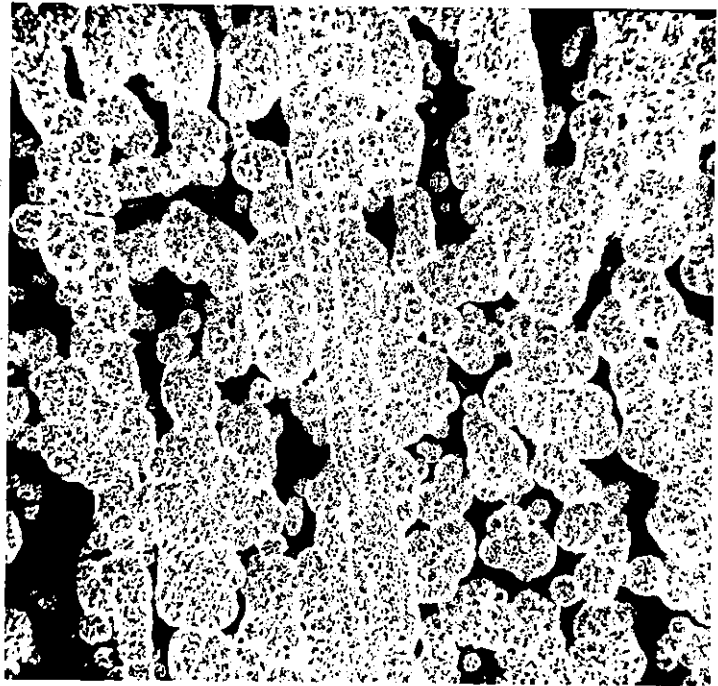
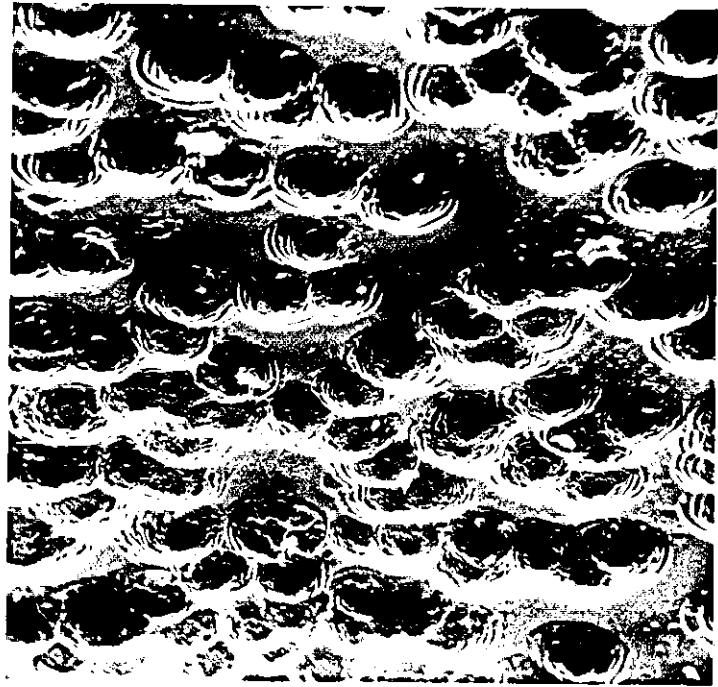
5 $\mu$ m

Fig. 52  
Surface of intermediate DDM content  
resin after cryogenic ion bombardment



10 $\mu$ m

Fig. 53  
Surface of polished stoichiometric  
resin after cryogenic ion  
bombardment







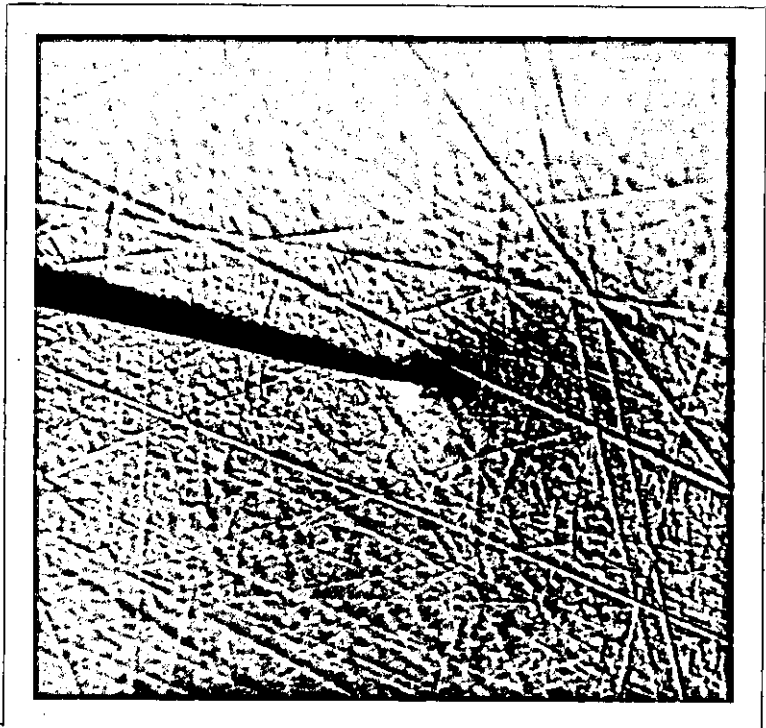
10 $\mu$ m

Fig. 54  
Meniscus of low DDM content cast  
slab after cryogenic ion  
bombardment



10 $\mu$ m

Fig. 55 (a)  
Surface deformation at the tip  
of a crack in a "tough" resin  
immediately after arrest



10 $\mu$ m

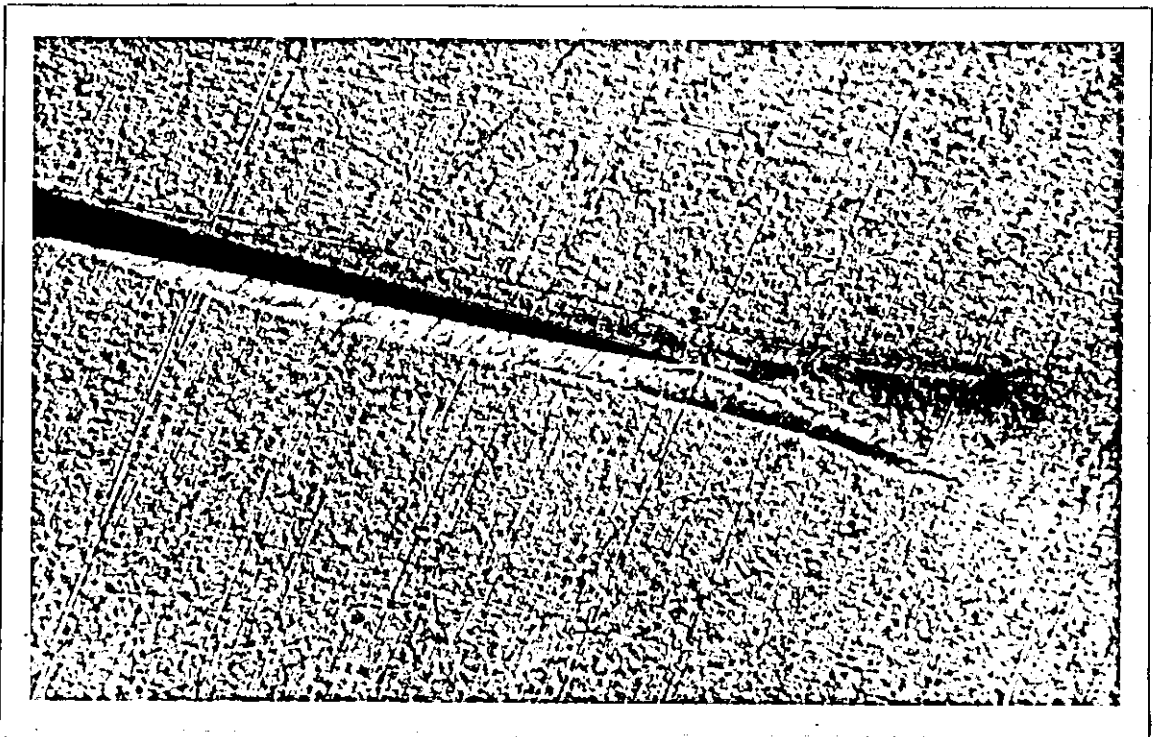
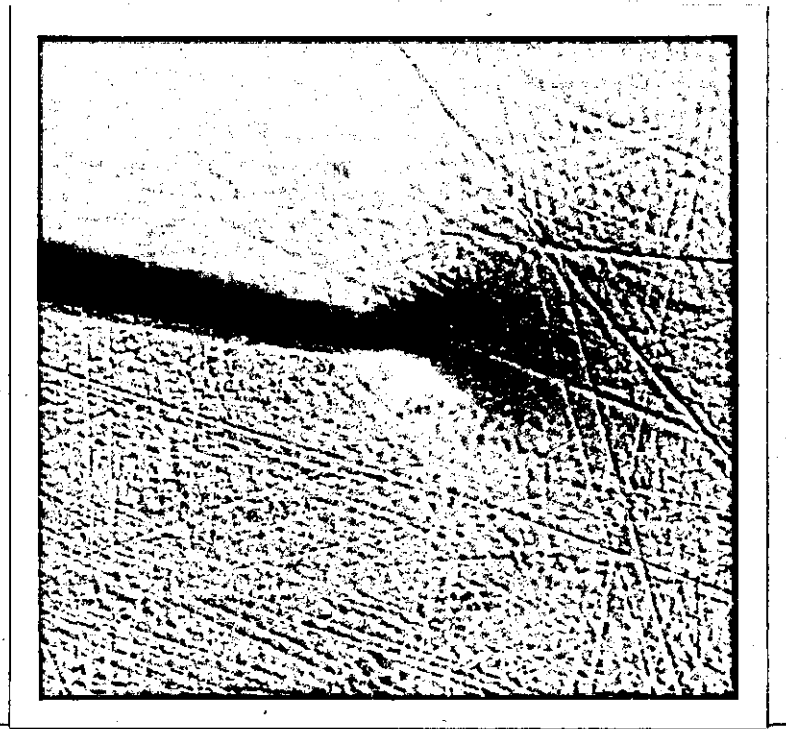


Fig. 55 (b)  
As Fig. 55 (a), after further strain

20 $\mu$ m



Fig. 56 (a)  
Surface deformation at the tip  
of a crack in low DDM resin  
immediately after arrest





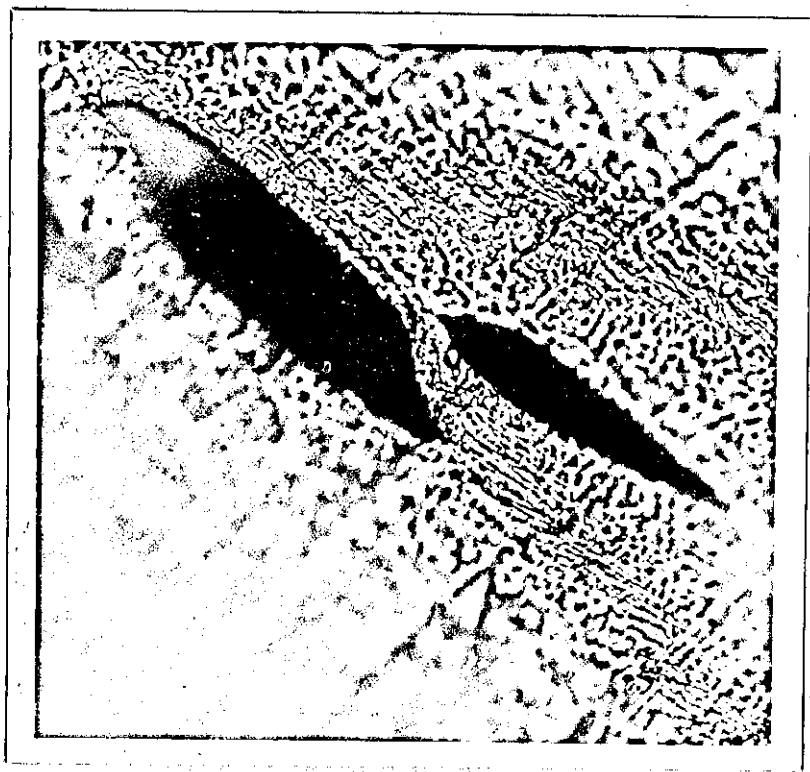
10µm

Fig. 56 (b)  
As Fig. 56 (a), after further  
crack movement



10µm


Fig. 57  
Surface region of a crack tip in  
a "tough" resin undergoing slow  
crack advance. (Specimen etched  
prior to testing)





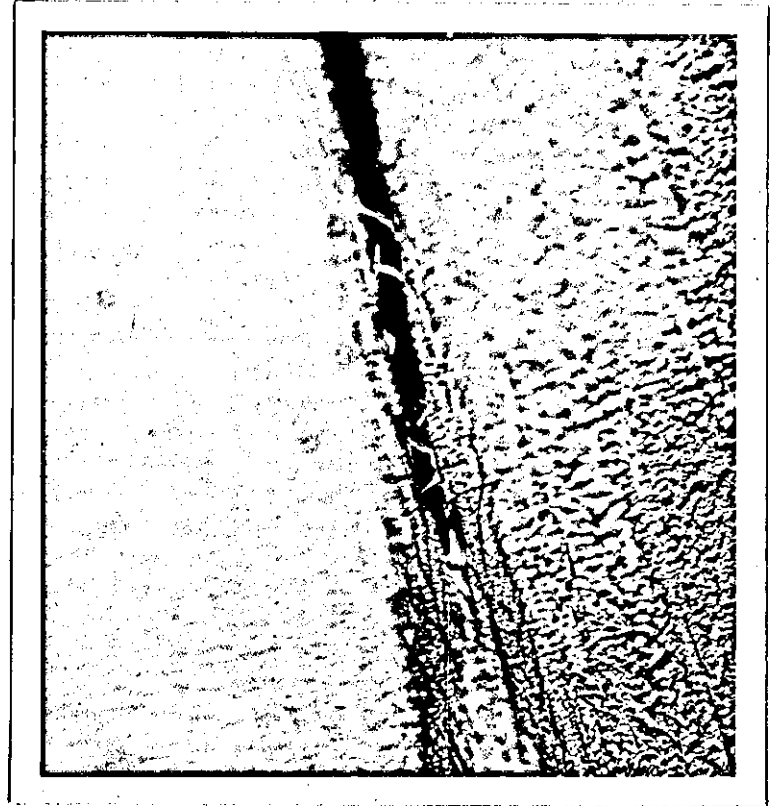
50 $\mu$ m

Fig. 58  
Surface region of a crack tip  
in low DDM resin - near an arrest  
location. (Specimen etched prior  
to testing)




12.5 $\mu$ m

Fig. 59  
Surface region of a crack tip in  
a "tough" resin after slow crack  
growth. (Specimen etched after  
testing)

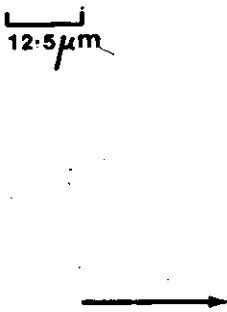






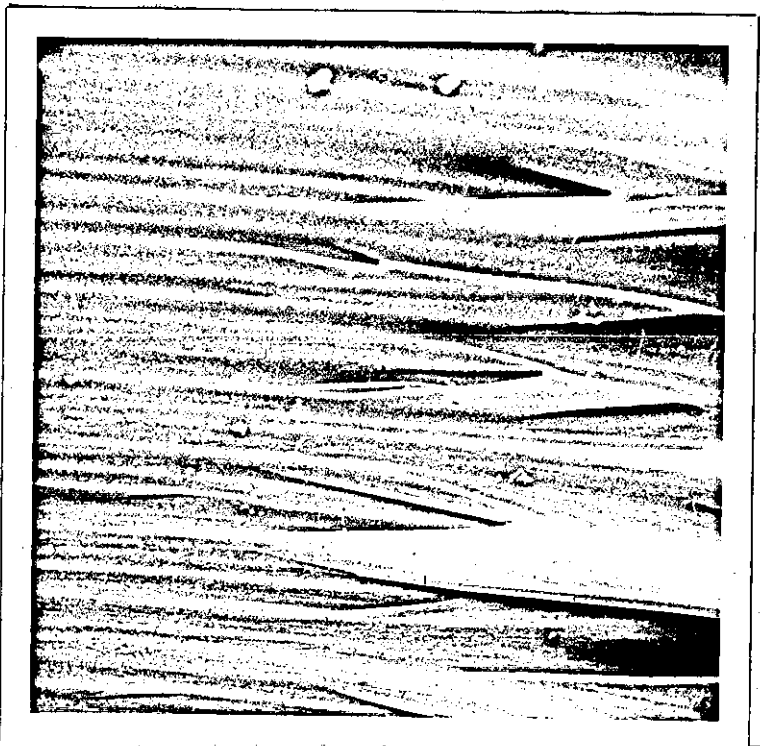
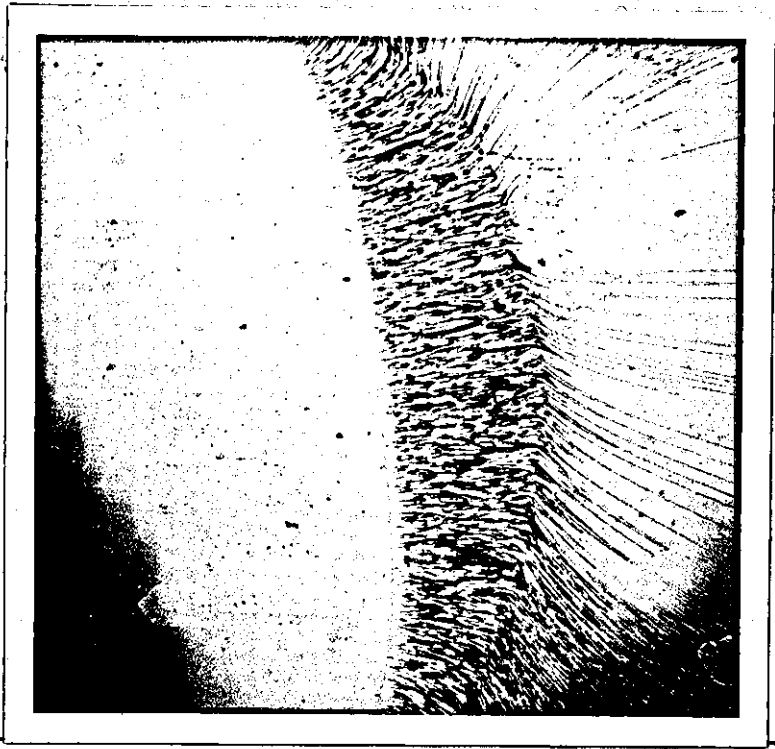
200  $\mu$ m

Fig. 60  
Arrest and slow growth region on  
a cleavage fracture surface of a  
"tough" resin. (Optical  
micrograph)



12.5  $\mu$ m

Fig. 61  
Scanning electron micrograph of  
transition from smooth area of  
a prior crack jump to the rough  
zone of the next jump. (35 parts  
DDM)





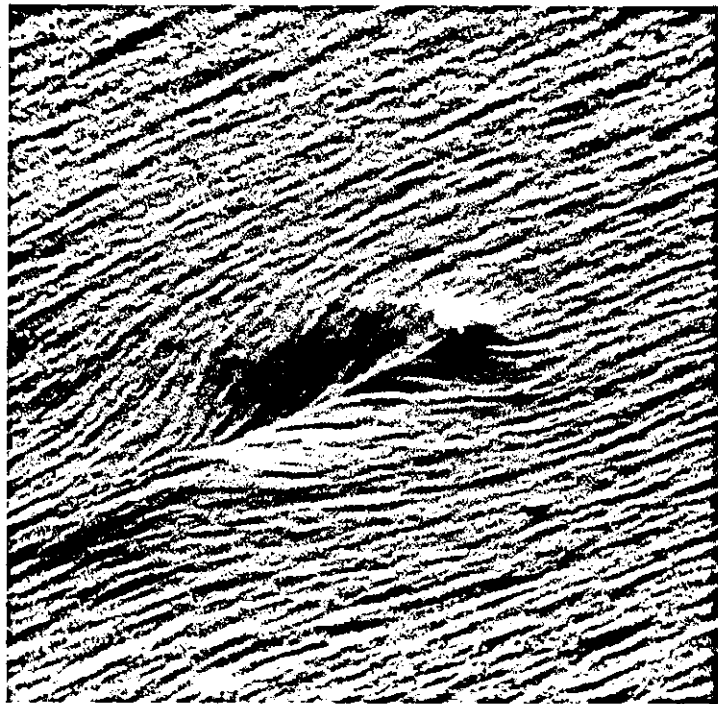
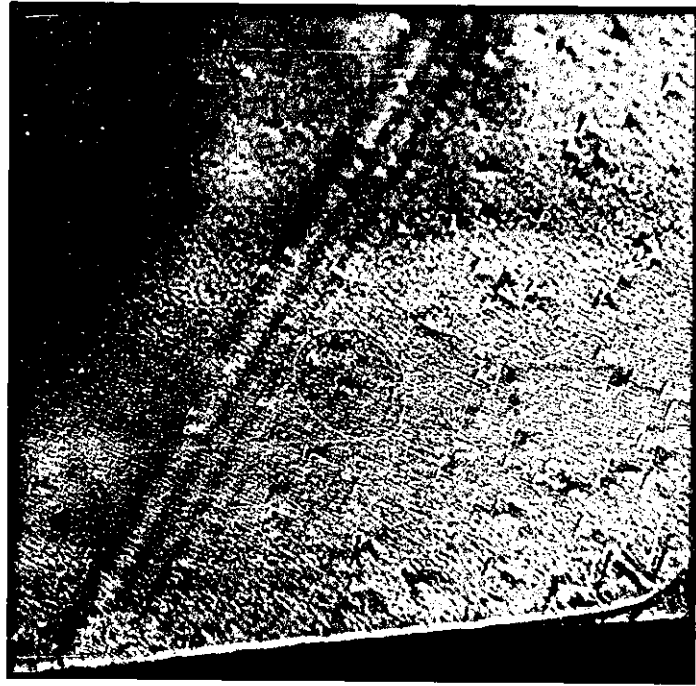
50µm

Fig. 62  
Arrest location on a (small)  
cleavage fracture surface of low  
DDM resin. (Optical micrograph)



1.8µm.

Fig. 64  
Scanning electron micrograph of  
an area corresponding to the  
triangular features in Fig. 62



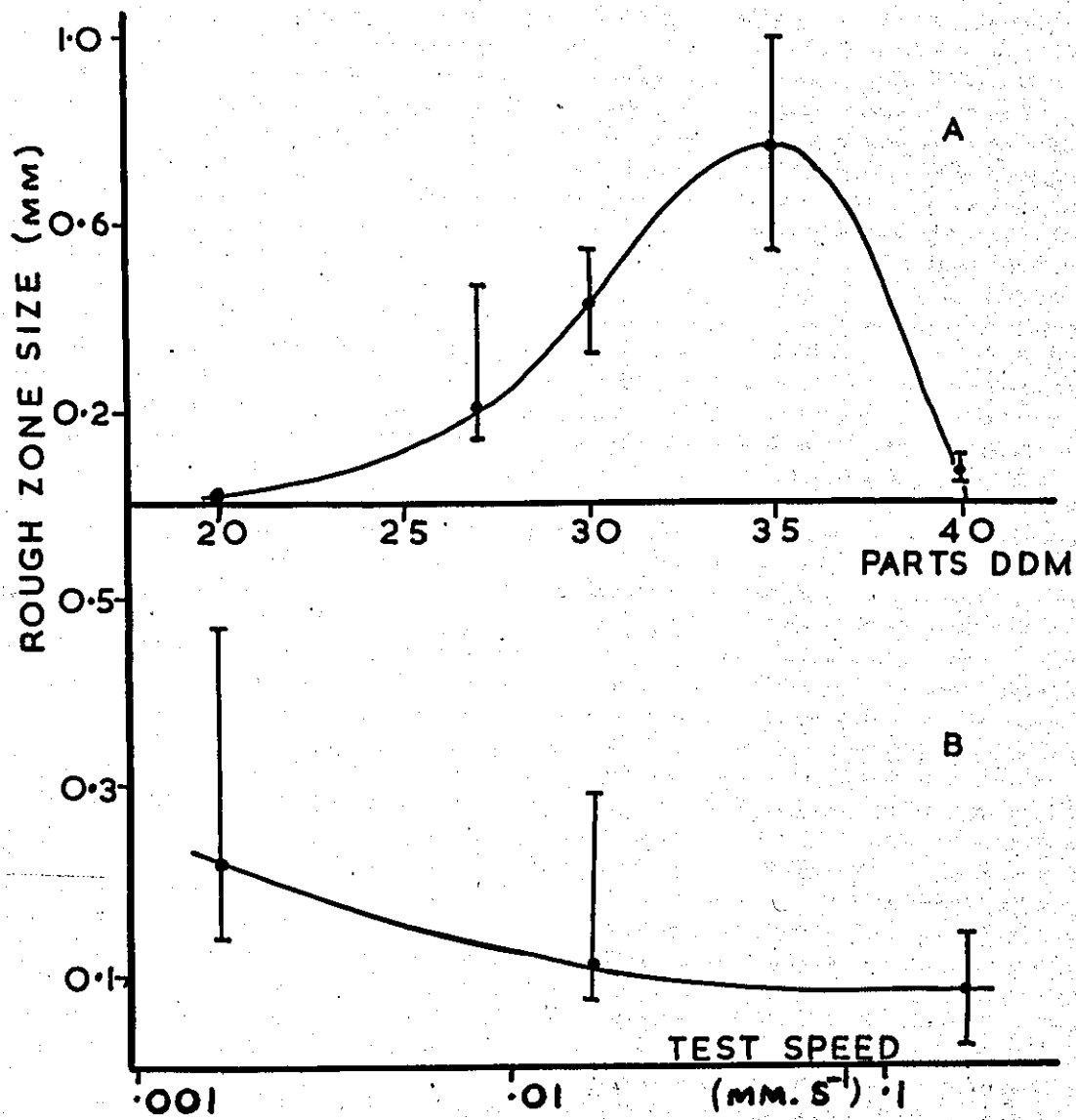


FIG. 63  
ROUGH ZONE SIZE v DDM CONTENT &  
TEST SPEED



4.4 μm

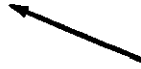
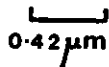


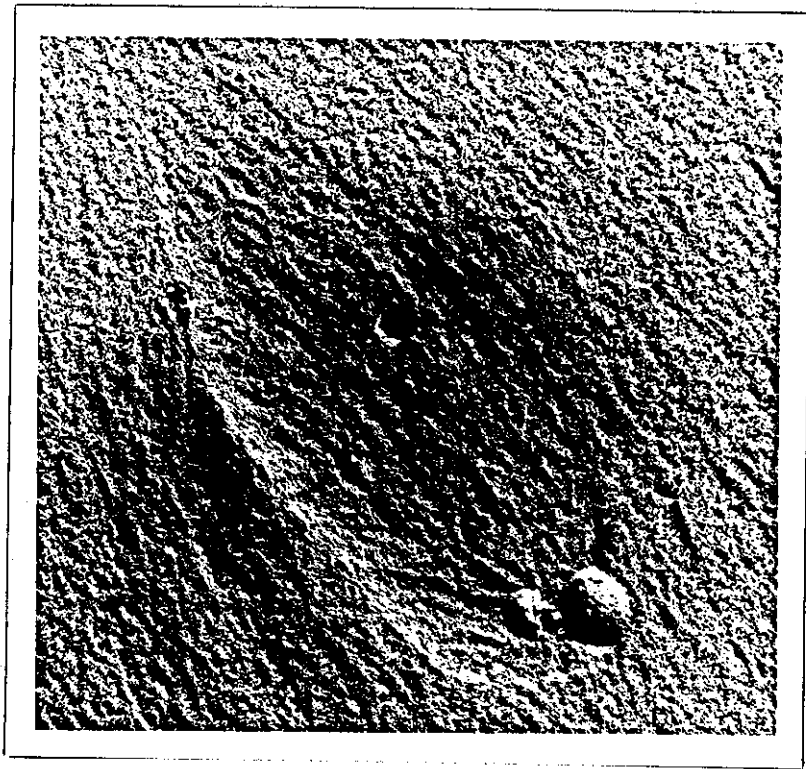
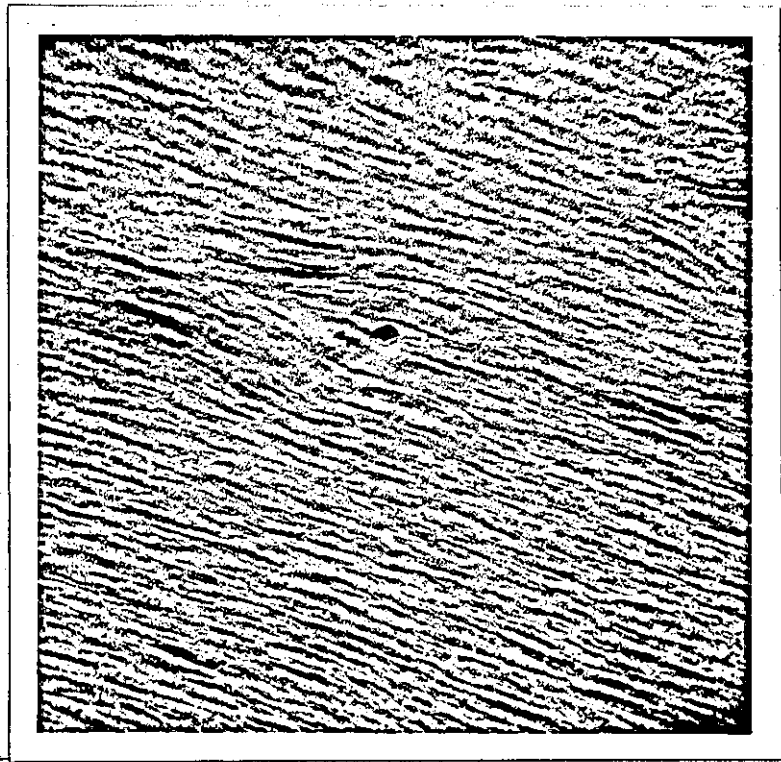
Fig. 65  
As Fig. 64, showing an associated  
pore



0.42 μm



Fig. 66  
Transmission electron micrograph  
of an area corresponding to the  
triangular features in Fig. 62.  
(Two-stage acetate-carbon replica)



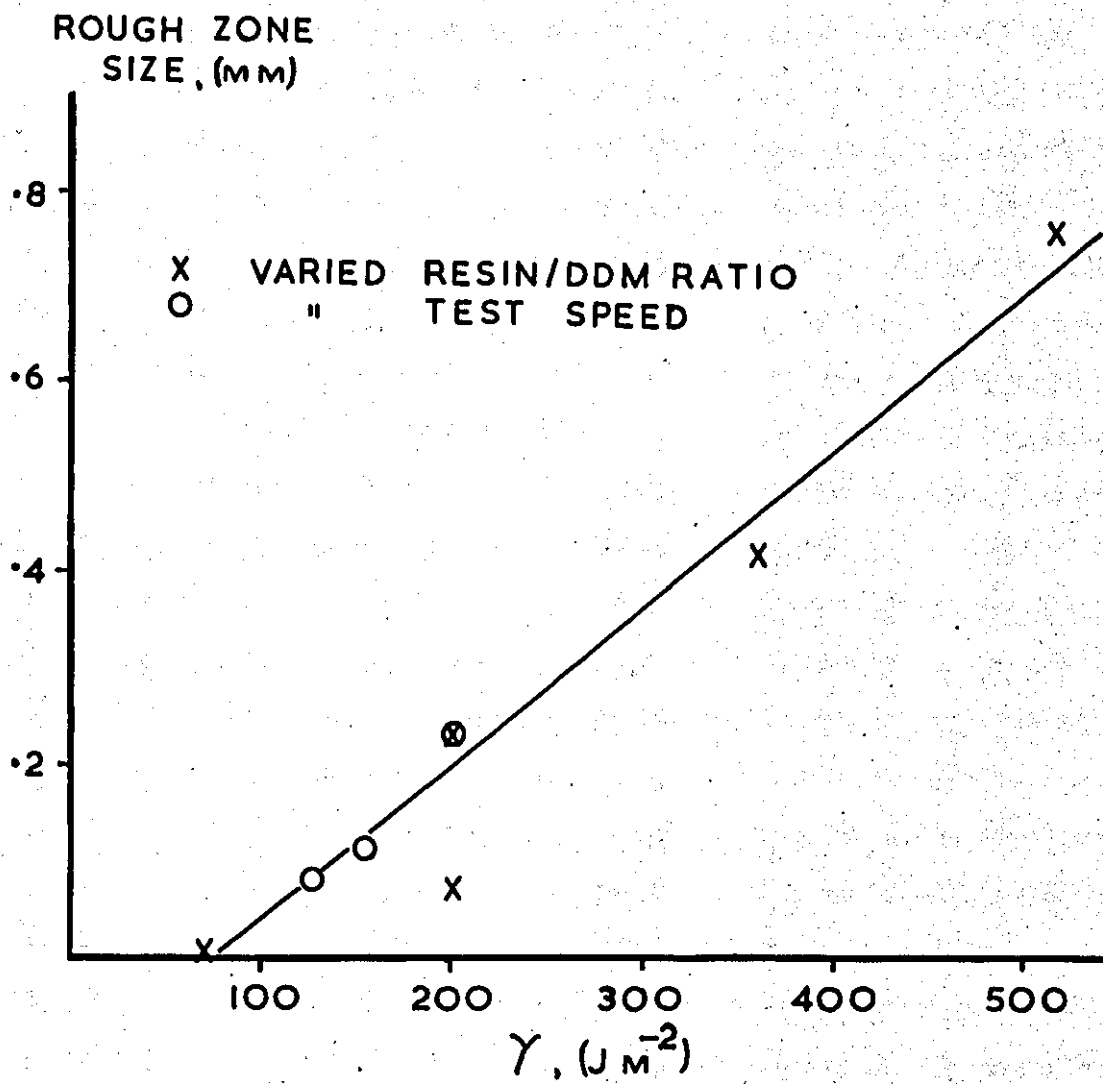
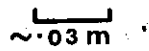


FIG. 67  
ROUGH ZONE SIZE v  $\gamma$





~0.3 m

Fig. A1  
Jig for groove-cutting of  
cleavage test pieces

